UNIVERSITÀ DEGLI STUDI DI PADOVA

Dipartimento di Ingegneria Industriale DII

Corso di Laurea Magistrale in Ingegneria Energetica

Techno-economic analysis of hydrogen separation and purification technologies for fuel cell application

Relatrice: Prof.ssa Stoppato Anna
Correlatore: Dott. Pratticò Luca

Laureando: Rizzo Michael
Matricola: 2026875

Anno accademico 2022/2023

Ringraziamenti
Desidero esprimere grande riconoscenza alle persone che hanno in vari modi supportato la stesura della tesi. Innanzitutto, il Dott. Luca Pratticò, supervisore del progetto, che con entusiasmo e competenza mi ha guidato in ogni fase del percorso, fornendomi i migliori consigli durante i numerosi meeting. Un ringraziamento va al Dott. Matteo Testi, Head of Area Hydrogen Technologies, per il suo aiuto nella modellazione dinamica di separazione dell'idrogeno allo stato solido basato sugli idruri metallici e per avermi dato l'opportunità di entrare a far parte del vibrante team Sustainable Energy della Fondazione Bruno Kessler (FBK). Infine, ringrazio la Prof.ssa Anna Stoppato per la sua disponibilità e l'interesse mostrato nel corso di questi mesi.

Acknowledgements
I would like to express great gratitude to the people who supported the writing of this thesis in various ways. First of all, Dr. Luca Pratticò, project supervisor, who with enthusiasm and competence guided me every step of the way, providing me with the best advice during the numerous meetings. My thanks go to Dr. Matteo Testi, Head of Area Hydrogen Technologies, for his help in the dynamic modelling of solid-state hydrogen separation based on metal hydrides and for giving me the opportunity to join the vibrant Sustainable Energy team of the Fondazione Bruno Kessler (FBK). Finally, I would like to thank Prof. Anna Stoppato for her helpfulness and interest over the past few months.

Abstract

The climate-environmental crisis the modern world is facing is mainly caused by an inefficient energy system based on fossil fuels. The decarbonization targets of 2050 call for early action, but it is crucial to avoid investing time and resources in the wrong direction. In this context, many research groups agree on the importance of hydrogen as a possible alternative energy source. In the use of hydrogen, especially in commercial fuel cell applications, hydrogen purity is crucial, as contaminants can negatively affect the efficiency and lifetime of the electrochemical device. The aim of this study is to contribute to the deployment of hydrogen as an energy carrier through a techno-economic analysis of available purification technologies that meet the purity requirements of ISO 14687:2019. Various purification technologies for hydrogen-containing gas mixtures are considered, including pressure swing adsorption systems, membranes, and metal hydrides. The techno-economic analysis is conducted on two specific study cases. The deblending of hydrogen from the natural gas transmission grid represents the case study of the purification of a hydrogen-lean gas mixture. In this context, with a stream containing 5% vol. of H_2 in the natural gas, metal hydride proves to be the most economical solution, with a final separation cost in the range of 1.1-1.7 €/kg_{H2}, and a specific energy consumption of 6.1 kWh/kg_{H2}, including hydrogen compression at high pressure and injecting the natural gas into the distribution grid. The second case study concerns the purification of a syngas with a high hydrogen content, obtained by a biomass gasification process. In this case, pressure swing adsorption technique remains the leading technology for this type of application. The different purification technologies examined show variable results depending on the use scenario analyzed and the relevant boundary conditions. Finally, a dynamic model for solid-state purification with doped $LaNi_5$ metal hydride is presented, studying the kinetics of adsorption and the thermal management. The results obtained through the model developed in the Dymola simulation environment confirm the feasibility of purifying mixture H_2:CH_4 5:95% vol., achieving a high hydrogen purity (99.97%) and a hydrogen recovery close to 80%.

Sommario

La crisi climatica-ambientale che il mondo moderno sta affrontando è principalmente causata da un sistema energetico inefficiente basato sui combustibili fossili. Gli obiettivi di decarbonizzazione al 2050 richiedono un intervento tempestivo, ma è fondamentale evitare di investire tempo e risorse nella direzione sbagliata. In questo contesto, numerosi gruppi di ricerca concordano sull'importanza dell'idrogeno come possibile fonte di energia alternativa. Nell'utilizzo dell'idrogeno, soprattutto nelle applicazioni commerciali delle celle a combustibile, la purezza dell'idrogeno è cruciale, poiché i contaminanti possono influire negativamente sull'efficienza e sulla durata del dispositivo elettrochimico. Lo scopo di questo studio è contribuire alla diffusione dell'idrogeno come vettore energetico attraverso un'analisi tecnico-economica delle tecnologie di purificazione disponibili che rispettino i requisiti di purezza richiesti dalla norma ISO 14687:2019. Sono state prese in considerazione diverse tecnologie di purificazione per miscele di gas contenenti idrogeno, tra cui i sistemi di adsorbimento a pressione oscillante, membrane e metalli idruri. L'analisi tecno-economica è stata condotta su due casi studio specifici. La separazione di idrogeno dalla rete di trasmissione del gas naturale rappresenta il caso studio di purificazione di una miscela gassosa povera di idrogeno. In questo contesto, con un flusso contenente il 5% vol. di H_2 nel gas naturale, il metallo idruro dimostra di essere la soluzione più economica, con un costo finale di separazione nell'intervallo 1.1-1.7 €/kg_{H2}, ed un consumo specifico di energia di 6.1 kWh/kg_{H2}, comprensivi della compressione dell'idrogeno ad alta pressione e dell'immissione del gas naturale nella rete di distribuzione. Il secondo caso studio riguarda la purificazione di un syngas ad alto contenuto di idrogeno, ottenuto tramite processo di gassificazione della biomassa. In questo caso, la tecnica dell'adsorbimento a pressione oscillante rimane la tecnologia principe per questo tipo di applicazioni. Le diverse tecnologie di purificazione prese in esame evidenziano risultati variabili in base allo scenario d'uso analizzato e alle relative condizioni al contorno. Infine, viene presentato un modello dinamico per la purificazione allo stato solido con idruro metallico $LaNi_5$ dopato, studiando la cinetica di assorbimento e la gestione dello scambio termico. I risultati ottenuti mediante il modello sviluppato in ambiente di simulazione Dymola confermano la fattibilità di purificare una miscela H_2:CH_4 5:95% vol., ottenendo un'elevata purezza dell'idrogeno (99.97%) e un recupero dell'idrogeno prossimo all'80%.

Contents

Abbreviations

IEA	International Energy Agency
LNG	Liquified natural gas
USD	United States dollar
PEM	Polymer electrolyte membrane
PEMFC	Polymer electrolyte membrane fuel cell
HFI	Hydrogen fuel index
NREL	National Renewable energy laboratory
PSA	Pressure swing adsorption
WGS	Water gas shift
MEMPHYS	MEMbrane based Purification of HYdrogen System
UNIFHY	UNIQUE gasifier for hydrogen Production
PCT	Pressure-Composition-Temperature
KPI	Key performance parameter
PDF	Process flow diagram
CMS	Carbon molecular sieve
STP	Standard pressure condition
EER	Energy efficiency ratio
COP	Coefficient of performance
GPU	Gas permeance unit
LHV	Low heating value
MH	Metal hydride
CAPEX	Capital expenditure
OPEX	Operational expense
LCOP	Levelized cost of purification
TCO	Total cost of ownership
CEPCI	Chemical Engineering Plant Cost Index
%wt	Weight percentage
TEA	Techno Economic Analysis
IF	Installation factor

Chapter 1

1 Broader context

1.1 Hydrogen as an energy carrier

Economies and governments around the world are looking for the best way to achieve carbon neutrality. Looking at carbon dioxide (CO_2) emissions by the economic sector, almost ¾ of emissions come from energy use, which includes electricity, heat, and transport [1]. Interventions to be applied to the energy system, currently largely based on fossil fuels, can be of the traditional type, such as improving process efficiencies and reducing losses, or of the innovative type, such as using carbon-neutral renewable sources. Such a scenario should ideally be based on an energy carrier. An energy carrier is a form of secondary energy that lends itself to being transported to the place of use. For example, electricity is an energy carrier because it can be transmitted via a grid and used even kilometers away from the place of generation. Any energy carrier that is not a primary source[1] suffers a loss of energy due to the transformation of one form of energy to another, and that one additional step in the whole process increases the cost of the unit of energy.

Hydrogen was first isolated by the English chemist Henry Cavendish in 1766 [2]. Around the 1970s, it began to gain interest as a replacement for hydrocarbon fuels for vehicle and air transport [3] and in the 2016 World Energy Outlook compiled by the International Energy Agency (IEA), hydrogen is mentioned 11 times [4]. It is only recently that hydrogen has started to receive real consideration, to the extent that some countries such as Japan have made it central to their decarbonization strategy, and around the world there are national hydrogen strategies either fully developed or in the preliminary stages [5]. However, most outlook studies do not agree on how or in which sector hydrogen will play a major role [6].

No hydrogen deposits exist in nature; this element must be produced from other compounds by consuming electrical or thermal energy. The success of hydrogen depends on the advantages its use can bring over other energy carriers. If used as a substitute for fossil fuels, it would remove CO_2 emissions in end uses, and make the carrier's local impact zero. Hydrogen is a gas that burns in the air, producing water as a product of combustion[2]. Fuel cells, on the other hand, exploit hydrogen electrochemically and make it possible to generate electricity with excellent efficiency.

If hydrogen is produced from renewable sources, the overall environmental impact would also be significantly decreased. It would be produced by electrolysis of water

[1] Fossil fuels are a primary form of energy carrier.

[2] Open flame hydrogen burners without catalytic combustion generate nitrogen oxides (NO_x), due to the elevated temperature of combustion [112]. NO and NO_2 are strong greenhouse gases.

using electricity supplied by renewable power plants. In 2021, according to data from IEA [7], the share of renewables in global electricity generation reached 28.7% with hydropower alone having a share of 15.22% and all others[3] accounting for 13.13% of the total.

Hydrogen is an element with a very high gravimetric energy density. Gravimetric energy density refers to the amount of energy that is contained in a given mass of material. In this sense, hydrogen can contain more energy than any other fuel for the same mass. In particular, as the values in Table 1 show, hydrogen outperforms diesel and petrol by a factor of 3 and liquified natural gas (LNG) by a factor of 2.6. This makes hydrogen an excellent fuel for rockets, where mass is a critical factor.

Table 1: Gravimetric and volumetric energy densities of common fuels [8].

	Energy per kilogram [MJ/kg]	Energy per liter [MJ/liter]
Hydrogen (ambient pressure)	143	5.6
Natural gas (liquid)	53.6	22.2
Gasoline (petrol)	46.4	34.2
Diesel	45.4	34.6

Energy density can also be expressed on a volumetric basis, and hydrogen needs a larger volume than other fuels to contain the same amount of energy, in fact the energy density of hydrogen is only 45% of that of LNG, as shown in the right-hand column of Table 1. Hydrogen can damage metals and alloys, according to the hydrogen embrittlement phenomenon [9]. Compared to all solid and gaseous fuels, it has the smallest molecule, which makes it more likely to escape through small openings. Finally, it is a highly explosive gas, presenting the greatest risk of fire or explosion because it has the widest flammability ranges, 4-75% in air and 4-94% in oxygen [10]. However, the assessment of fuel hazards must be more comprehensive, taking into account various aspects such as flame visibility, heat radiation, and fire incidents in the event of leaks in closed spaces. Certain properties of hydrogen, such as its high diffusivity in air, can be advantageous for fire prevention.

Hydrogen is mainly required by the chemical and petrochemical industries as a chemical feedstock. In 2021, the global demand for hydrogen was 94 million tonnes (Mt) [5], 40 Mt of which were used for petroleum refining in fuel desulphurization and hydrogenation processes, and 54 Mt used for the synthesis of ammonia, ethylene, and methanol. Only a negligible share was used in the transport, buildings, and power sector (about 40 kilotonnes). The 94 million tonnes of H_2 are associated with more than 900 Mt CO_2 emissions. This is because hydrogen only occurs in nature in compound form in water, hydrocarbons, and organic compounds.

To obtain hydrogen in its pure state it is necessary to break down the molecule of these substances by an energy-intensive process. Hydrogen production can be

[3] Wind, solar photovoltaic, bioenergy, others.

distinguished according to where this energy comes from. If it is primary energy, it is produced from natural gas, coal, and oil, today accounting for about 80% of all hydrogen produced. Electricity is the only secondary form of energy used to produce hydrogen either by electrolysis of water (0.04% of the total production) or by chlor-alkali electrolysis, a process in which hydrogen is the waste product (18% of the total). In 2021, global carbon dioxide emissions from fossil fuels and industry amounted to 37 billion tons [11], with hydrogen-production-related emissions accounting for 4%.

1.2 Hydrogen supply side

Of the 94 Mt of hydrogen marketed worldwide in 2021, the vast majority comes from fossil sources. The most widely used process is called steam reforming of light hydrocarbons such as methane (CH_4). The steam reforming process involves the endothermic conversion of CH_4 and water vapor into hydrogen and CO_2. The process requires the substance to be reformed and heated to carry out the reaction at temperatures between 700 and 1100°C [12]. The heat is provided by the hydrocarbon, while the hydrogen comes from both the hydrocarbon and the water. Depending on regional natural gas prices, the levelized cost of hydrogen production from natural gas ranges 1-2.5 USD[4]/kg_{H2} [5].

There is also the possibility of producing hydrogen by coal gasification, a partial oxidation of the fuel. Taking all capital and operating costs into account, the production cost in 2023 is 1-2 \$/kg_{H2} [13]. The cost of producing hydrogen using hydrocarbons and coal in the absence of carbon capture and storage is expected to triple and the increase is mainly attributable to the cost of CO_2, which is expected to be in the range of 55-250 USD/tonne in 2050.

Biomass gasification is a process that convers biomass to hydrogen and other products, without combustion. Solid or liquid organic compounds are converted into a gas phase called syngas and a solid phase called char [14]. Syngas can be used for power generation or biofuel production. The conversion is a partial oxidation carried out in the presence of a gasifying carrier such as air, oxygen, steam, or CO_2.

Hydrogen can also be produced from water by splitting it into its components (hydrogen and oxygen) through various processes, the most established of which is electrolysis. Renewable resources produce the electricity needed for this purpose. Electricity is a commonly used energy carrier but does not lend itself to storage, so the electrochemical process enables it to be converted into hydrogen, which is more prone to storage. The device used to separate water molecules into their constituent elements using electricity is known as an electrolyzer. Most commercial electrolyzers are of the alkaline type and use an aqueous solution of potassium hydroxide as the electrolyte [15]. There are also electrolyzers with a solid electrolyte instead of a liquid called PEM, which stands for polymer electrolyte membrane. The cost of hydrogen by electrolysis is composed of the cost of renewable energy, replacement operating costs, and the capital cost of the electrolyzer. Given the continued reduction in the cost of renewable energy worldwide, electrolyzer learning rates around 18% [15], and major reductions in capital costs, many analysts predict a reduction in the cost of production from the current 4-9 \$/kg_{H2} [5] to a cost of 1.3-3.3 \$/kg_{H2} in 2050 [16]. To make

[4] USD: United States dollar.

hydrogen produced from renewable sources competitive with other types of production processes, a huge amount of money will be invested in the hydrogen supply side in the coming years, mainly to cover the electrolyzer capex and to reach 1300 gigawatts (GW) of capacity in Europe in 2050 [6]. For perspective, the peak electrical load reached in Europe in January 2016 was 546 GW [17]. The industrial sector, responsible for 20% of global carbon emissions [18], presents a significant challenge in terms of decarbonization. Green hydrogen has the potential to address this issue in hard-to-abate industries like steel, cement, and petrochemicals, which are difficult to decarbonize.

Currently, hydrogen is mainly used at the same location where it is produced, and the implementation of hydrogen on a large scale as an energy carrier requires efficient storage systems. The technological challenge of storage systems depends on the chemical and physical characteristics of hydrogen. As already introduced, among the most common fuels, hydrogen has the highest energy density on a mass basis, but the lowest energy density on a volume basis, both in the gas and liquid phase. But if for mobility applications the large size penalizes storage, in other stationary applications the problem would not exist. Furthermore, to assess the suitability of the storage system other characteristics must be considered such as the system's working temperature, pressure, kinetics, stability, or security.

An established technology is the storage of hydrogen in the form of compressed gas [19]. Due to the low energy density per unit volume, it is necessary to raise the gas pressure. At present, tanks are made of carbon steel, stainless steel, or even composite materials and allow pressures of up to 700 bar [20]. However, the advantage of the low mass of hydrogen can be lost as the thickness of the tank increases with increasing pressure to provide mechanical strength, which leads to an increase in the mass of the tank material. In addition, high pressures result in high energy expenditure for compression.
Energy density can be improved by storing hydrogen in liquid form by decreasing its temperature to around 20 K (-253 °C). However, hydrogen liquefaction is an energy-intensive process, increasing the final fuel cost and introducing the need for effective system insulation. Hydrogen liquefaction currently consumes 1/3 of its energy content [21], compared to no more than 10% for LNG.
There is also solid-state hydrogen storage, and it is done in two ways as nanostructured materials and hydrides. Nanostructured materials such as carbon nanotubes and metal-organic framework systems can store hydrogen by either physisorption or chemisorption processes [22]. In metal hydrides, hydrogen can chemically bond with various metals and metal alloys to form hydrides, compounds that can trap hydrogen. The gas penetrates the crystalline lattice of the metal, occupying the interstitial sites. Further information is presented in the following chapters to understand the functioning of metal hydride, not as a storage application, but used for purification processes.

When hydrogen needs to be transported, it can be accomplished through pipelines or by utilizing cryogenic liquid tanker trucks or gaseous tube trailers, moving it from the

production site to the intended destination. Hydrogen is transported through pipelines in areas with substantial, stable demand from large users like refineries and chemical plants, following a similar method to natural gas transport. Although the transport of hydrogen gas in pipelines requires appropriately engineered valves, compressors, and tanks, it is an economical solution compared to other alternatives. Typical capital costs for onshore transmission networks (high pressure transmission pipelines) including compression will range between USD 0.6-1.2 million per km for retrofit and USD 2.2-4.5 million per km for newly built H_2 pipelines, resulting in H_2 transport costs of 0.13-0.23 USD/kg/1000km. Distribution pipelines (pipelines for last-mile gas delivery to end users) are substantially cheaper than transmission pipelines given their smaller diameter and lower pressures [23].

1.3 Hydrogen demand side: fuel cells and fuel quality

Fuel cells are a key technology for developing hydrogen as an energy carrier due to their ability to utilize hydrogen optimally. The technology is used in:

- Electric power generation system in commercial, residential, industrial sectors.
- Backup power generation in temporary or emergency situations.
- Power sources in remote locations.
- Cogeneration where the system generates continuously electrical energy and heat from residues of hot air and water.
- Fuel cell electric vehicles for mobility.

Hydrogen fuel cells, as electrochemical systems, can directly convert the chemical energy of hydrogen into electrical energy without the need for a thermal cycle, thus overcoming the limits of the Carnot cycle and achieving higher conversion efficiencies than traditional thermal machines like gas turbines, steam turbines, and internal combustion engines [24]. A conventional combustion-based power plant typically generates electricity at efficiencies of 33 to 35%, while fuel cell systems can generate electricity at efficiencies up to 60%.

A fuel cell can produce electricity as long as hydrogen and oxidant (air) are supplied to the system through an electrochemical process. There are different cell technologies, with different characteristics and different degrees of development. Normally, cells are classified based on the electrolyte used or the operating temperature (low-temperature and high-temperature cells). Table 2 shows some of the more common fuel cells and the type of membrane each uses.

Table 2: classification of fuel cell systems based on the employed membrane [25].

Fuel cell	Membrane	Abbreviation
Solid oxide fuel cells	Yttria-stabilized zirconia	SOFC
Direct methanol fuel cell	Solid polymer electrolyte (Nafion)	DMFC
Phosphoric Acid fuel cell	Phosphoric Acid	PAFC
Polymer electrolyte fuel cell or Proton exchange membrane	Solid polymer electrolyte (Nafion)	PEMFC
Alkaline fuel cell	Aqueous solution Potassium Hydroxide	AFC

In the global fuel cell market in 2021 [26], most of the shipments are PEMFCs, corresponding to an overall capacity of 1973 MW, followed by SOFCs and DMFCs. Approximately half of the fuel cells are used for stationary applications, a smaller portion is used for transport, and a further negligible amount of 6000 units is destined for portable applications (size from a few watts to a few kW).

To be used in refineries, ammonia production, and fuel cells, hydrogen must undergo an ultra-purification process. For other applications such as methanol synthesis, steel production with direct reduced iron technology, or others, hydrogen does not need to be purified and can be used mixed with other gases, such as CO_2. Pure hydrogen means that small amounts of contaminants or additives are present and can be tolerated by specific applications. For many years, there was great difficulty in defining quality specifications for hydrogen, each requirement being established within a commercial relationship between customer and supplier [27]. This reason, together with the spread of fuel cells, and the search for uniformity led to the standard BS ISO 14687:2019 "Hydrogen fuel quality - Product specification". This document specifies the minimum quality characteristics of distributed hydrogen fuel for use in vehicle and stationary applications. Table 3 is an extract from the standard for type 1 hydrogen (gaseous hydrogen).

Table 3: Fuel hydrogen grades and their applications according to the standard ISO 14687 for type 1 (hydrogen gaseous).

Grade	Applications		Purity
A	Gaseous hydrogen; internal combustion engines for transportation; residential/commercial combustion appliances (boilers, cookers and similar applications)		98.0
B	Gaseous hydrogen; industrial fuel for power generation and heat generation except PEMFC applications		99.90
C	Gaseous hydrogen; aircraft and space-vehicle ground support systems except PEMFC applications		99.995
D	Gaseous hydrogen; PEMFC for road vehicles		99.97
E	PEMFC for stationary appliances	Cat.1	50
		Cat.2	50
		Cat.3	99.9

Purity is based on the Hydrogen fuel index (HFI) concept to indicate the purity of hydrogen fuel as a percentage (or mole fraction) of a gaseous hydrogen mixture, so HFI can be obtained by subtracting non-hydrogen gases from 100 percent:

$$HFI = 100\% - \sum Non\ hydrogen\ gas\%$$

Eq. 1

And so in the case of grade D hydrogen, the maximum mole fraction of other gases is 0.03% (or 300 μmol/mol). In certain non-commercial applications, hydrogen must also meet ultra-pure requirements. For these specific cases, the standard dictates that gaseous and liquid hydrogen used in aircraft and space-vehicle on-board propulsion applications should have an HFI value of 99.995%. Table 4 presents specified maximum permissible limits for individual components.

Table 4: impurity levels for grade D of gaseous hydrogen fuel extract from ISO 14687.

Contaminants	Maximum concentration [μmol/mol]
Water	5
Total hydrocarbons except methane	2
Methane	100
Oxygen	5
Helium	300
Nitrogen	300
Argon	300
Carbon dioxide	2
Carbon monoxide	0.2
Total Sulphur compounds	0.004
Formaldehyde	0.2
Formic acid	0.2
Ammonia	0.1
Halogenated compounds	0.05
Maximum particulate concentration	1 mg/kg

The impurities in hydrogen affect the performance and durability of the fuel cell in different ways. Table 5 shows the main effects of each contaminant. The probability of each impurity being present in hydrogen is highly dependent on the hydrogen production method [28]. Out of the gaseous contaminants specified in ISO 14687, only three are likely to be present in electrolytic hydrogen: nitrogen, oxygen and water [29]. In the process of steam reforming methane are generated impurities such as CO_2, carbon monoxide (CO), hydrocarbons, nitrogen, argon, helium, ammonia, halogens, sulphur compounds and other substances [30].

Table 5: Action of contaminants of hydrogen on fuel cell (Rev = reversible, Irr = irreversible).

Contaminants	Effect	Damage
Water	No direct degradation	
Total hydrocarbons except methane	Inhibiting access of hydrogen on the catalyst surface	
Methane	Inert, problems at high concentration for hydrogen dilution	
Oxygen	Inert	
Helium, Nitrogen, Argon	Inerts, hydrogen dilution	
Carbon dioxide	Hydrogen dilution High concentration lead to the formation of CO	
Carbon monoxide	Severe catalyst poisons	Rev.
Total Sulphur compounds	Severe catalyst poisons	Irr.
Formaldehyde and Formic acid	Similar or more severe effect than that of CO	Rev.
Ammonia	Affect the ion exchange capacity of the fuel cell	Irr.
Halogenated compounds	Degradation of the fuel cell catalyst	Irr.
Particulates	Erosion of gaskets, clogging filters and valves	Irr.

Dawood et. al [31] point out that it is rare in the literature to find a direct connection or inclusion of the purification process in the hydrogen production's techno-economic assessment. The authors concluded that the cost of hydrogen purification needs to be considered for meeting endpoint application requirements, determining the hydrogen production pathway choice, and assessing hydrogen cycle feasibility. Luo et al. [32] state that the cost of hydrogen is mainly affected by its production cost, transportation cost, and purification cost, as well as the carbon trading cost and that if the raw gas is derived from water electrolysis the purification cost can be considered to be 0 USD/kg_{H2}. The model is applied to the Chinese market for hydrogen used in fuel cells in the transportation field and explicitly calculates the purification cost for hydrogen production from coal and natural gas. For hydrogen production from natural gas relative to a demand of 1000 Nm^3/h, the purification cost is 0.96 USD/kg_{H2}, with a reduction of 63.33% if the demand increases to 10000 Nm^3/h for large-scale economy. For hydrogen production from coal, the cost is higher, 1.47 USD/kg_{H2}, due to the low hydrogen content of the raw gas and high equipment investment costs.

Wickham et al. in their work [33], in which is proposed an optimized hydrogen supply chain model for the transport sector focus on hydrogen purity and purification requirements, reviewed many supply chain models and concluded that production, transportation (transmission and distribution), storage, and hydrogen fueling stations are always considered, but the inclusion of separation/purification technologies is missing in all of them, underestimating the total supply chain costs. Purification technologies found to contribute 14% and 30% of total capital expenditure and operational expense.

Separation and purification can be implemented at different stages of the supply chain. In a centralized facility, it can enhance the purity of hydrogen obtained from transmission and supply it to the distribution system. This approach offers the advantage of economies of scale. However, it requires transporting pure hydrogen to the refueling station, leading to potentially higher transportation costs. Alternatively,

separation and purification can be conducted locally at the refueling site. This allows for flexibility in the hydrogen grade resulting in reduced transportation costs. Nevertheless, a drawback of this method is the lack of economies of scale due to the small-scale localized purification process.

1.4 Case study 1: Hydrogen deblending from natural gas grid

There are about 2600 km of hydrogen pipelines operating in the United States and about 2000 km in Europe [34], but there is currently no widespread infrastructure for the transport of hydrogen gas that can distribute hydrogen in line with the user demand expected in the coming years. In contrast, more than 1.2 million km of transmission pipelines are installed globally for the transport of natural gas [35], so it has been proposed to inject hydrogen into the already existing infrastructure with H_2 percentages of no more than 30% by volume. In this strategy, several users would benefit from an appropriate deblending phase, in other words, the separation of the components of the mixture, starting from hydrogen fuel cells that require pure hydrogen, but also hydrogen-sensitive consumers such as gas turbines or natural gas vehicles that do not accept hydrogen higher than 1-2%. Figure 1 [36] illustrates some examples of this, although these examples are not comprehensive.

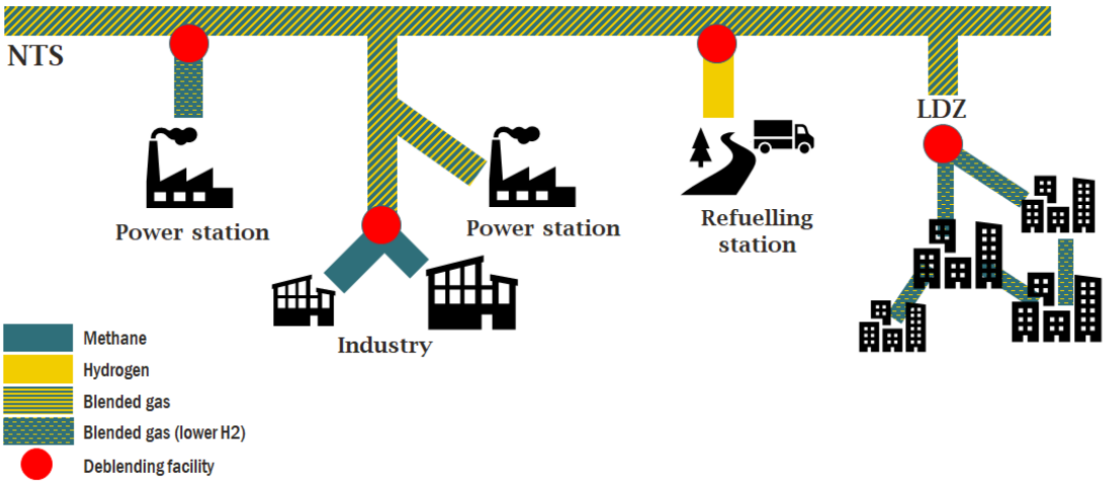

Figure 1: Deblending could help meet different customer needs. NTS = national transmission system, LDZ = Local distribution zones.

One of the first publications covering the economics of hydrogen separation from blended natural gas is the work of the National Renewable Energy Laboratory (NREL) [37], which performed a cost estimation for hydrogen extraction using pressure swing adsorption (PSA) units. With an assumed hydrogen recovery factor of 80%, the extraction cost is 3.3-8.3 $\$/kg_{H2}$ depending on the scale of extraction in kg/day, for a 10% hydrogen in the initial blend. With the increase of the blend to 20%, the extraction cost drops to 2.0-7.4 $\$/kg_{H2}$. The extraction cost is largely due to high capital costs, especially for compressors that have to re-inject natural gas into the network at 20 bar. However, if the deblending is done at a pressure-reduction facility, the recompression costs are reduced, bringing the extraction cost to range between 0.3-1.3 $\$/kg_{H2}$.

More recently, National Grid proposed a feasibility study [38] for deblending in the UK transmission and distribution network, comparing different separation technologies, such as cryogenic separation or a hybrid system with PSA and polymeric membranes. Minimum specific cost of hydrogen recovery for 20 mol% hydrogen in feed is in the range 1.0-1.6 £/kg_{H2} for the membrane/PSA scheme and 0.9-1.4 £/kg_{H2} for the cryogenic process without natural gas recompression. For recompression to feed gas pressure, costs are about 50-80% higher.
In 2016, the European research project HyGrid [39] started to develop a technology to separate hydrogen from low hydrogen streams (e.g. 2-10% vol). The project targets a pure hydrogen separation system with power and cost of <5 kWh/kg_{H2} and <1.5 €/kg_{H2} through a combination of membranes, electrochemical separation and temperature swing adsorption. The electrochemical separator, membrane production and membrane separators were expanded, and the membranes were tested under industrial conditions up to 50 bar. The complete modelling of the system demonstrated 25 to 40 % lower costs compared to the use of state-of-the-art technology.
The HylyPure process [40], developed by the research group at TU Wien, consists of a membrane pre-enrichment step followed by a pressure swing adsorption. The results show that for fuel-cell quality hydrogen at 25.81 bar the required specific energy demand is in the range of 0.8–1.5 kWh/m^3. Further information on deblending can be found in the European project Naturalhy [41].

1.5 Case study 2: Derived-biomass hydrogen purification

Fossil fuel-based thermochemical routes are currently the leading methods for large-scale H_2 production in industries. Green hydrogen can be generated through thermochemical processes by utilizing biomass as the source material. The production of hydrogen from fossil fuels and biomass involves conversion techniques like reforming, gasification, and pyrolysis [42]. These processes provide a synthesis gas, mainly consisting of hydrogen and is subjected to downstream processes in order to produce pure hydrogen.

Gasification is the thermochemical conversion of a carbonaceous solid fuel into a product gas in the presence of a specific gasification agent. Figure 2 shows a general process layout for hydrogen production via gasification and table 6 shows examples of syngas compositions depending on the gasifying agent and gasification reactor technology.

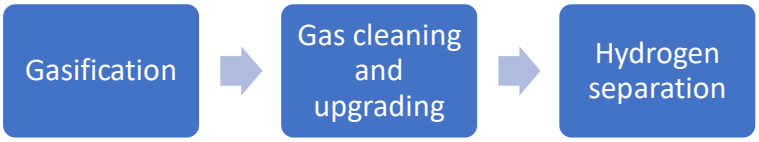

Figure 2: General process layout for hydrogen production via gasification.

Table 6: Overview of producer gas compositions from biomass [43].

Gasification technology	Typical hydrogen content in the product gas vol% (dry bases)	Gasifying agent
Downdraft	12-20	Air
Bubbling fluidized bed	7-9	Air
Entrained flow	23	Oxygen
ICBFB ENEA	30-33	Steam/oxygen
Circulating fluidized bed	30-31	Steam/oxygen
Dual Fluidized Bed	36-42	Steam

Gas cleaning and upgrading is necessary in order to remove bulk CO and CO_2, and trace components like hydrogen sulfide (H_2S), ammonia (NH_3), hydrochloric acid (HCl), and tar. Water gas shift (WGS) reaction is the intermediate step used for CO reduction and hydrogen enrichment in the synthesis gas.

The reaction, expressed in equation 2, was discovered by the Italian physicist Felice Fontana in 1780 [44]. The WGS reaction converts CO and steam to hydrogen and CO_2.

$$CO + H_2O \leftrightarrow H_2 + CO_2$$

Eq. 2

WGS reaction is a well-established technology in industrial large-scale plants producing hydrogen or setting the CO/H_2 ratio of synthesis gas [45]. A wet scrubber is a commonly used to control and remove particulate matter, tar, and other impurities from the gas.
Several approaches have been conducted with the aim of producing fuel cell-grade hydrogen from the product gas generated in biomass steam gasification plants. In the study conducted by Fail et al. [46], the process consisted of four operational units: catalyzed WGS reaction, gas drying and cleaning with a wet scrubber, hydrogen purification through PSA, and utilization of the produced biohydrogen in PEM fuel cell. The project MEMPHYS (MEMbrane based Purification of HYdrogen System) [47], develops an innovative electrochemical membrane hydrogen purification system for the extraction of hydrogen from multiple hydrogen sources, for instance hydrogen recovery from biomass fermentation.
The UNIFHY project (UNIQUE gasifier for hydrogen Production) [48] is focused on the production of pure hydrogen from biomass gasification. Hydrogen production at 99.99% was achieved with an H_2 yield from PSA of 66.4%.

When considering the purification of hydrogen gas, the cost of purification becomes a significant factor that can impact the overall cost of hydrogen production. This is particularly challenging for small-scale systems, as ensuring reliability and convenience while dealing with purification can be more complex. Even if the biomass cost is low and the system has a larger size and relatively high efficiency, the cost of purification becomes a significant aspect to consider. The expenses associated with removing impurities and achieving high-purity hydrogen can add up and affect the overall production cost. Therefore, while other factors such as biomass cost, system

size, and efficiency play a role in achieving a low hydrogen production cost, the purification cost becomes a critical consideration in the overall economic analysis.

1.6 Objectives

The aim of this thesis is to carry out a technical-economic comparison of hydrogen purification and separation systems. In particular, the stream of hydrogen leaving the purification unit must be suitable for use in fuel cells, according to the purity parameters indicated by the ISO 14687 standard. The work will proceed through various phases including:

- Propose study cases.
- Identify conventional purification technologies.
- Develop designs for each component of the purification unit.
- Create an economic database of cost items.
- Undertake technical-economic assessment declined in the study cases and evaluate the feasibility with technical and economic key performance indicators (KPI), listed and described in table 7.
- Application of a kinetic model of the sorption process in metal hydride to verify the preliminary design.

Table 7: List of technical and economic KPIs.

KPI	Unit	Description
Hydrogen purity	%	Hydrogen purity (expressed as a percentage) reached at the purification system outlet.
Hydrogen recovery	%	Amount of hydrogen (expressed as a percentage) extracted compared to the maximum amount of hydrogen potentially extractable from the feed stream.
Specific energy consumption	kWh/kg	Energy required to separate 1 kg of H_2.
Lifetime	years	Life of the purification system.
CAPEX	€	Cost of hydrogen purification system including direct capital costs and indirect capital costs.
OPEX	€/y	Annual O&M cost, including operating costs (electricity, heating and cooling water), labor, maintenance and repairs.
TCO	€	Total cost of ownership (sum of CAPEX and OPEX over the entire useful life).
LCOP	€/kg_{H2}	Levelized purification cost (within the battery limits exposed in chapter 5) evaluated considering the ratio between the TCO and the hydrogen purification potential over the entire useful life.

As regards the technical KPIs, the parameters are evaluated by observing updated bibliographic references and technical data sheets of commercial products. For the economic KPIs, an analytical model has been implemented to estimate all the desired indicators: the description of the model and the assumptions will be explained in next chapters.

In this study, two different usage scenarios and their related boundary conditions are identified. Specifically, the first case deal with de-blending upstream of a REMI cabin (REgolazione e MIsura), a regulation and metering plant that corresponds to a delivery point of the transmission network and is responsible for decompressing natural gas and its metering. The first case study involved two variations: a feed gas with a CH_4/H_2 concentration of 95% and 5% respectively, and a case with a much higher percentage of hydrogen in the feed gas (30% H_2 in methane). The second case study instead analyzed the purification of H_2 from a biomass gasification feed stream. In all scenarios, the purpose of the feed gas separation operation is to obtain a high purity hydrogen stream that can be used to power fuel cells. More details are given in Chapter 5. For all the cases it is assumed that the feed stream is free of sulfur-containing components or humidity, this occurs through special desulfurizers and dehumidifiers.

1.7 Thesis Outline

Chapter 2 describes the three hydrogen purification technologies selected for the study, pressure swing adsorption, membranes, and metal hydride, trying to briefly express the underlying physical phenomena.

Chapter 3 describes the methods for making an initial design of the three purification systems, producing estimates of some parameters which then allow an evaluation of the economic analysis.

Chapter 4 describes the economic assumptions, the cost functions found in the literature, and the construction of the LCOP (levelized cost of purification) index.

Chapter 5 shows the results of the technical-economic analysis for case study 1, for two different compositions of hydrogen in the natural gas grid (5% and 30%), and for case study 2.

Chapter 6 wants to verify the possibility of separate hydrogen from a H_2:CH_4 5:95% vol. mixture through a metal hydride tank using a doped $LaNi_5$ metal alloy, adopting a dynamic model for the study of the kinetics of absorption and desorption reactions.

Chapter 2

2 Purification technologies - State of art

2.1 Pressure swing adsorption (PSA)

PSA has been the dominant technology for hydrogen recovery from a wide range of gaseous streams for decades. After commercialization in 1966, the breakthrough came with the Polybed units increasing capacity to 265000 Nm^3/h of ultra-pure hydrogen produced by meeting the increased hydrogen consumption of refineries, and with H_2 recovery that can exceed 90% [49].

At the core of this process lies the principle that an adsorbent material possesses the capability to adsorb impurities to a greater extent at high partial pressures, as compared to adsorption at low partial pressures. Hydrogen is not adsorbed, and impurities trapped in the fixed high-pressure adsorbent bed are released when the system goes to a lower level, from which it takes the name 'swing'. A PSA system primarily comprises a carbon steel adsorbent vessel that is filled with the solid adsorbent material, complemented by the inclusion of a valves and control system.
Activated carbon, silica gel, and zeolite are used as adsorbents hydrogen purification applications at ambient temperature, sometimes even used simultaneously in the same bed where each layer adsorbs different impurities due to different affinity between species and solid adsorbent.

The overall performance of a PSA process depends on both equilibrium and kinetic factors [50]. When the solid adsorbent is placed in contact with a gas phase for a certain time, equilibrium can be reached. The behavior at equilibrium is described qualitatively by expressing the amount of adsorbed gas as a function of the partial pressure of the gas at a fixed temperature. This model of equilibrium is called isothermal, and depending on the type of curve trend, various models have been proposed. An example is given in figure 3, where the isotherm is expressed in terms of the amount of adsorbate adsorbed per unit weight of the adsorbent, which is generally well described by Langmuir's isothermal model. This type of isotherm is also characterized as favorable because adsorption is high at low partial pressure. Physical adsorption from the gas phase is an exothermic process, which is not favored at high temperatures. For this reason, the process operates at room temperature, because at a given pressure the amount of adsorbate at equilibrium decreases with increasing temperature, as shown in figure 3 [51].

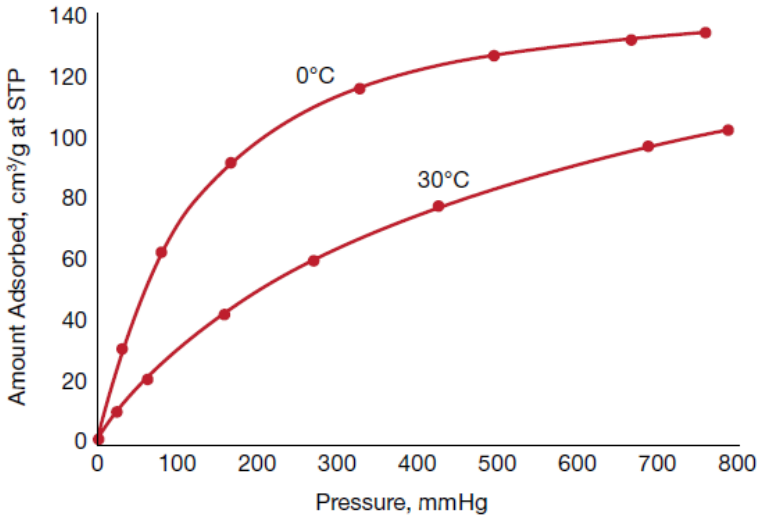

Figure 3: Data for the adsorption of ammonia onto charcoal follow the Langmuir isotherm reasonably closely.

From a kinetic point of view, for a molecule to be adsorbed by the adsorbing particle, it must diffuse, reach an adsorption site and then adsorb on the surface. Mass transfer is therefore the controlling mechanism of the process as the actual rate of equilibrium at a surface is usually very rapid [52].

A batch process is one in which a series of operations are carried out over a period of time on a separate, identifiable item or parcel of material [53]. PSA belongs to this type of process, but the use of multiple adsorbents in a staggered sequence makes the process continuous. Regardless of the number of adsorbent vessels, the main steps for a pressure swing cycle are (table 8):

1) Adsorption: the adsorbent bed receives the raw H_2 stream at high pressure, the impurities are adsorbed into the different adsorbent layers and a pure hydrogen stream is taken as product at the opposite side of the feed stream. The high-purity hydrogen product then leaves the system at a pressure close to that of the feed stream minus pressure drop. Once the bed is fully saturated, the feed is shut off and the feed gas is directed to another fresh bed. This allows for constant feed and outlet flows.

2) Co-current depressurization: the pressure is lowered to an intermediate level between maximum and minimum. This step recovers the hydrogen trapped in the gaps in the adsorbent, a depressurization takes place on the product side and in the same direction as the feed stream (named co-current). The extracted hydrogen stream is used to repressurize another adsorbent bed, which then undergoes a depressurization (or equalization) phase, and to purge other adsorbents. The hydrogen recovery phase is complete.

Table 8: PSA process steps.

Step 1	Step 2	Step 3	Step 4	Step 5
Adsorption	Co-current depressurization	Counter-current depressurization	Purge	Pressurization
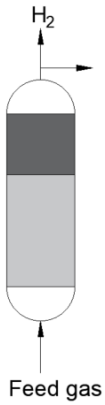	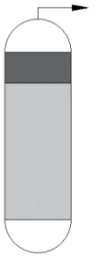			

3) Counter-current depressurization: at this point, the fully saturated bed begins the regeneration phase. The pressure is further lowered to the minimum level on the feed side, allowing the off-gas flow of impurities to escape.

4) Counter-current purging: to achieve further regeneration of the adsorbent bed, a purging step is performed by sending a flow from the product side consisting of pure hydrogen from another adsorbent that is performing co-current depressurization (step 2).

5) Pressurization: the bed is repressurized counter-current with hydrogen. Hydrogen is supplied by both the co-current depressurization step (step 2) of another adsorbent and a portion of the hydrogen produced (step 1). When the maximum pressure is reached, the cycle is complete, it is in the same condition as at the start, and the bed is ready to begin new adsorption.

To assess how well a PSA works, performance indicators should be introduced [54]. With reference to figure 4, it is defined purity:

$$Purity = \frac{C_{H_2}^P}{\sum_{i=1}^{N} C_i^P} = x_{H_2}^P$$

Eq. 3

where $C_{H_2}^P$ is the concentration [mol/m^3] of hydrogen in the product stream, i is the i-th component, N the total number of components in the gas mixture, $x_{H_2}^P$ is the molar fraction of hydrogen in the product stream. Denoting by Q the volumetric flow rate [m^3/s], and by superscript f the parameters for the feed stream, recovery is defined:

$$Recovery = \frac{\int_0^t C_{H_2}^P Q_{H_2}^P dt}{C_{H_2}^F Q_{H_2}^F}$$

Eq. 4

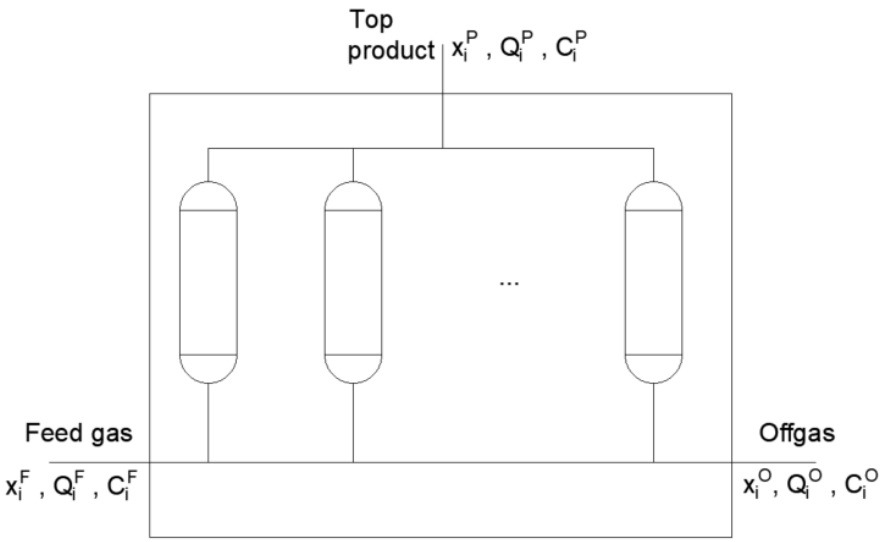

Figure 4: "grey-box" generic example of a pressure swing adsorption process. The inlet and exit streams are characterized by molar fraction (x_i), volumetric flow rate (Q_i), and gas concentration (C_i).

2.2 Membrane gas separation

The main disadvantage of PSA is the substantial loss of H_2 that takes place during the pressure release stage of desorption, resulting in significant waste of hydrogen resources. PSA method is costly due to its high equipment expenses and energy consumption, not suitable for the recovery of hydrogen from a stream containing low-purity or low-pressure hydrogen. In this context, membrane separation technology is emerging as a highly promising industrial process and has the potential to compete with and eventually replace traditional separation techniques. Membrane technology was first commercialized in the 1980s for the sweeting of natural gas[5] and for the recovery of hydrogen from ammonia purge gas [55]. There are currently several types of membranes for gas separation, and in this chapter the membranes are organized according to membrane structure and only those used for the techno-economic analysis of the thesis: metal membranes and carbon membranes. The two types make it possible to explain the two mechanisms of species permeation in the membrane, in other words the ability of the gas to pass through.

Metallic membranes are classified as inorganic membranes. Several metals are candidates for hydrogen permeable membranes, but among them palladium has

[5] Natural gas sweetening is a process that removes acidic impurities like CO_2 and hydrogen sulfide from natural gas to meet pipeline dry gas quality levels.

received considerable attention for the following reasons: extraordinary permeability, high tolerance to hydrocarbon flows and essentially impermeable to all other gases. The multistep mechanism of gas transport across a metal membrane is well illustrated in figure 5 from Baker [56]. The hydrogen molecule is sorbed onto the surface where it dissociates into atoms. Each hydrogen atom loses its electron and diffuses into the metal structure as an ion. On the permeate side, the atoms that have diffused reassociate to form the hydrogen molecule H_2 and desorbs, completing the process. Only the hydrogen gas manages to pass through the membrane, all other gases are excluded. At high temperature (> 300°C), the controlling mechanism governing the entire process is the diffusion of atomic hydrogen through the metal.

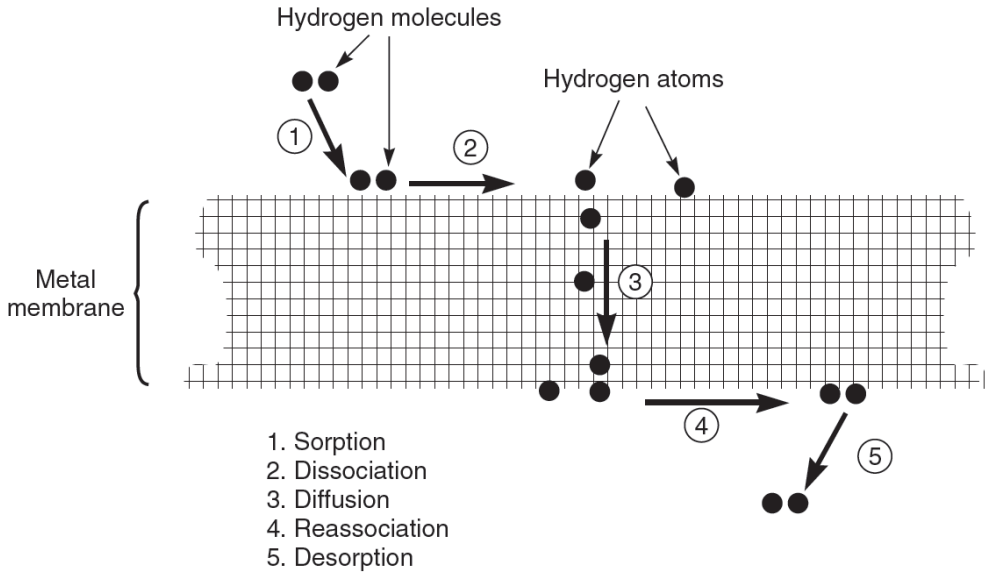

Figure 5: Mechanism of hydrogen permeation through metal membranes.

Despite palladium's excellent characteristics, its use is limited by certain disadvantages. The pure metal is prone to embrittle at temperatures below 300 °C and pressures below 2 bar [57], it can also be poisoned by Sulphur, and finally the high cost of commercial palladium foils. Therefore, to promote a long useful life of the membrane, pure palladium is alloyed with other metals, such as aluminum, copper, and silver, just to name a few, allowing the limits of pure palladium to be overcome.

Carbon membranes also belong to the inorganic category but work differently. There are several mechanisms for transporting gas through a carbon membrane. The most common is called molecular sieving and is depicted in Figure 6 [58]. In the carbon matrix, there are microscopic-scale constrictions that only allow species with the smallest molecule to pass through, trapping larger molecules. Transport through this type of membrane is complex and includes both diffusion in the gas phase and diffusion of adsorbed species on the surface of the pores.

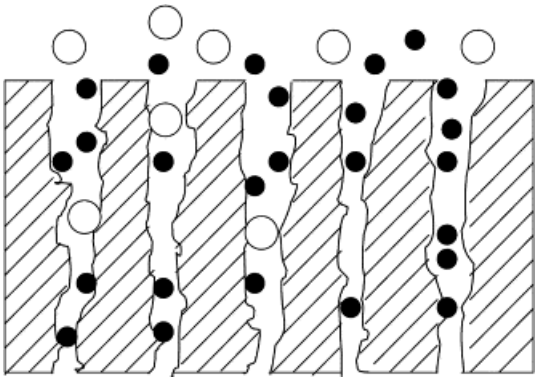

Figure 6: Typical molecular sieving transport mechanism.

Regardless of the transport mechanism, a membrane is a physical barrier that allows the selective transport of mass species. The result of the intervention of a membrane is a flow called retentate that is depleted of some initial component, and another flow called permeate that is the concentrated component (hydrogen in this context). The ability to effectively separate a mixture of gases is expressed through two important parameters, permeability and selectivity. Permeability P is a molar or volumetric flux per unit area of the membrane, normalized for pressure driving force, and membrane thickness. Selectivity $\alpha_{A/B}$ is a relative parameter, assessing the membrane's ability to separate species A from species B. The permeability of a pure gas is expressed as:

$$P = Q \cdot s = \frac{N \cdot s}{A \cdot \Delta p}$$

Eq. 5

where A is the membrane area, Δp is the driving force for separation, the partial pressure difference across the membrane, s is the thickness, N is the normalised flux. The term $N/A{\cdot}\Delta p$ is also called permeance and is often measured in terms of gas permeation units (gpu), where 1 gpu is defined as $1{\cdot}10^{-6}$ $cm^3(STP)/cm^2{\cdot}s{\cdot}cmHg$, STP being standard temperature and pressure.
Pure gas selectivity or ideal selectivity is a measure of the effective ability to separate a single gas A from another gas B and is defined as the ratio of the permeabilities of the two gases:

$$\alpha_{A/B} = \frac{P_A}{P_B}$$

Eq. 6

The expression of the permeability (Eq. 5) allows some important considerations: generally, if the permeability is high, less membrane area will be required, positively impacting the investment costs of the membrane system. Furthermore, the higher the selectivity, the lower the partial pressure difference between the feed and permeate side must be, with the same separation efficiency of the process and thus reducing the operating costs of the system, in particular reducing any energy consumption to maintain the driving force Δp.

2.3 Metal hydride

The generic reversible reaction of transforming a metal, or a metal alloy, into a metal hydride is reported in equation 7:

$$M + \frac{x}{2} H_2 \leftrightarrow MH_x \pm \Delta H$$

$Eq.7$

where M and H represent the metal and hydrogen atoms respectively, x is the non-stoichiometric coefficient and ΔH is the enthalpy of reaction.

Reaction kinetics is a critical aspect to consider in solid-state purification/storage technology because although the hydrogen accumulation or desorption reaction is favored in specific temperature and pressure conditions it does not necessarily occur with adequate rate, and suitable for practical applications. To go into the details of the hydrogenation and dehydrogenation processes the sequence includes the following steps provided by Martin et al. [59]:

1) physisorption of hydrogen molecules on the metal surface;
2) dissociation of hydrogen molecules;
3) penetration of hydrogen atoms from the surface into the bulk of the metal;
4) diffusion of hydrogen atoms through the hydride layer, involving interstitial and/or vacancy mechanism;
5) finally hydride formation at metal hydride interface by nucleation and growth.

The absorption process is exothermic when hydrogen is absorbed and endothermic when hydrogen is desorbed from the alloy. The thermodynamic aspects of metal hydride formation are described using Pressure-Composition-Temperature curves (PCT), an example is shown in Figure 7 from [60].

As the hydrogen amount and pressure increase, the metal hydride phase begins to be thermodynamically favored, referred to as the β phase in Figure 7, nucleating and growing within the metal phase. The number of hydrogen atoms in the crystal relative to the metal atoms varies from the type of hydride, and expresses the storage capacity by weight, most often expressed as a percentage.

The upper curve represents the equilibrium pressure measured when hydrogen is added to a metal alloy; the lower curve shows the equilibrium pressure when hydrogen is removed from the system. The different behavior is an hysteresis and represents a loss in the efficiency of the hydride due to irreversible degradations of materials during hydrogenation/dehydrogenation processes. At low hydrogen-to-metal ratios the hydrogen dissolves with heat release (exothermic reaction in the metal). This solid solution is what is referred to as the α-phase in Figure 7. Taking into account a single PCT curve, the plateau present at a certain pressure in the intermediate zone between the two phases occurs at a pressure called equilibrium pressure p_{eq}.

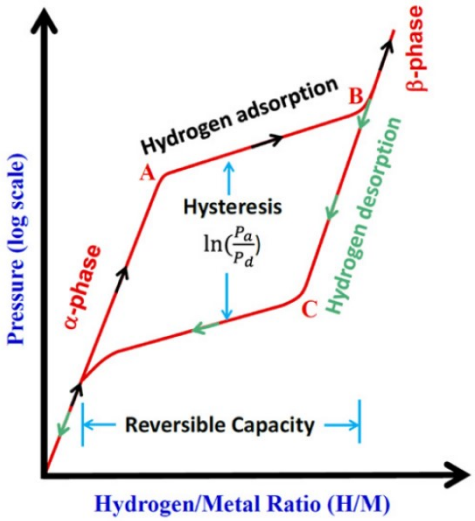

Figure 7: The typical PCT curves for the hydrogenation and dehydrogenation of a metal hydride under a fixed temperature T.

Above the p_{eq} the metallic material and hydrogen gas tend to form the hydride phase. Conversely, when the operating pressure is lower than the equilibrium pressure, the hydride tends to return to the metallic phase, releasing hydrogen. From Figure 8 [61], it can be seen that higher operating temperatures correspond to higher equilibrium pressures.

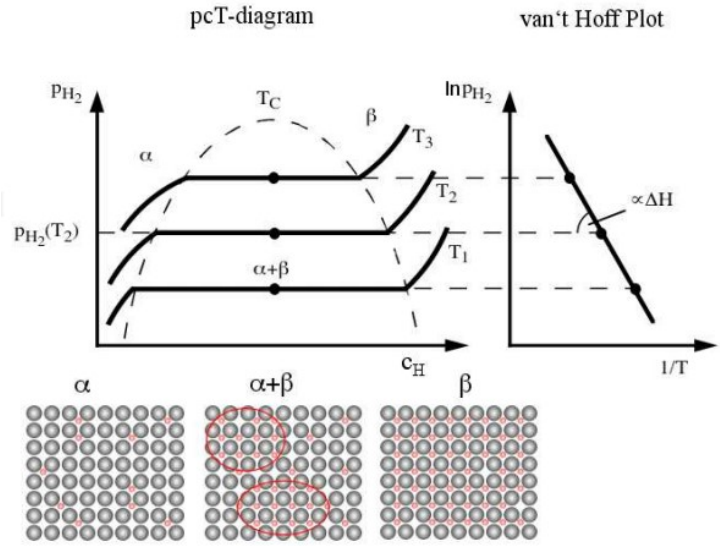

Figure 8: Schematic PCT-diagram and van't Hoff plot. The α-phase is the solid solution phase, the β-phase the hydride phase. Within the (α-β) two phase region both the metal-hydrogen solution and the hydride phase coexist.

The evolution of the equilibrium pressure as a function of temperature is described by the Van't Hoff equation:

$$\ln P = \frac{\Delta H}{RT} - \frac{\Delta S}{T}$$

Eq. 8

where P is the equilibrium pressure, T is the temperature, R is the universal gas constant, ΔH the enthalpy variation and ΔS the entropy variation of the hydrogenation and dehydrogenation reactions, respectively.

Pure materials most often have non-optimal characteristics, in fact compounds are often used to improve their characteristics. The basic idea is to alloy two metals in an $A_xB_yH_z$-type alloy in which: element A has the strongest hydrogen bond and element B the weakest. The alloy between the two will obtain intermediate characteristics between the two components. There is a wide variety of possible compounds, but the most used ones can be reduced to three main categories: AB, AB_2 and AB_5. The most widely used alloy for category AB is the Iron-Titanium (FeTi) alloy. The most representative alloy in category AB_5 is $LaNi_5$. The use of metal hydrides of the AB_5 type can be a solution for the purification of hydrogen destined for fuel cells. The success depends mainly on the fact that they have temperatures and pressures very close to normal conditions (temperature 0-100 °C and pressure 1-10 bar) thus reducing the heat exchange requirements of the system.

A hydride metal-based purification system has several similarities with the classic PSA process, but with the substantial difference that it selectively adsorbs/traps hydrogen itself instead of contaminants. The sequencing of the process in a metal hydride system is slightly different, as the product is obtained from the desorption step and not the adsorption step as in the PSA process. Typical steps in a metal hydride purification process are:

1) Absorption: The mixture is fed to the metal hydride reactor and the hydrogen is selectively absorbed from the bed with the formation of the metal hydride, the heat of the reaction is removed by a cooling heat transfer medium. The hydrogen absorption reaction is considered complete if the hydrogen that has passed through the rector begins to escape together with the other gaseous components.

2) Depressurization: the bed is preparing to regenerate the absorption capacity, allowing a second tank that has finalized the regeneration to be partially pressurized.

3) Desorption: is the crucial phase in obtaining purified hydrogen, where the hydrogen outlet pressure is controlled by heating through the heat transfer fluid.

4) Pressurization: to restart the cycle, the tank must return to the initial pressure conditions, and it does so using the discharge phase of a twin tank.

The operation of several beds in alternating phases allows the process to be considered continuous at the battery limits, and can be evaluated with the same parameters introduced with the PSA.

Table 9 summarizes technical parameters of the hydrogen separation technologies under considerations.

Table 9: Hydrogen Separation Technology Summary.

Technology	Capacity (Scale)	Typical feed H2 content	Typical feed pressure [bar]	Typical feed temp. [°C]	Hydrogen product pressure	Residue gas pressure	Hydrogen recovery [mol%]	Hydrogen purity [mol%]
PSA	Large	>50%	10-150	Ambient	High (feed pressure)	Low (atm)	80-90%	>99.7%
Palladium membrane	Small	>98%	<20	300-450	Low	High (feed pressure)	95-99%	99.995%
Carbon membrane	Small	5-25	<50	50-100	Low	High (feed pressure)	>70%	>99.7%
Metal hydride	Medium	10-50	10-100	20-150	Low	High (feed pressure)	75-90%	99.999%

Chapter 3

3 Models and methodology

The following chapter explains how the models for the selected purification technologies are constructed. These models enable the design of the components necessary for the purification process, which will then determine the costs that will be incurred. Since purification processes are inherently complex, in this analysis, a simplified approach is taken by initially assuming the performance of the processes, which is expressed through KPIs (Key Performance Parameter). These KPIs are not the output results, but rather assumed values based on the state-of-the-art technologies.

3.1 PSA design

The PSA process designed for this study is based on one of the first patented and commercialized configurations, namely the 4-bed system developed by Batta [62]. The adsorption vessel can be sized as a cylindrical pressure vessel using the pressure vessel design method given by Seider et al. [63], that contains the adsorbent volume. These vessels are cylindrical with an internal diameter D_T and a length H_{TL}, often referred to as the tangent-to-tangent length. Two elliptical heads are usually welded to the ends of the cylindrical body. The fixed bed may consist of single or multiple adsorbent layers, depending on the impurity present in the feed mixture.

The main model assumptions of the process are:

- Ideal gas mixtures.
- Isothermal conditions.
- Neglecting the thermodynamic and kinetic aspects that contribute to the formation of concentration profiles.
- The exothermic nature of the adsorption process is not taken into account.
- Pressure drops across the bed due to gas flow are neglected.
- The adsorbent is not irreversibly poisoned by any component of the gas phase.

The partial pressures of each component in the PSA feed mixture are determined using the equation:

$$p_i = x_i P_T \qquad Eq.9$$

where P_T is the total pressure of the feed stream [bar], and x_i is the molar fraction of the i-th component in the feed stream.

When sizing a PSA process, one of the first steps is to choose the appropriate adsorbent based on various considerations, such as the nature of the stream to be treated, the characteristics of the adsorbates to be removed, required throughput, and process objectives [51]. Although proprietary adsorbents are used in industrial

applications without any available data, isotherm data for commonly used adsorbents such as activated carbon, alumina, silica gel, and zeolites can be found in the literature. The required amount of adsorbent can be estimated by considering the flow rate of the adsorbed species and the change in bed loading during the adsorption cycle. The mass of adsorbent per bed, M_a, is determined from the mass balance equation provided by Towler and Sinnot [64]:

$$(F_1 x_1 - F_2 x_2) t_a = (m_{max} - m_{min}) M_a f_L$$

$Eq.10$

where F_1 is the feed molar flow rate [mol/h], F_2 the product molar flow rate, x_1 the feed molar fraction of adsorbed component, x_2 the product mole fraction of adsorbed component, t_a is the time when the bed is in the adsorption stage of the cycle [s], m_{max} is the maximum adsorbent loading [mol/kg], m_{min} is the minimum adsorbent loading, M_a the mass of adsorbent per bed [kg], and f_L is the fraction of the bed that is fully loaded at end of the adsorption phase of the cycle. Towler [64] suggests that a loading fraction f_L close to 1 can be achieved by using four or more beds, indicating a high degree of adsorbent saturation.

The difference between the maximum and minimum loading is the column capacity and represents the amount of adsorbed gas between the pressure conditions corresponding to the high-pressure adsorption phase and the pressure conditions in the regeneration phase. These parameters are related to the isotherm data of the pure gases adsorbed in their respective adsorbents. It is therefore important to know the partial pressure and temperature of the i-th component during the feed and discharge phases.

Given that the influence of adsorption rate, mass transfer, and heat exchange on the process has been neglected, in this preliminary analysis it is assumed a value for the adsorption step time. This phase is shorter than the overall cycle duration, which can be determined as the product of the adsorption time and the number of beds used in sequence.

The volume V [m^3] of each adsorbent bed can be estimated from the calculated mass of the adsorbent and the bulk density of the adsorbent ρ_b [kg/m^3]:

$$V = \frac{M_a}{\rho_b}$$

$Eq.11$

According to Yussof [65] up to 20% of the volume between the tangent lines of the vessel is packed with inert material, like a ceramic ball, to ensure a uniform flow profile and a better flow distribution (figure 9). The head space is left empty and the ratio between the length and the diameter of the bed is 3:1 to guarantee an efficiently used of the bed.

Based on the previous considerations the volume of the cylindrical vessel is:

$$V = \frac{\pi D_T^2 H_{TL}}{4} = \frac{3\pi D_T^3}{4}$$

Eq. 12

where D_T is the diameter of the vessel [m], H_{TL} is the total height of the bed [m].

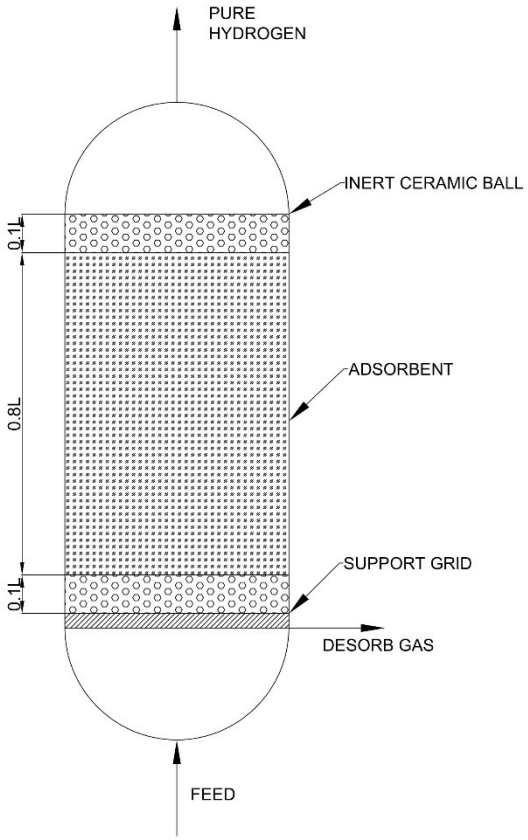

Figure 9: Adsorption vessel internals.

The approximate weight W of a pressure vessel with 2:1 elliptical heads can be calculated as follows:

$$W = \pi(D_T + t_s)(H_{TL} + 0.8 \cdot D_T)t_s \cdot \rho$$

Eq. 13

where ρ is the density of the carbon steel, which can be taken as 0.284 lb/in^3 and t_s is the reactor thickness. D_T, H_{TL}, and t_s are in inches.

The cylindrical shell wall thickness is computed from the ASME pressure-vessel code formula:

$$t_s = \left(\frac{P_d \cdot D_T}{2 \cdot S \cdot E - 1.2 \cdot P_d}\right)$$

Eq. 14

where P_d is the internal design gauge pressure in psig, D_T is the inside shell diameter in inches, S = 13750 is the maximum allowable stress of the shell material at the design temperature in pounds per square inch, and E = 0,85 is the fractional weld efficiency. For operating pressures greater than 1000 psig, Seider et al. [63] recommends a design pressure equal to 1.1 times the operating pressure.

The calculation of these parameters is sufficient to carry out an economic evaluation of the PSA system, presented in chapter 4. The process is assumed to operate by alternating between the adsorption and regeneration phases. The use of multiple columns allows for a continuous process and ensures a constant purification of hydrogen.

3.2 Membrane design

The membrane separation design aims to calculate the area necessary to purify the feed stream. Simple equations can be used for this type of problem, but it is first necessary to establish the flow pattern within the membrane as the calculations depend on it [66].

Complete mixing condition [67] is defined when the gas concentration inside the membrane is uniform at every point within the membrane module, both on the high-pressure side (feed side) and on the low-pressure side (permeate side). On the feed side, the gas concentration is constant at every point within the membrane module and equal to the concentration of the gas on the retentate side. Similarly, on the permeate side, the gas concentration is uniform at every point within the membrane module.
Cross-flow condition [67] is defined if it is considered that the gas concentration on the feed side varies gradually along the flow direction, from an inlet concentration to the retentate concentration, so it depends on the location within the membrane being considered. On the other hand, on the permeate side, the gas concentration is very similar to the average gas concentration on the membrane surface. This means that, although the mixing condition on the permeate side is not perfect, the gas concentration is still uniform over the entire membrane surface.

Any model, regardless of the flow configuration, must include mass balance relationships. Let q_f be the volumetric feed flow in [m^3(stp)/h], the overall mass balance is expressed as the sum of the permeate flow q_p and the retentate flow q_r:

$$q_f = q_p + q_r$$

Eq. 15

The mass balance can also be expressed for each i-th component of the gas mixture:

$$q_{f,i} = q_{p,i} + q_{r,i}$$

Eq. 16

Or in other words, denoting x as the molar fraction of the i-th component:

$$q_f \cdot x_{f,i} = q_p \cdot x_{p,i} + q_r \cdot x_{r,i}$$

Eq. 17

Assuming perfect mixing conditions, the permeate flow of the i-th component is given by:

$$q_{p,i} = q_p \cdot x_{p,i} = J_i \cdot A = A \cdot P_i\left(x_{r,i} \cdot p_f - x_{p,i} \cdot p_p\right)$$

Eq. 18

where J_i is the flux of the i-th component obtained from Fick's law, A [m^2] is the membrane area, P_i [GPU] (1GPU = $2.76 \cdot 10^{-3}$ m^3(STP)/(m^2·h·bar)) is the permeance of the i-th component, p_f [bar] is the pressure in the feed side and p_p is the pressure on the permeate side. A similar expression is valid for the j-th component.

In addition to mass balances, partial pressure relationships are used to evaluate the molar fractions of the components:

$$x_{f,i} = \frac{p_{f,i}}{p_f}$$

Eq. 19

$$x_{p,i} = \frac{p_{p,i}}{p_p}$$

Eq. 20

In cross-flow models, the feed gas is introduced on one side of the membrane and flows parallel to it. The gas becomes depleted of hydrogen, and the permeate passes through the membrane perpendicular to it. Models that describe gas permeation through a membrane can be distinguished as analytical or numerical models. For the case of cross-flow, Thundyl and Koros [68] have proposed a numerical approach based on the finite difference method, also called the succession of states, where the membrane is reduced to a succession of small elements with equal constant properties.

This thesis uses a numerical approach based on the cross-flow model, where the membrane is discretized into small parts, assuming the presence of complete mixing conditions in each discretization. The mass balance is calculated for each of them, and it is assumed that the permeances remain constant and that the separation occurs under isothermal conditions. Additionally, the regime is steady-state, and pressure losses are neglected.
The fundamental equation of the model is the one that relates the permeate flow and molar fraction $x_{p,i}$ in cross-flow regime with the feed molar fraction $x_{f,i}$, the pressure ratio $P_r = \frac{p_f}{p_p}$ and the selectivity α. The equation is given by Baker [56]:

$$x_{p,i} = \frac{1}{2} \cdot \frac{B - \sqrt{B^2 - \frac{4\alpha x_{f,i}}{(\alpha - 1) \cdot P_r}}}{\frac{1}{P_r}}$$

Eq. 21

where

$$B = x_{f,i} + \frac{1}{P_r} + \frac{1}{\alpha - 1}$$

Eq. 22

To allow the passage of the component i through the membrane, the partial pressure of i on the feed side of the membrane must be greater than that on the permeate side of the membrane, satisfying the following equation:

$$x_{f,i} \cdot p_f > x_{p,i} \cdot p_p$$

Eq. 23

Or rearranging:

$$\frac{x_{p,i}}{x_{f,i}} \leq P_r$$

Eq. 24

regardless of the selectivity of the membrane. In the absence of such conditions, there would be a reversal of flow due to the higher partial pressure of a specific component in the permeate relative to that in the feed flow.

The algorithm proceeds from the feed stream inlet and, thanks to equation 21, calculates the composition of the permeate. The volumetric flow rate of component i that crosses the membrane is then:

$$q_{p,i} = dA \cdot P\left(x_{f,i} p_f - x_{p,i} p_p\right)$$

Eq. 25

The method consists of repeating the composition and flow calculations through the membrane for each surface interval dA, updating the values of the volumetric flows and, therefore, the compositions on the feed side and permeate side until the desired recovery is obtained. Figure 10 gives schematic representation of the cross-flow case.

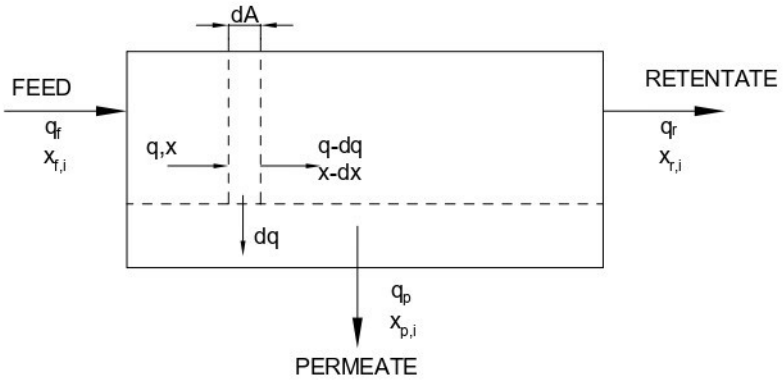

Figure 10: Flow diagram of a cross-flow design.

The membrane area can then be determined as $A = dA \cdot n$ where n is the number of iterations required to reach the target recovery. The purity of hydrogen can be evaluated as the ratio of the cumulative volumetric flow rate of hydrogen in the permeate of each discretization, divided by the cumulative volumetric flow rate of the permeate.

If the hydrogen purity at the end of the separation process is not higher than the requirements outlined in Chapter 1, the model will be applied again to size the next membrane. This way, the system design will be of the multistage type, where each stage represents a membrane. For simplicity, in the studied cases, a multistage configuration with a single pass is assumed, meaning that the feed solution passes through the single membrane only once. The permeate flow is sent for possible further purification, thus generating a series of membranes configuration, or compressed to the specific conditions of the use case. The retentate, instead, is not recirculated, resulting in a loss of hydrogen.

In a multistage configuration, the overall recovery is calculated as the product of the recovery of every single stage [69], that is:

$$R = \prod R_k \qquad \textit{Eq. 26}$$

where R_k is the recovery of the k-stage.

Therefore, the model requires the overall recovery as input and calculates the hydrogen purity in the permeate as output.

3.3 Metal hydride design

The design of a metal hydride system for hydrogen purification is based on the use of metal hydrides packed in absorption beds. When the gas mixture to be purified passes through the absorbent bed, hydrogen is absorbed while impurities flow toward the outlet. Although the absorption process is chemical in nature, the cycle principle is the same as that of PSA and TSA systems [70].

The metal hydride absorbs and releases hydrogen according to the working temperature and pressure [71]. Conceptually, the system is very similar to the one proposed by Taniguchi and Ishida [72] and called Metal Hydride Intermediate Buffer (MIB) for the purification of hydrogen from reformed gas.

The idea is to estimate the amount of metal alloy needed, with the equation 10, to absorb the hydrogen feed flowrate to obtain the required volume of the absorbent bed and allow for an economic evaluation of the system. The entire system is composed of 4 absorbent beds, as in the PSA system, to allow the process to operate continuously, to always have a flow of highly pure hydrogen.

The choice of hydrogen absorbent is guided by the following properties [73]:

- Absorption capacity and selectivity.
- The isothermal curve for the working temperature.
- Resistance to poisoning.
- Industrial technological maturity.

The absorption capacity of metal or metal alloys can be identified by consulting reviews or reports in which the maximum weight percentage of hydrogen, expressed in %wt, is provided under certain temperature and pressure conditions, as in reference [74]. The absorbent must be selective for the absorption of hydrogen compared to other gases present in the feed stream.

The saturation of the metal hydride can be visually observed in the isotherm curve of the metal alloy. The absorption capacity is plotted as a function of the partial pressure of hydrogen on a semi-logarithmic axis (figures 7 and 8). As the absorption capacity increases, the partial pressure does not increase significantly, resulting in a plateau of the curve [75], which depends on the working temperature.

As in the simplified PSA model, the absorption kinetics is neglected, and the enthalpy of absorption is considered only for the calculation of the thermal power required to facilitate the desorption of hydrogen. Similar to the model for physical adsorption, a time for chemisorption is assumed.

To use metal hydride as an absorbent, it must be stable enough to resist the impurities in the gas mixture, as some metals easily bond with chemically aggressive species such as O_2, H_2O, CO, etc. [76]. Therefore, the choice of material to use is also directed by the need to avoid seriously penalizing the absorption capacity of hydrogen. For example,

alloys of the AB_5 type based on $LaNi_5$ have a high tolerance to poisoning by CO_2 when CO_2 is present in the gas mixture with a percentage of 20-25% [77]. In this regard, the adoption of surface fluoridation is assumed to increase the resistance and the possibility of regeneration of the material in addition to the pre-filters present for all the technologies analyzed for the desulphurization and dehumidification of the incoming flow.

The feasibility of industrial production of the material must also be considered. In fact, among the materials that have attracted more attention due to their superior thermodynamic properties and reasonable reaction pressures, few exceed 2-3% in gravimetric percentage. This indicates that the amount of metal or metal alloy to be produced is significantly relevant for every kg of absorbed hydrogen and can easily reach values that are incompatible with laboratory processes and therefore may require industrial systems.

3.4 Utilities

One or more compression systems are necessary for the considered purification systems. For gas compression, only reciprocating displacement compressors have been chosen, particularly the oil-free variety which is commonly used for hydrogen applications when the desired pressure level exceeds 3 MPa [78]. For addressing compression costs for each of the considered purification options, it is necessary to calculate the compression power P [kW] using the following formula [79]:

$$P = Q \cdot \frac{Z \cdot T \cdot R}{MW_{H_2} \cdot \eta_{comp}} \frac{N \cdot \gamma}{\gamma - 1} \left[\left(\frac{P_{out}}{P_{in}} \right)^{\frac{\gamma - 1}{N \cdot \gamma}} - 1 \right]$$

Eq. 27

where Q is the flow rate [kg s^{-1}], Z the gas compressibility factor set as a mean value between inlet and outlet conditions, T the temperature at the inlet of the compressor in Kelvin, R the ideal gas constant equal to 8.314 J K^{-1} mol^{-1}, MW_{H_2} the molecular mass of the gas [g mol^{-1}], η_{comp} the compressor efficiency chosen as the product of isentropic, mechanical, and electrical efficiencies of the compressor, N the number of compressor stages, γ the diatomic constant factor defined as the ratio c_p/c_V where c_p is mass specific constant volume specific heat and c_v mass specific constant pressure specific heat. P_{in} is the inlet pressure of the compressor [bar], P_{out} is the outlet pressure of the compressor. This formula enables the calculation of the necessary compressor power based on the flow rate and the required pressure difference to be overcome.

An iterative methodology is followed to determine the number of stages where the maximum discharge temperature is set. The discharge temperature T_{out} [K] and the temperature at each stage is calculated using the following formula assuming an isentropic behavior:

$$T_{out} = T_{int}\left(\frac{P_{out}}{P_{in}}\right)^{\frac{\gamma-1}{N\cdot\gamma}}$$

Eq. 28

where T_{int} is the inter-cooling temperature, constant for each stage following the procedure of the system designed in [80].

The ratio of the discharge pressure to the inlet pressure is called pressure ratio r. The total power requirement is a minimum when the pressure ratio in each stage is the same [81]. This may be expressed in equation form as:

$$r = \left(\frac{P_{out}}{P_{in}}\right)^{\frac{1}{N}}$$

Eq. 29

If a unitary flow rate Q is set, the compressor's energy consumption in kWh/kg is obtained, which will be required in the economic analysis to determine the annual cost related to the energy consumption of the compressors by multiplying the cost of electricity.

It is assumed that the water needed to cool the exhaust gas is produced through a chiller with fixed EER. The electrical power required to produce the cooling water, for multi-stage cooling, can be estimated from the equation:

$$P_{el} = \frac{\dot{m}_2}{EER}\sum_{j=1}^{n}\left(h_{j,H_2}^{in} - h_{j,H_2}^{out}\right)$$

Eq. 30

where h_{j,H_2}^{in} and h_{j,H_2}^{out} are the specific enthalpy of hydrogen or methane entering and leaving the j-th stage, $\dot{m}_2$ the mass flow of hydrogen or methane and n the total number of stages. The enthalpy is evaluated in kJ/kg.

For the metal hydride purification system, it is necessary to evaluate the power of the thermal machines for heating or cooling to desorb or absorb the hydrogen. The power in kW of the heat pump and chiller can be evaluated using the following equations:

$$P_{\substack{heat\\pump}} = \frac{\dot{m}_{H_2}\cdot\Delta H}{COP}$$

Eq. 31

$$P_{chiller} = \frac{\dot{m}_{H_2}\cdot\Delta H}{EER}$$

Eq. 32

where $\dot{m}_{H_2}$ [kg/s] is the flow rate of hydrogen to be absorbed/desorbed (ideally the same), ΔH is the enthalpy of absorption and desorption in kJ/kg$_{H2}$, COP is the

coefficient of performance of the heat pump, and EER is the energy efficiency ratio of the chiller.

In the membrane purification system, the entire stream must be heated to temperatures above 400 °C if palladium-based metal membranes are used to function effectively, or up to 50 °C for carbon membranes[6]. Research to date indicates that elevated temperatures are required for palladium membranes to avoid issues related to a phase transition of the palladium.

Heat duty is provided by a gas burner heater placed just before the membrane burning a stream of natural gas from retentate side. To estimate the energy consumption of the electric heater, the power to be installed in [kW] is:

$$P_{\substack{heat \\ duty}} = \frac{q \cdot \Delta h}{LHV_{CH4}}$$

Eq. 33

where q [kg/s] is the mass flow rate of hydrogen to be heated, Δh the enthalpy difference [kJ/kg], and LHV_{CH4} is the lower heating value of methane in [kJ/kg]. Heating of gas would be required prior to treatment which would add to capital and operational costs.

The overall energy consumption [kWh/y] by the utilities when compared with the total amount of purified hydrogen makes it possible to evaluate the consumption to be incurred for each kg of purified hydrogen. The electrical equivalent of the thermal consumption is obtained considering a transformation with a conventional efficiency of 33%.

[6] Membranes become hydrogen selective at elevated temperatures as a result of increase in diffusivity.

Chapter 4

4 Economic analysis

This chapter provides an economic analysis of hydrogen purification technologies. It describes the basic economic assumptions and presents capital costs as well as operational, maintenance, and replacement costs. Additionally, the construction of specific cost of hydrogen purification is shown. These economic analyses are crucial for evaluating different hydrogen purification technologies in various scenarios and making informed decisions on the choice of the most suitable technology based on specific application requirements.

In economic analysis, all monetary values are expressed in euros and the cost of electricity is used to evaluate the energy consumption costs of utilities in the system. The table 10 provides values for the conversion of monetary quantities from dollars to euros and the cost of electricity.

Table 10: Economic assumption.

		Unit	Ref.
Conversion $ to €	1		[82]
Electricity cost	100	€/MWh	Assumption

To estimate equipment costs, various studies, and cost data are taken into consideration. Therefore, each cost will be related to its reference year, in which it was evaluated. For this reason, it is necessary to discount all costs to a reference year, which for this study is 2023. This is done using the Chemical Engineering Plant Cost Index (CEPCI).

$$Cost_{2023} = Cost_{ref} \cdot \frac{CEPCI_{2023}}{CEPCI_{ref}}$$

Eq. 34

where $Cost_{ref}$ and $CEPCI_{ref}$ are the cost and CEPCI index relative to the reference year. The following table shows values for the last 20 years.

Table 11: Annual plant cost indexes [83].

Year	CEPCI	Year	CEPCI	Year	CEPCI
2023 march	799.5	2015	556.8	2007	525.4
2022	816.3	2014	576.1	2006	499.6
2021	708.8	2013	567.3	2005	468.2
2020	596.2	2012	584.6	2004	444.2
2019	607.5	2011	585.7	2003	401.7
2018	603.1	2010	550.8	2002	395.6
2017	567.5	2009	521.9	2001	394.3
2016	541.7	2008	575.4	2000	394.1

Hydrogen and natural gas, as well as other gas mixtures, are considered within the battery limits and are assigned a zero-cost flow.

4.1 Capital cost

Capital costs are the initial investment costs. They consist of direct costs for equipment purchase and indirect costs, such as those necessary for design, construction, and others. Costs are therefore expressed at two different levels:

- Equipment/uninstalled costs.
- Total installed costs.

Total installed costs refer to equipment costs plus indirect capital costs. Indirect capital costs include site preparation, engineering and design, project contingencies, and others. Each of these items is included in an installation factor IF.

The compression system is evaluated using a cost function provided by the H2A model [80] that expresses the uninstalled capital costs for reciprocating compressors:

$$Cost = 19207 \cdot (Motor\ rating, kWe)^{0.6089}$$

Eq. 35

An installation factor of 2 is adopted.

The investment cost associated with the inter-cooler is calculated using a specific investment cost of 650 €/kW [84]. An installation factor of 1.3 is adopted. The investment cost associated with the heat pump is calculated using a specific investment cost of 700 €/kW [84]. An installation factor of 1.3 is adopted.

For the estimation of PSA capital costs, it was decided to follow the method proposed by Seider et al. [63] for the evaluation of pressure vessels cost, and then add the adsorbents costs:

$$C_P = [F_M \cdot (C_V + C_{ads}) + C_{PL}] \cdot N$$

Eq. 36

This formula is adjusted using the CEPCI index value of 500 as the base index for cost estimation. C_V is the empty vessel cost, C_{ads} the adsorbents costs (for one vessel), F_M is the material factor (= 1 for Carbon Steel), C_{PL} is added costs (for one vessel), N is the number of vessels used equally to the adsorbent beds. The cost of valves and connections is neglected.

C_V for a vertical vessel is estimated from the following equation:

$$C_V = e^{\{7.0132 + 0.18255 \cdot \ln W + 0.02297 \cdot \ln W^2\}}$$

Eq. 37

where W is the weight of the empty vessel in lbm.

The cost of the adsorbent is calculated from the following formula:

$$C_{ads} = \text{volume of adsorbent per column} \cdot \text{adsorbent cost}$$

Eq. 38

Table 12 shows the prices of commercially available adsorbents.

Table 12: Adsorbent cost for the pressure swing adsorption process [85].

Adsorbent	Cost [$/m^3]
Silica gel	3000
Activated carbon	700
Zeolite	26000

C_{PL} for a vertical vessel is estimated from the following formula:

$$C_{PL} = 361.8 \cdot D_T^{0.7396} \cdot H_{TL}^{0.70684}$$

Eq. 39

Where D_T is the diameter of the vessel in feet (ft), H_{TL} is the length of the vessel in feet (ft).
It is worth mentioning that the material of construction of the vessels is chosen to be Carbon Steel at 6.0 mm corrosion allowance since the temperature is not above 200°C. An installation factor of 1.17 is adopted [86].

For the membrane purification plant, a specific cost including the installation factor is used. The relative costs (indicative) of palladium membranes per unit of surface area is about 60 times the cost of carbon membranes (table 13).

Table 13: membrane unit cost.

Membrane	Abbreviation	Specific Cost	Ref.
Carbon molecular sieve	CMS	100 $/m^2	[87]
Palladium-silver	Pd-Ag	6000 €/m^2	[88]

For the metal hydride separation system, cost estimation is made by considering a single storage tank, including metal hydride pellets, a heat exchange section, and the tank itself. Regarding the tank, both cost functions considered show a similar trend for medium sizes of absorbed hydrogen, although Ganda and Maronati [89] have proposed a scaling exponent of 0.7509 while Amos [90] has proposed a constant specific CAPEX (scaling exponent equal to 1), figure 11. For large sizes, only one cost data has been found, which is quite in line with Ganda's scaling law. The latter shows good consistency with literature data even for small and medium sizes. Considering all these aspects, the cost function proposed by Ganda is used for the cost assessment of metal hydride hydrogen separation systems:

$$MH\_cost = 13744 \cdot (Hydrogen\ Capacity\ [kg]\ )^{0.7509}$$

Eq. 40

The overall concept of the metal hydride storage system requires further consideration due to the different expected lifetimes of the storage container and the metal hydride pellets. Therefore, to estimate equipment replacement costs, the total cost of the system must be divided between the metal hydride pellets and the storage container. For simplicity, the cost of the storage container (including the heat exchange portion) has been assumed to be 40% of the total plant cost, regardless of size. The chosen installation factor for the storage tank is 1.3 [80].

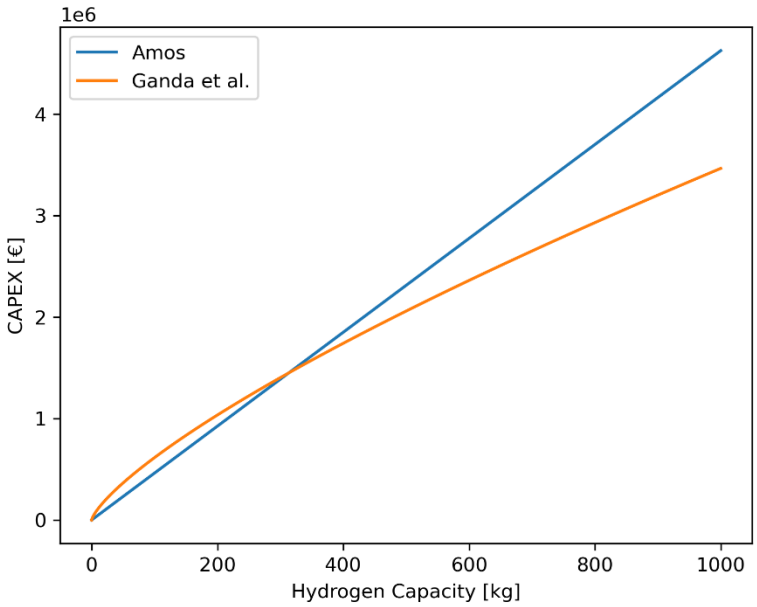

Figure 11: Capital cost function overall metal hydride storage system from literature data.

4.2 Operational cost

Operating and maintenance (OPEX) costs are the ongoing expenses associated with the operation and upkeep of a facility or equipment. These costs can include expenses for labor, materials, utilities, and other services required to keep the facility or equipment in working order. Fixed O&M costs are those costs that remain relatively constant regardless of the level of production or operation, while variable O&M costs are those costs that change with the level of production or operation.

Fixed operating and maintenance costs are often expressed as a percentage of uninstalled capital costs. For example, it is assumed that the maintenance cost of the hydrogen PSA purification system is 2% of the CAPEX on an annual basis. Table 14 shows the summary of annualized maintenance costs used in this study.

Table 14: Summary of fixed maintenance costs on an annual basis adopted.

Component	Fixed O&M	Ref.
PSA	2%	[85]
Membrane	2%	[69]
Metal hydride alloy	1.5%	Assumption
Metal hydride vessel	1.5%	Assumption
Compressor	4%	[91]
Inter-cooler	1%	[84]
Heat-pump	1%	[84]

The comparison of all purification options is based on a project duration of 30 years. Different components have different lifetimes and, therefore, different numbers of replacements during the considered plant lifetime. Once a macro-component reaches the end of its useful life, it must be replaced, resulting in a new capital cost expenditure. Table 15 shows the assumed lifetimes for the various macro-components considered in this study.

Table 15: Assumptions on the useful life of components.

Component	Lifetime	Ref.
PSA adsorbents	30	[49]
PSA vessel	20	[92]
Pd-Ag Membrane	3	[88]
CMS Membrane	5	[69]
Metal hydride alloy	30	Internal information
Metal hydride vessel	20	Internal information
Compressor	15	[91]
Inter-cooler	20	[84]
Heat-pump	20	[84]

The metal hydride performance in terms of hydrogen absorption might be significantly restored with the application of a regeneration approach. Consequently, the bed can be regenerated through powder recycling, lowering the investment cost, and it is assumed that the regeneration cost is incurred every 5 years and equal to 10% of the investment cost of the metal alloy.

It is possible that, in the 30th year of operation, some components still have a high residual useful life and, therefore, a high residual value. Once the residual useful life of the component has been calculated, the amortized residual value can be determined by using a fixed depreciation rate (eq. 41). 5% fixed depreciation rate in this study. For all components with a remaining useful life, it is assumed that the recovery value is 10% of the initial installed equipment cost.

$$residual\ [€] = salvage + depreciation \cdot (CAPEX - salvage)$$

Eq. 41

To calculate the variable operating costs, which are mainly comprised of the electricity costs required for the purification system utilities, the following values must be used: operating hours per year, the power in kW of the component to estimate the annual

energy consumption in kWh, and the cost of electricity to obtain the annual energy consumption cost.

4.3 Specific cost of purification

The total cost of ownership (TCO) represents the sum of CAPEX and OPEX over the chosen analysis period. The TCO can be calculated using the following equation:

$$TCO = CAPEX + lifetime_{proj.} \cdot OPEX$$

Eq. 42

The levelized cost of purification (LCOP) is defined as the ratio of the TCO and the amount of hydrogen separated/purified over the entire lifetime. In this study, two versions of this parameter are calculated: a non-discounted LCOP simply given by the equation 43, and a discounted LCOP over the system lifetime:

$$LCOP = \frac{TCO}{H_{2,tot}}$$

Eq. 43

$$LCOP_{act} = \frac{\sum_{i=0}^{i=lifetime_{proj.}} TCO_i \cdot (1+r)^{-i}}{\sum_{i=0}^{i=lifetime_{proj.}} H_{2,tot,i} \cdot (1+r)^{-i}}$$

Eq. 44

where r is the discount rate. The discount rate assumed for this project is 8%.

For all economic figures of interest, an estimated error range for the different technologies is given, depending mainly on the maturity of the purification technology and the degree of accuracy that can be achieved with respect to the final system and, thus, the associated costs; for PSA it is estimated at 10%, for metal hydrides and membranes at 20% and 5% respectively.

Chapter 5

5 Results

5.1 Case study 1 - Deblending hydrogen from the natural gas grid

For all different technologies, the system control volume must have the same input and output conditions, in order to ensure correct and consistent evaluation. For the hydrogen deblending case study in natural gas pipelines, a gas feed flow of 500 Sm^3/h [7] is being considered, which corresponds to the demand of a civilian user or an industrial hub that can in turn distribute hydrogen to appropriate customers. Two different cases are being studied based on the amount of H_2 blend present in the pipeline: 5%, which reflects the minimum acceptable hydrogen content in a preliminary phase, and 30% to simulate an extensive blending experiment as used in major projects regarding blended hydrogen transportation [93]. The feed flow is at ambient temperature and at the operating pressure of the transmission pipeline, 70 bar, as indicated in Figure 12. The purified hydrogen is then compressed to the typical high-pressure storage pressure of 350 bar. The residual natural gas is being reinjected into the distribution grid at 24 bar.

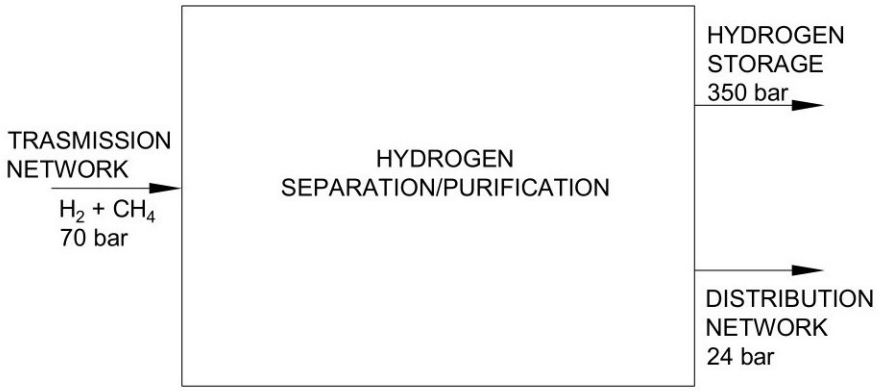

Figure 12: Battery limits for hydrogen deblending.

The compressors for natural gas and hydrogen are of the reciprocating multi-stage type with inter-cooling stages to maintain the discharge temperature below a chosen value. Table 16 summarizes the operating parameters of the compressors, which are common to all separation technologies. It is assumed that the cooling water is being produced through a refrigeration unit with an energy efficiency ratio of 2.5. The techno-economic analysis is designed for a lifetime of the entire project of 30 years, operating 8000 hours per year, with the compressors working at nominal capacity 90% of the time.

[7] Sm3 stands for standard condition, 0°C and 1 atm.

Table 16: Compressors parameters.

	Units	Natural gas [94]	Hydrogen [80]
Isentropic efficiency	%	90	90
Electrical efficiency	%	95	95
Mechanical efficiency	%	90	90
Maximum discharge temperature	°C	155	135
Temperature after inter-cooling	°C	50°C	37.8
EER inter-cooling		2.5	2.5

For the sake of simplicity, the process streams are approximated as a binary mixture of H_2 and CH_4. However, natural gas also contains other compounds that cannot be neglected, especially if the purified hydrogen is required to meet the purity requirements for fuel cells. Table 17 reports the average composition of natural gas from the northern European Passo Gries intake point, expressed as a molar fraction and the new composition of natural gas with 5% addition of hydrogen.

Table 17: Average natural gas composition in Passo Gries intake for the thermal year 2021–2022 [95].

CH_4	C_2H_6	C_3H_8	C_4H_{10}		C_5H_{12}		C_6H_{14}	CO_2	N_2	He	H_2
Methane	Ethane	Propane	I-butane	N-butane	I-pentane	Pentane	n-Hexane	Carbon dioxide	Nitrogen	Helium	Hydrogen
93.075	4.12	0.71	0.185	0.121	0.046	0.024	0.047	0.629	1.019	0.024	0.0
88.421	3.91	0.674	0.175	0.114	0.043	0.022	0.044	0.597	0.968	0.022	5

PSA: Assuming hydrogen purity (99.97%) and hydrogen recovery (80%), it is possible to calculate, through mass balances, a hydrogen separation of 43 kg/day. The chosen adsorbent for methane adsorption is activated carbon. The experimental data for the pure gas adsorption isotherms of CH_4 and CO_2 on activated carbon at 298 K are plotted in figure 13 (data from [96]).

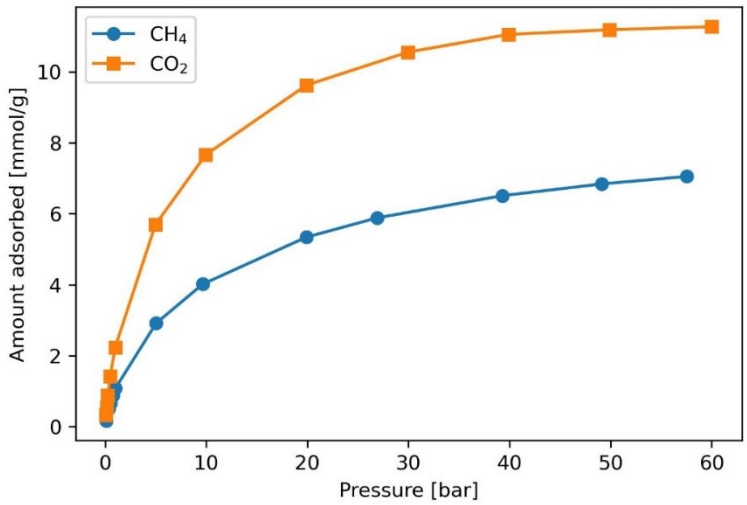

Figure 13: Measured amounts adsorbed of the pure gases CH_4 and CO_2 on AC Norit R1 at T = 298 K.

The processing conditions of the PSA are tabulated in Table 18. To the calculated volume of activated carbon are added a layer of zeolite for N_2 adsorption and a layer of silica gel for heavy hydrocarbon adsorption, each with a length of 0.1 m.

Table 18: Processing conditions for PSA in deblending with 5% hydrogen.

			Ref.
Feed pressure	70	bar	
Desorption pressure	1	bar	
Feed gas H_2 molar fraction	5	%	
Flow rate	500	Sm^3/h	
Operating temperature	298	K	
Column height	2.3	m	
Column inner diameter	0.7	m	
Number of beds	4		
Adsorption time	300	s	
Bulk-density activated carbon	450	kg/m^3	[97]
Feed mixture density	0.68	kg/Sm^3	Coolprop[8]
Hydrogen density	0.08	kg/Sm^3	
Methane density	0.71	kg/Sm^3	

Within the battery limits, as shown in figure 14, there is the PSA system with 4 adsorbing beds and the two compression trains necessary to compress the purified hydrogen and the natural gas retained and adsorbed during the process to the desired conditions. The compressor for hydrogen has power of 1.6 kW and 2 stages, and a specific power of 0.76 kWh/kg_{H2}. The compressor for methane requires 3-stage compression with a power of 69 kW, with 0.172 kWh/kg_{CH4}.

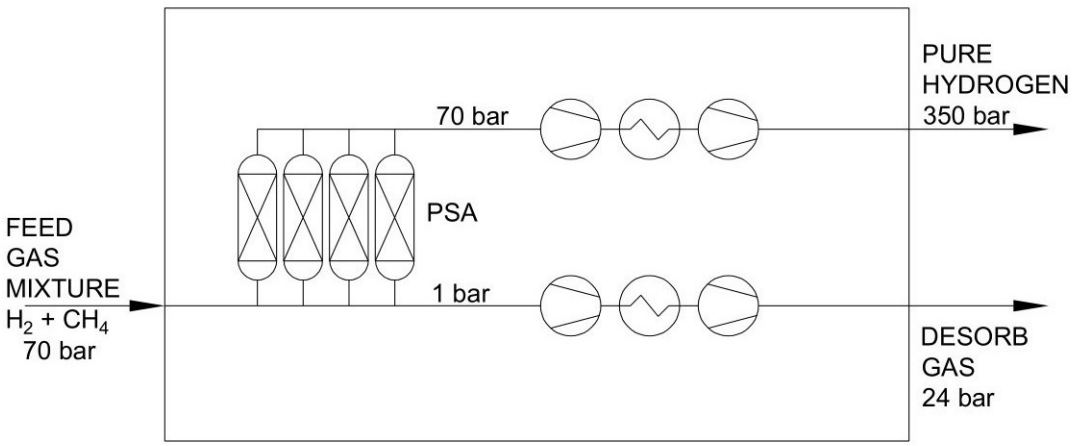

Figure 14: PFD for PSA separation system in deblending hydrogen from natural gas grid.

[8] CoolProp is an open-source software library that calculates thermodynamic and transport properties for fluids.

The impact of the gas inlet flow rate on the length of the adsorbent bed in the PSA system is depicted in Figure 15. The graph in the figure represents the flow rate of gases into the PSA 4-bed system and demonstrates that the bed length is directly proportional to the flow rate. As the flow rate increases, the bed length also increases, resulting in the requirement for more adsorbent to absorb the gases.

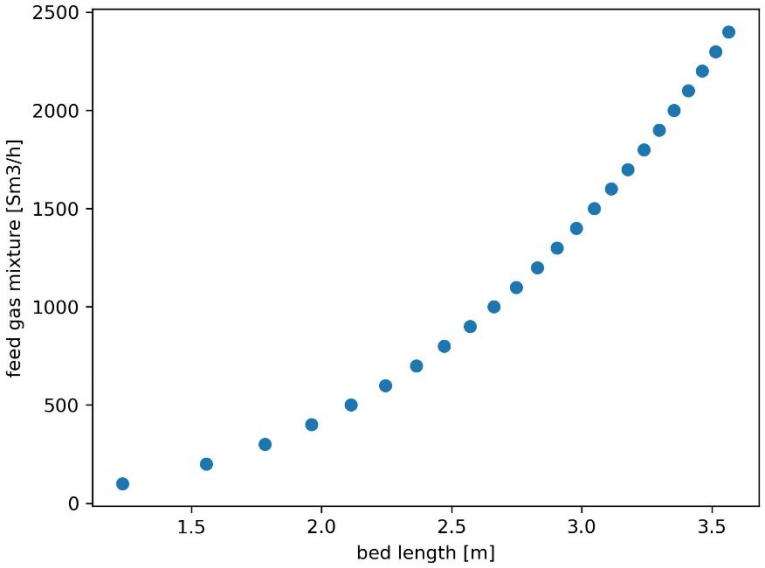

Figure 15: Effect of inlet flowrate on the bed length.

The impact of the adsorption step time on the length of the adsorbent bed is depicted in Figure 16. The graph in the figure displays the adsorption time ranging from 100 s to 30 minutes, and it reveals that the bed length increases with the adsorption time.

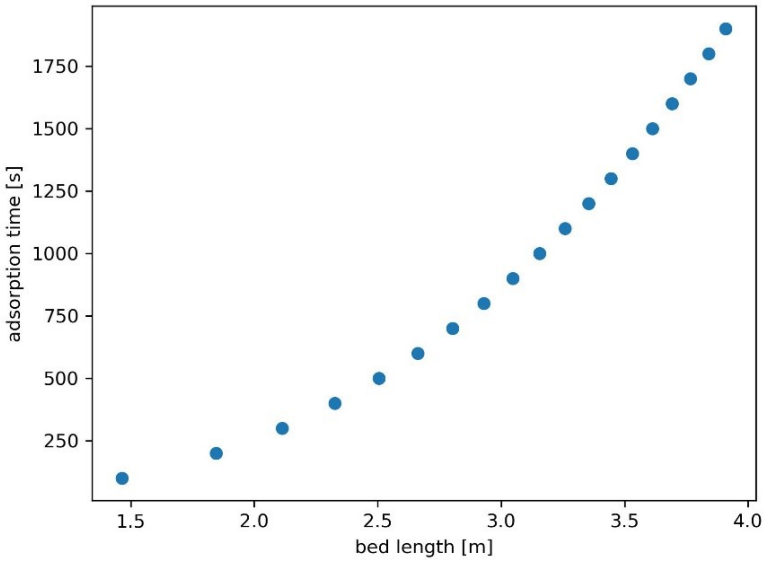

Figure 16: Effect of time on the bed length.

Membrane gas separation: for the membrane separation, a high-performance cellulose-derived asymmetric carbon hollow fiber membrane has been selected as the first stage, whose performance is reported in figure 17 [87], where the hydrogen

permeance and the H_2/CH_4 selectivity are function of the feed pressure. Major gas components have a smaller permeability than hydrogen.

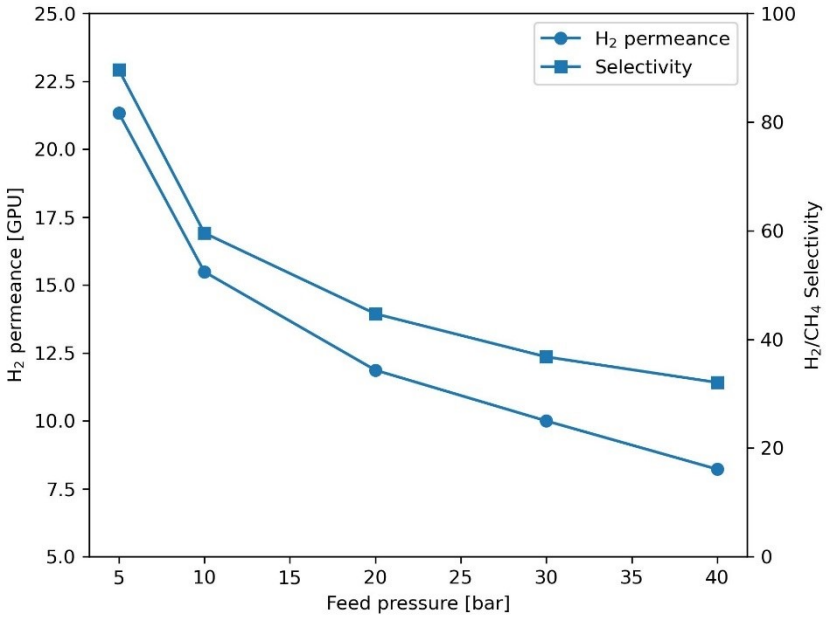

Figure 17: H_2 permeance and H_2/CH_4 selectivity vs pressure feed difference across the membrane (permeate pressure of 1 bar), for 10 vol% H_2 in CH_4 gas mixture.

The first stage is not sufficient to reach the target purity of 99.97%. The membrane can obtain hydrogen permeate molar fraction 30.34% with a surface area of 1160 m^2. The performance of the first single stage membrane for the feed gas composition under consideration is shown in figure 18. Residue gas from the membrane is available at high pressure, similar to feed gas pressure and therefore does not need recompression for injection into gas networks operating at lower pressures.

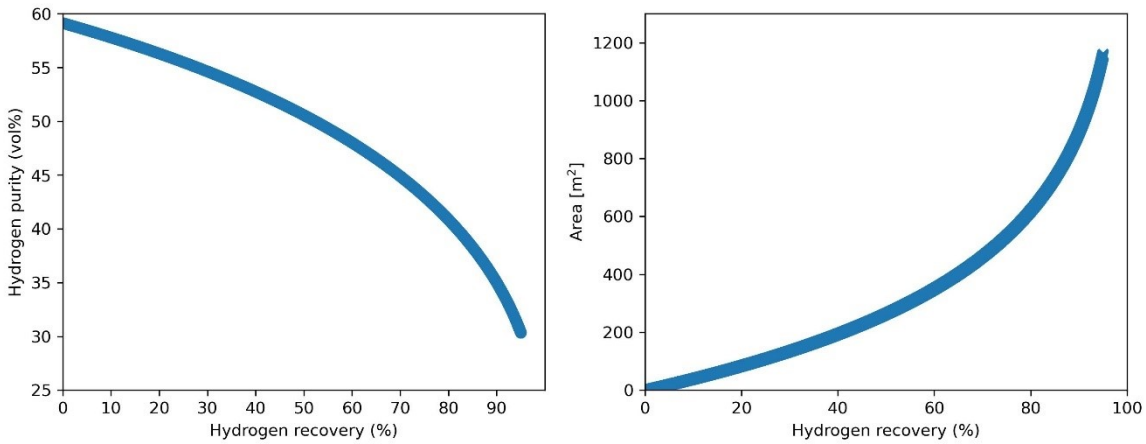

Figure 18: 1st stage membrane performances in deblending hydrogen from natural gas grid with 5 % H_2 vol.

To purify the flow of permeate produced by the first stage it is decided to use the same type of membrane, which works at a lower pressure difference. The hydrogen purity obtained in the second stage permeate stream does not reach the fuel cell purity requirement. A metal alloy membrane is then added, in particular, a Palladium-Silver membrane which has hydrogen permeance of 5914 GPU and H_2/CH_4 selectivity = 65000 at 8 bar operating pressure [87]. Although metallic membranes have high

performance for the purification of hydrogen and are also very expensive due to the noble metals they are made, therefore their use is justified by the fact that the area of the 3rd stage is small, 0.2 m^2.
All components within the battery limits are shown in figure 19, including the 3-way valves which allow natural gas to be re-injected. The hydrogen obtained is extremely pure 99.9988%, with a production of 43 kg/day. The heating necessary to heat the streams (50°C for CMS membrane and 400°C for Pd-Ag membrane) can be accomplished by combusting natural gas, preferably from the retentate with a gas-fired heater.

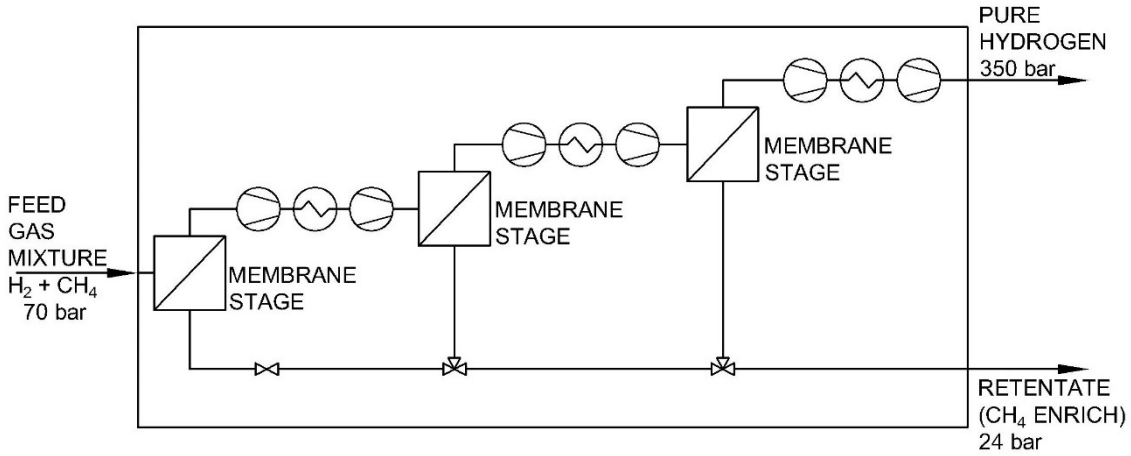

Figure 19: PFD for membrane system in deblending from natural gas grid.

As the pressure difference across the 1st stage membrane increases, more area is required to achieve the specified H_2 recovery, as shown in figure 20. However, the use of 1st stage permeate pressure values under vacuum conditions is not justifiable from a cost perspective due to increased energy consumption and capital costs.

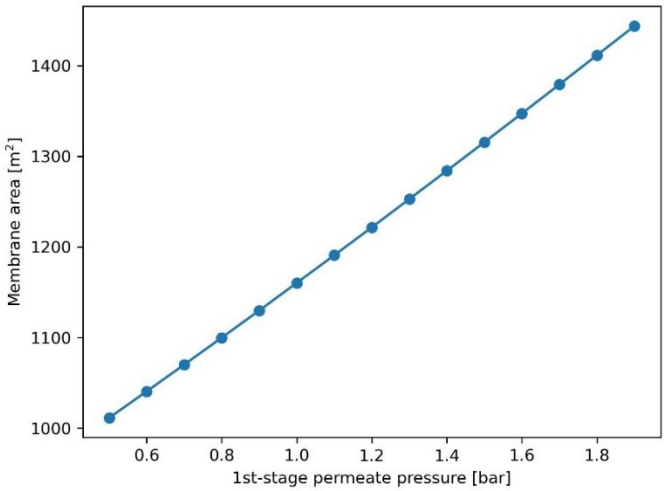

Figure 20: The effect of the 1st-stage permeate pressure on the first membrane area.

Table 19 summarizes the performance and results of the membrane system for hydrogen separation.

Table 19: Configuration of the membrane separation system.

	Membrane	H2 Purity [%]	H2 Recovery [%]	Membrane area [m^2]	Feed pressure [bar]	Permeate pressure [bar]
1st stage	CMS	30.34	95	1160	70	1
2nd stage	CMS	80.72	95	356	24	1
3rd stage	Pd-Ag	99.99	90	0.2	10	1
Overall			80			

The first compression train requires a 3-stage compressor of 66 kW and specific power of 1.36 kWh/kg. As the product flow decreases, the compression power decreases, worth 16 kW for the compressor between the 2nd and 3rd membranes and 5.8 kW for the last compression train, where the compressed flow is mainly hydrogen.

Metal hydride: for the separation with metal hydride, an alloy already experimentally tested for this application was chosen [98], which belongs to the AB_5 category. It is a lanthanum-nickel alloy with doping elements added, $LaNi_{4.8}Mn_{0.3}Fe_{0.1}$. In the event that there is a data deficit relating to material $LaNi_{4.8}Mn_{0.3}Fe_{0.1}$, those available for material $LaNi_5$ are used.

Table 20: Metal hydride absorption processing conditions.

	Unit	$LaNi_{4.8}Mn_{0.3}Fe_{0.1}$	$LaNi_5$	Ref
Desorption enthalpy	kJ/mol_{H2}	34		[98]
Desorption entropy	J/mol_{H2}	108		
Max adsorption capacity	wt%	1.35		[98]
Absorption time	s	300		
Hysteresis $ln(p_{abs}/p_{des})$		0.13		
Density	kg/m^3		8400	[99]
Adsorption capacity	mmol/g		7	[100]
Specific heat	J/kgK		419	
Thermal conductivity	W/mK		1.087	

The metal hydride separation system and the components required for the system are depicted inside the control volume, shown in figure 21. Each of the four vessels requires a quantity of $LaNi_{4.8}Mn_{0.3}Fe_{0.1}$ equal to 21 kg. It is assumed that the hot water for the desorption phase is being produced through an heat pump unit with COP of 2.5.

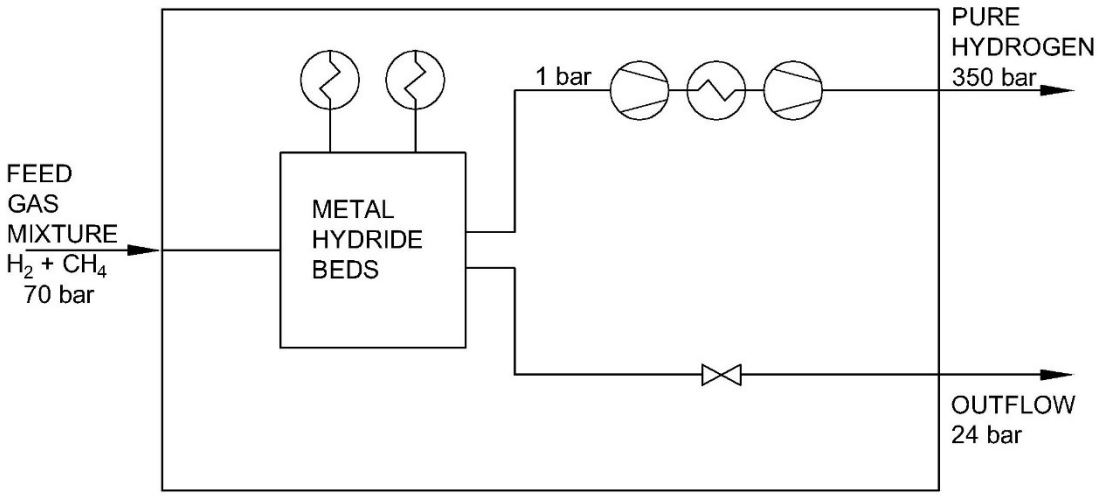

Figure 21: PDF for metal hydride system in deblending from natural gas grid.

With a hydrogen amount of 5%, the partial pressure of the gas in the feed is 3.5 bar. This does not allow for a maximum reversible capacity of 1.35% but 1.2% under these conditions. A safety coefficient of 2 is used when sizing the amount of metal alloy to account for the kinetics of the absorption reaction. The compression power is related only to the compression of hydrogen, through a 7-stage train for a power of 5.7 kW.

The three separation technologies are analyzed to purify a flow of 500 Sm^3/h of gaseous mixture CH_4:H_2 = 95:5 vol.% and to obtain hydrogen suitable for use in fuel cell applications.

Table 21: Description of overall configurations in deblending hydrogen from natural gas with 5% H_2.

	Hydrogen recovery [%]	Hydrogen separated [kg/day]	Hydrogen purity [%]	CH_4 molar fraction in non-product stream	Specific energy consumption [kWh/kg_{H2}]	LCOP [€/kgH_2]
PSA	80	43	99.97	98.95	39.7	8.6
Membranes	80	43	99.99	97.64	41.5	10.9
Metal Hydride	80	43	99.97	98.95	6.1	1.43

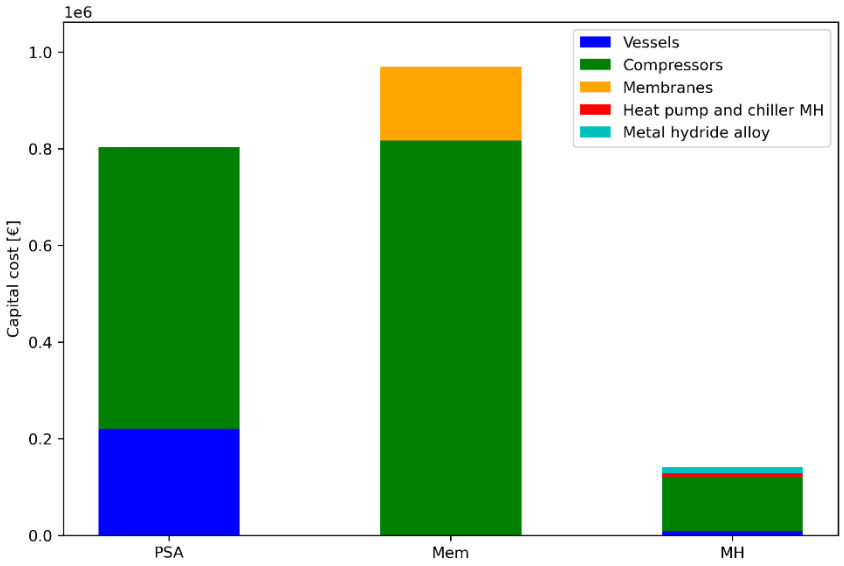

Figure 22: Capital cost distribution for the different technologies to separate hydrogen from natural gas grid with 5% H_2 in the blend mixture.

As figure 22 shows, the highest investment cost is related to membrane separation, where about 80% represents the capital cost of compressors. In all three technologies, the largest capital share relates to compressors (and their intercoolers). Metal hydride achieves an important result, the investment cost is about 5 times lower than in the other two technologies. In figure 23 below, the distribution of cost items affecting the final separation cost is shown.

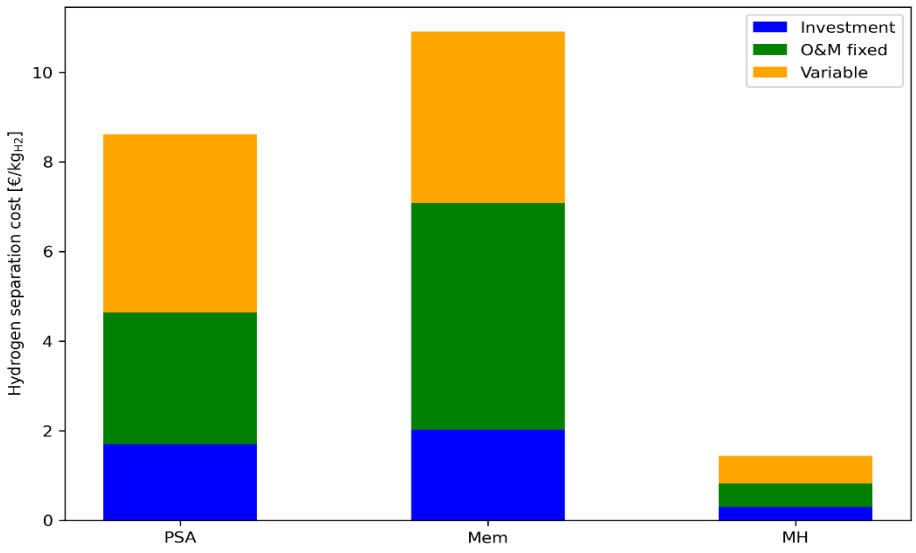

Figure 23: Final hydrogen separation cost distribution for the different technologies to separate hydrogen from natural gas grid with 5% H_2 in the blend mixture.

The replacement of compressors and carbon membranes have a heavy impact on the fixed operating costs of the membranes system. Since the PSA system and the membranes require about the same compression power the contribution related to the variable operating costs of electricity are about the same.

The quality of the natural gas re-introduced into the distribution network could require a limit to the quantity of hydrogen present required by some sensitive consumers, such as methane cars (1-2% hydrogen). All technologies guarantee compliance with this constraint. In the pie chart in Figure 24, it can be seen that more than half of the operating costs in metal hydride technology is electricity consumption. Table 22 summarizes all the cost items which determine the final cost of separation.

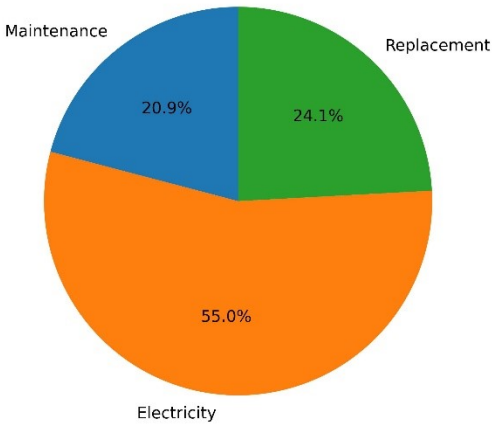

Figure 24: OPEX breakdown cost for metal hydride with 5% H_2 in the blend mixture.

Table 22: cost items for deblending at 5% H_2.

	CAPEX [€]	OPEX [€/y]	LCOP actualized [€/kgH_2]	TCO [€]
PSA	804040	108823	11.1	4068743
Membranes	970657	142180	13.8	5236072
Metal hydride	141599	17895	1.8	678468

In the 30% case of hydrogen in the blend, the configurations, from a technical point of view, remain unchanged compared to the 5% H_2 case. The PSA system is sized according to the amount of impurities in the mixture, at low hydrogen amount the adsorbent bed is larger than at high amount. In table 22 there are the technical results of the 30% H_2 case and in the following table 23 the economic results for this case.

Table 23: Description of overall configurations in deblending hydrogen from natural gas with 30% H_2.

	Hydrogen recovery [%]	Hydrogen separated [kg/day]	Hydrogen purity [%]	CH_4 molar fraction in non-product stream	Specific energy consumption [kWh/kgH_2]	LCOP [€/kgH_2]
PSA	80	258	99.97	92.1	5.6	1.3
Membranes	80	258	99.99	97.67	10.2	2.2
Metal Hydride	80	258	99.97	92.1	6.1	1.0

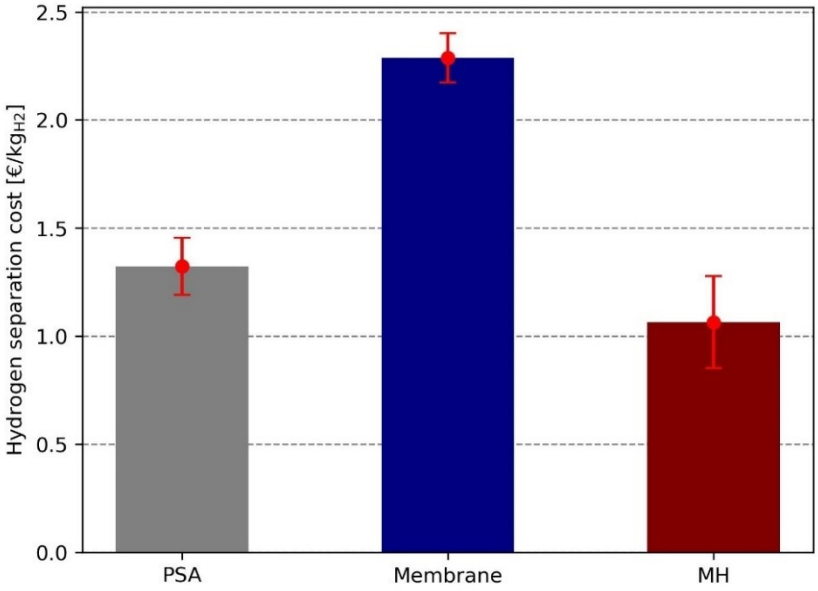

Figure 25: Final hydrogen separation cost for the different technologies to separate hydrogen from natural gas grid with 30% H_2 in the blend mixture.

The increase of up to 30% of the amount of hydrogen for the same volume has significantly reduced the final cost of separation especially for the PSA system and the membranes (figure 25). Metal hydride still remains the cheapest solution thanks to the reduced investment cost. In general, the costs have increased but the increase in the amount of purified hydrogen is much more relevant in the evaluation of the LCOP.

Table 24: results of the economic analysis for hydrogen deblending from natural gas with 30% H_2 in the feed.

	CAPEX [€]	OPEX [€/y]	LCOP actualized [€/kgH_2]	TCO [€]
PSA	783228	98881	1.7	3749678
Membranes	1149040	181152	2.8	6583614
Metal hydride	477622	84739	1.3	3019821

Compared to the 5% H_2 case, in the operating costs of the metal hydride system the share relating to the variable costs linked to electricity consumption has increased, going from 55% to approximately 70%. Figure 26 shows the comparison of the specific cost of separation between the case of 5% and 30% blend in the natural gas grid.

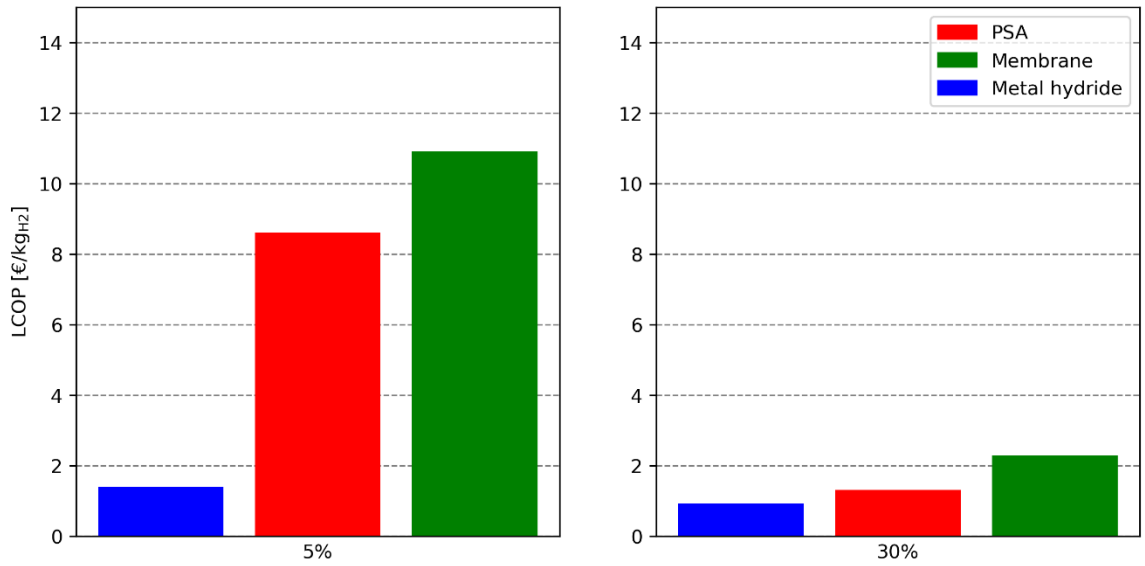

Figure 26: Comparison of the final hydrogen separation cost for 5% and 30% H_2.

Increasing the molar fraction of H_2 in the feed gas (% by volume) can significantly reduce the amount of 1st membrane area required for hydrogen recovery (figure 27). This reduction in membrane area can help to lower the overall cost of recovering hydrogen from the feed gas.

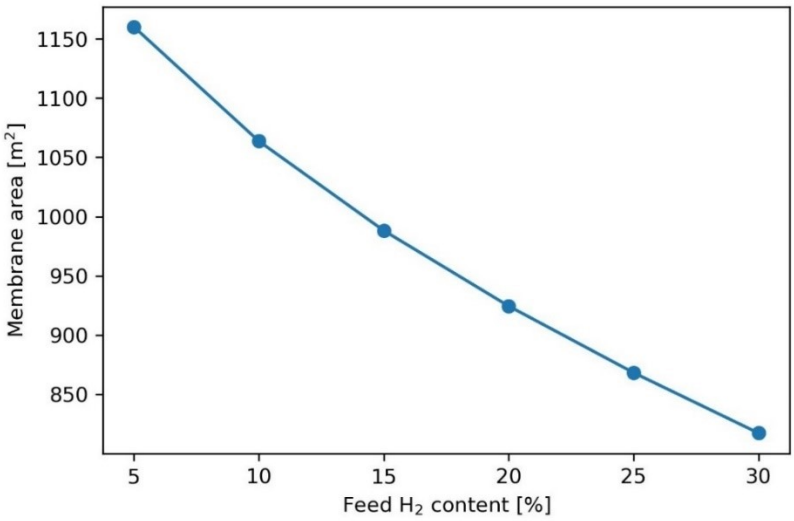

Figure 27: The effect of the 1st-stage feed H2 content on membrane area.

The power and energy consumption of the compressors hold significant importance. Hence, Figure 28 illustrates a comparison of the total installed power for the mechanical compressors. For the metal hydride and membrane purification units, the compression power increases as the percentage of hydrogen in the feed increases. In the case of the PSA system, despite the increased power required for hydrogen compression, the corresponding decrease in power needed for reinjecting natural gas outweighs it, leading to an overall reduction in the total installed power. In general, increasing the amount of purified hydrogen reduces specific energy consumption.

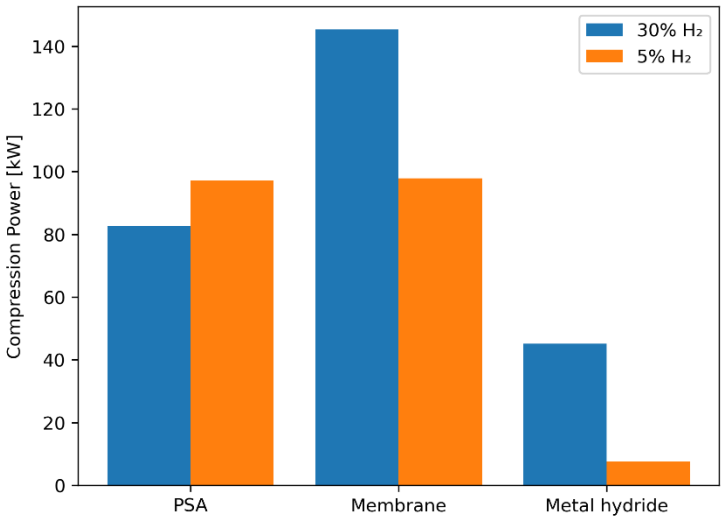

Figure 28: Compression power comparison.

The process has been shown to be very sensitive to the H_2 feed concentration. In particular, very low concentrations significantly increase the required amount of energy.

5.2 Case study 2 - Purification of biomass-derived hydrogen

For the purification of hydrogen coming from biomass, it is decided to study a flow rate of 500 Sm^3/h with composition H_2:CO_2 70:30 %vol. The assumption of a binary mixture, in addition to simplifying the analysis, represents the composition of syngas originating from biomass gasification followed by a WGS reaction. The composition of the syngas, and thus the amount of hydrogen present, depends on the characteristics of the biomass and the operating conditions [101]. If the syngas is further treated through the WGS reaction, the amount of CO can be reduced [102]. Also, in fermentation-based processes, hydrogen and carbon dioxide are the main products, and CO_2 must be removed before hydrogen utilization [103]. The average composition of dry syngas after the WGS reaction is shown in table 24 as a molar fraction. The gas stream that comes out from the WGS reactor is dehydrated to remove most of the water vapor. In the case of biomass, a desulphurization stage is included in the system to get rid of the sulfur contained in the syngas. The tail gas from the purification unit is recycled upstream to heat the gasifier or reformer, or both.

Table 25: Composition of the dry syngas, after the shift reaction [104].

H_2	CO_2	CO	CH_4
67.7	29.8	0.9	1.6

The syngas enters the purification unit at ambient temperature and a pressure of 20 bar. The hydrogen purified at 99.97% is then compressed to a pressure of 700 bar by a train of mechanical compressors. Figure 29 shows the battery limits of the biomass-derived hydrogen purification.

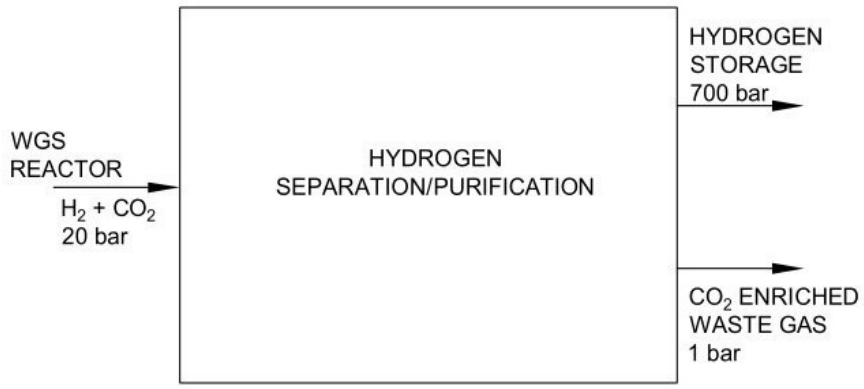

Figure 29: Battery limits for biomass-derived hydrogen.

PSA: the adsorbent chosen for CO_2 adsorption is zeolite LiX, whose isothermal curve is shown in figure 30 [105], evaluated at a temperature T = 293 K. Lee et al [106] indicate that zeolite can excellently remove CO_2, compared to activated carbon or silica gel. PEM fuel cells are very sensitive to carbon monoxide, which can be considered the main issue regarding the purification of syngas produced from biomass gasification. To ensure the absence of carbon monoxide, a 0.1 m high layer of activated carbon is added.

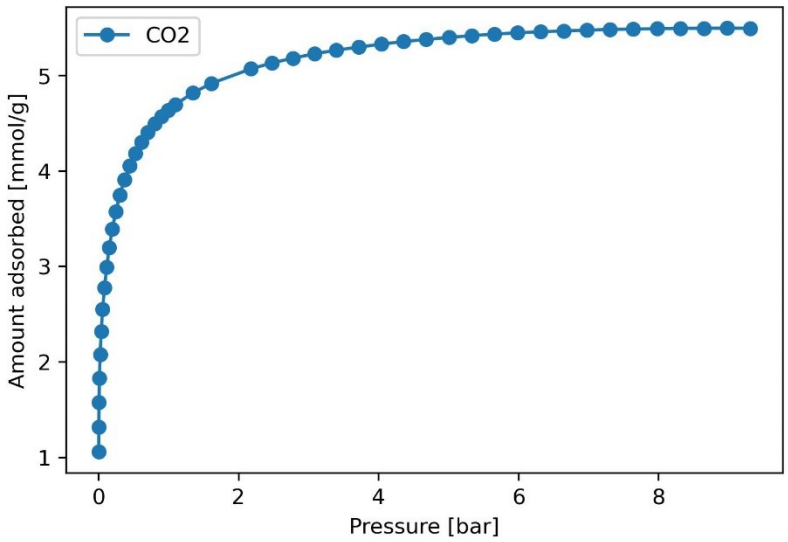

Figure 30: Adsorption isotherms on zeolite LiX for CO_2 at T = 293 K.

With the achievable recovery assumption of 80% and a purified hydrogen purity of 99.97%, it is possible to determine the amount of purified hydrogen, 604 kg/day. Within the battery limits, as shown in figure 31, there is the PSA system with four adsorbing beds and the compression train necessary to compress the purified hydrogen at 700 bar. The process conditions of the PSA are tabulated in Table 26.

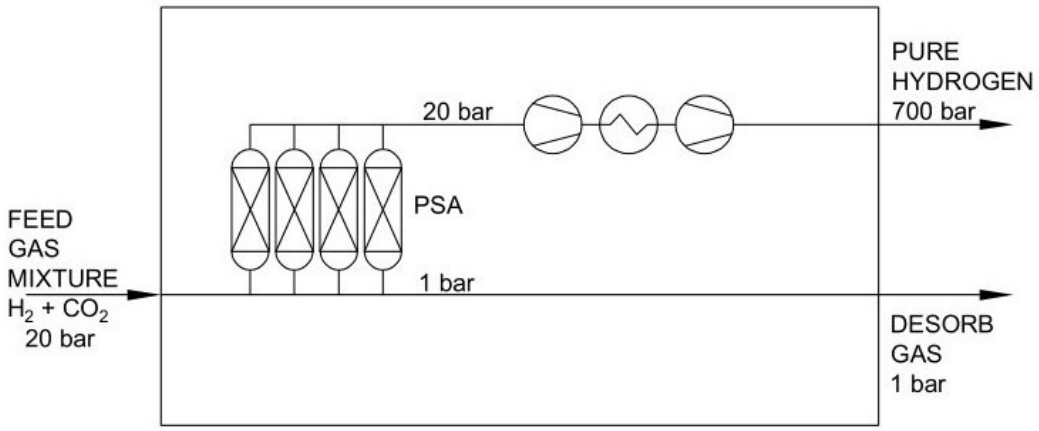

Figure 31: PFD for PSA system in purification biomass-derived hydrogen.

Table 26: Processing conditions for PSA in purification of hydrogen from biomass.

			Ref.			
Feed pressure	20	bar		Feed mixture density	0.65	kg/Sm^3
Desorption pressure	1	bar		Hydrogen density	0.08	kg/Sm^3
Feed gas H_2 molar fraction	70	%		CO_2 density	1.97	kg/Sm^3
Flow rate	500	Sm^3/h				
Operating temperature	298	K				
Column height	2.4	m				
Column inner diameter	0.8	m				
Adsorption time	300	s				
Bulk density zeolite LiX	790	kg/m^3	[107]			

Membrane gas separation: the membrane purification system provides purification in 3 stages (figure 32) to achieve the desired purity. They are 3 asymmetric carbon molecular sieve membranes whose performances are shown in figure 33, [108]. The relatively dry gas is fed into the 1st-stage membrane unit after it is pre-heated to a given operating temperature (100 °C) with an electrical heater.

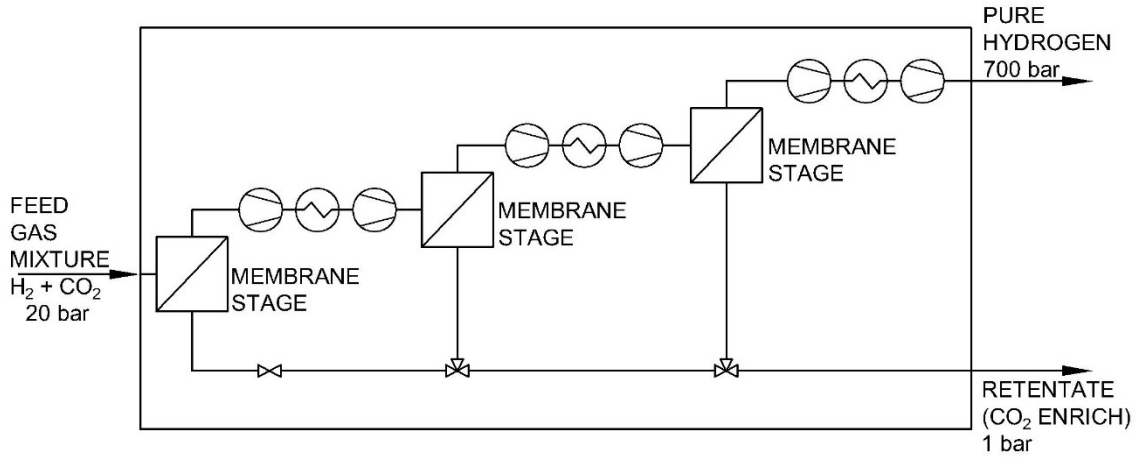

Figure 32: PFD for membrane system in purification biomass-derived hydrogen.

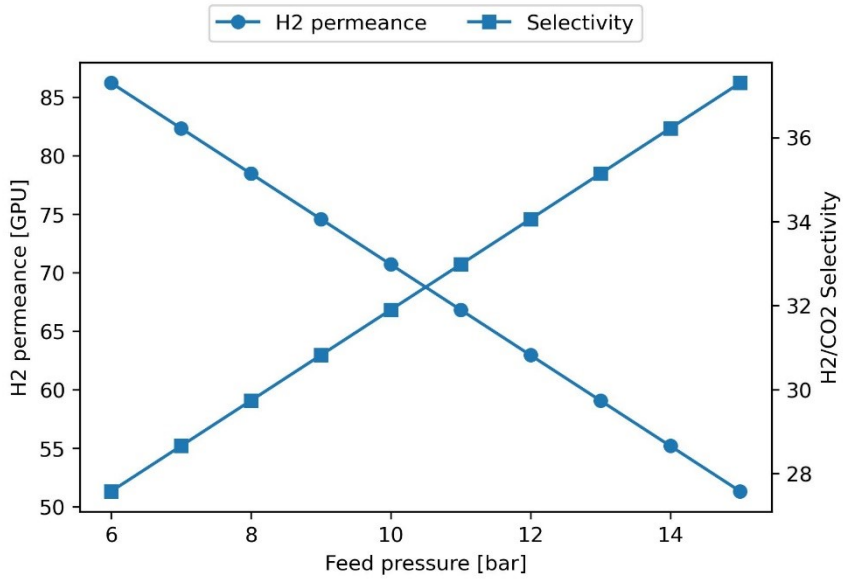

Figure 33: Mixed gas separation performances using a 50 vol% H_2/50 vol% CO_2 gas mixture as a function of total feed pressure tested at T = 90 °C.

As mentioned, after 3 purification stages it is possible to reach a hydrogen purity greater than 99.97%. The performance of the last stage of membrane purification is shown in figure 34.

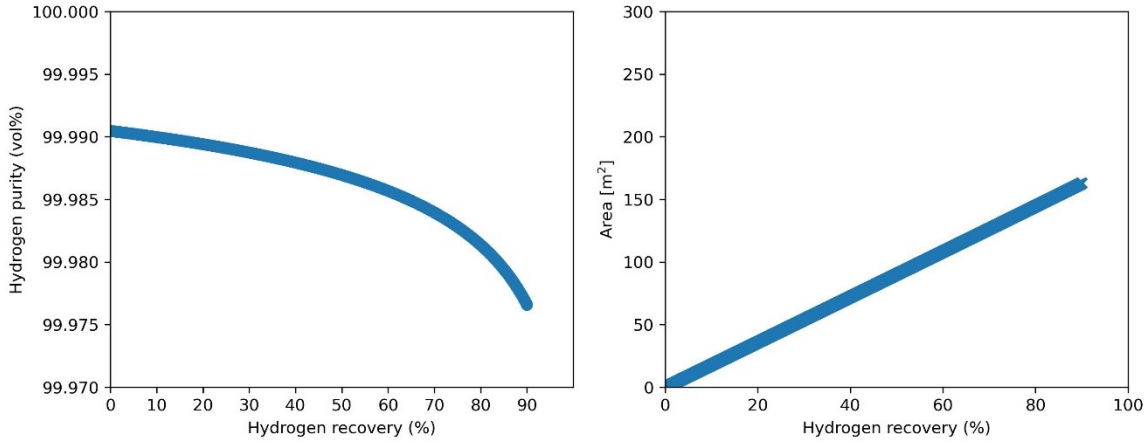

Figure 34: 3rd stage membrane performances.

A high feed pressure induces a high driving force for permeation, increasing the flux and reducing the membrane area. However, as pressure increased, the considered membrane demonstrates a reduction in H_2 permeance, increasing membrane area. All this is shown in figure 35.

The change in feed pressure showed a change in membrane area, which impacts capital costs. But the feed pressure variation also affects the compression power and therefore the operating costs. When the 1st-stage feed pressure is increased from 10 to 25 bar the power demand for the compressors is slightly decreased, figure 35.

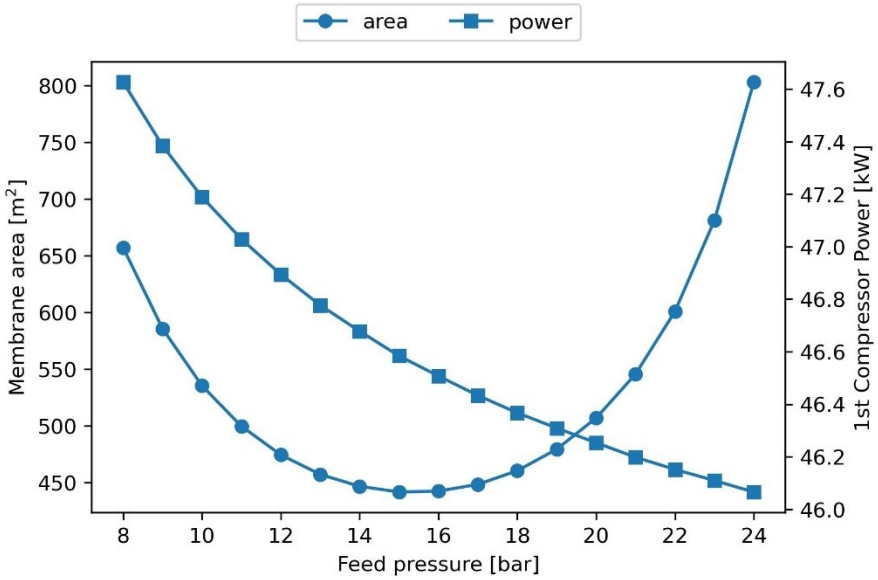

Figure 35: The influence of the 1st-feed pressure on the required membrane area and power demand.

The lower transmembrane pressure at the 1st-stage unit caused by the higher permeate pressure requests a larger membrane area to fulfill the required H_2 loss, figure 36.

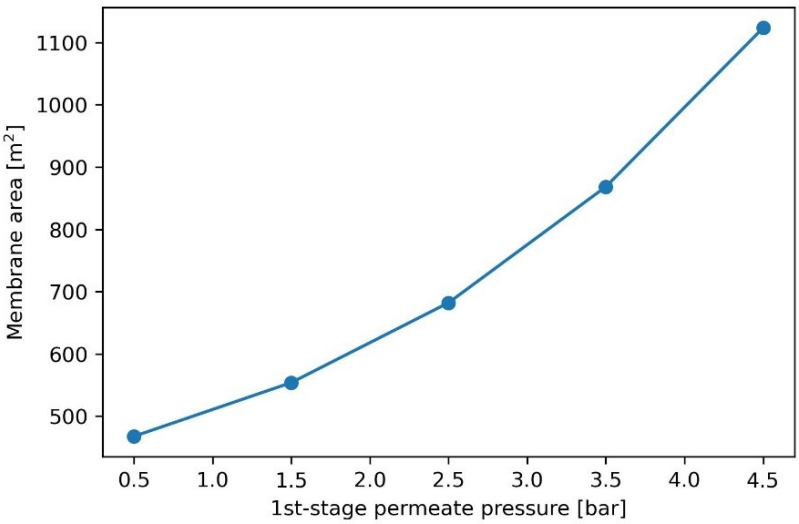

Figure 36: The influence of the 1st-stage permeate pressure on the membrane area.

Table 27 summarises the performance and results of the membrane system for hydrogen purification.

Table 27: Configuration of the membrane separation system for purification of biomass-derived hydrogen.

	Membrane	Hydrogen purity [%]	Hydrogen recovery [%]	Membrane area [m²]	Feed pressure [bar]	Permeate pressure [bar]
1st stage	CMS	96.49	95	506	20	1
2nd stage	CMS	99.72	95	210	20	1
3rd stage	CMS	99.97	90	163	10	1
Overall			80			

Metal hydride: the same metal alloy used in the deblending hydrogen from natural gas is used in this case study. Dunikov et al. [109], have demonstrated the separation of hydrogen/carbon dioxide mixture using the AB_5 type, in particular, $LaNi_{4.8}Mn_{0.3}Fe_{0.1}$. The configuration with metal hydrides is presented in figure 37.

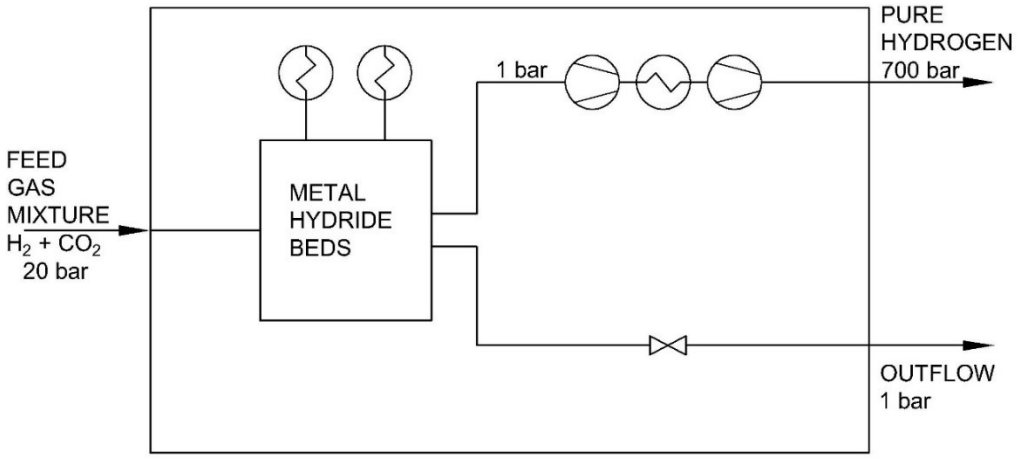

Figure 37: PFD for metal hydride system in purification biomass-derived hydrogen.

The 3 technologies are again analyzed in the new case study, to find the most economical solution for hydrogen purification and suitable for use in fuel cell applications. When hydrogen amount exceeds 50% the PSA system demonstrates its unrivaled strength. In all cost items, CAPEX, OPEX, and LCOP (figure 38), the PSA is the cheapest solution, and also the one with the lowest specific energy consumption (figure 39).

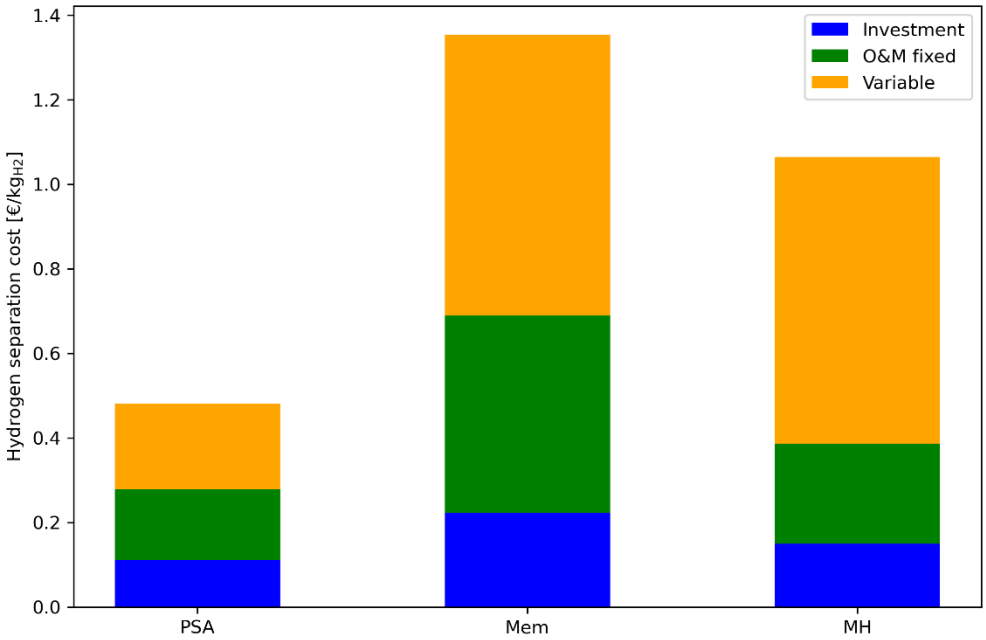

Figure 38: Final hydrogen separation cost distribution for the different technologies to purify hydrogen from biomass gasification.

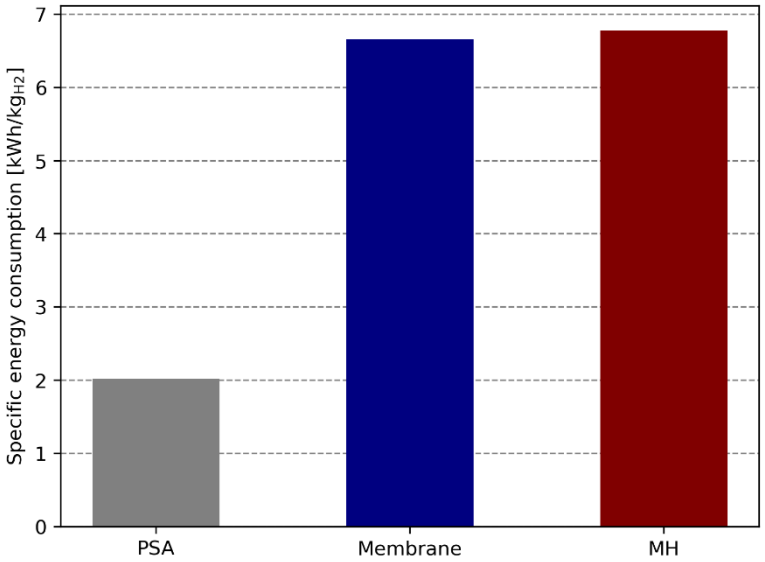

Figure 39: Specific energy consumption for the different technologies to purify hydrogen from biomass gasification.

The results of the techno-economic analysis are reported in tables 28 and 29 for the case study of hydrogen purification produced by biomass gasification. In capital expenditure, the metal hydride system and the membranes reach one million euros. The trend is repeated and indeed expanded also for operating costs. As easy to expect, the TCO reflects the first two contributions, in which PSA has a cost more than half of metal hydride which in turn are better than membranes. The levelized cost presents no particular surprises with very good performance of PSA systems that even reach a levelized cost of purification of about 0.5 €/kg$_{H2}$. In the breakdown of the annual operating costs of the metal hydride purification system, it is noted that electricity costs have further increased their share, reaching almost 75%, increasingly confirming themselves as the main cost driver while the percentage of maintenance and replacement has decreased. This is due to the higher amount of separated hydrogen than in the previous case study.

Table 28: Description of overall configurations in the purification of biomass-derived hydrogen.

	Hydrogen recovery [%]	Hydrogen separated [kg/day]	Hydrogen purity [%]	Specific energy consumption [kWh/kg$_{H2}$]	LCOP [€/kg$_{H2}$]
PSA	80	604	99.97	2	0.4
Membranes	80	604	99.97	6.7	1.3
Metal Hydride	80	604	99.97	6.7	1.0

Table 29: results of the economic analysis purification of biomass-derived hydrogen.

	CAPEX [€]	OPEX [€/y]	LCOP actualized [€/kgH_2]	TCO [€]
PSA	741465	81317	0.6	3181004
Membranes	1491683	253570	1.6	9098797
Metal hydride	990583	201715	1.2	7042053

Chapter 6

6 Dynamic modeling

The pre-design of the purification processes explained in Chapter 3 provided indicative values on which the techno-economic analysis was based. Aware of the fact that the processes of adsorption, membrane separation and chemisorption are complex phenomena, it is decided to investigate the most relevant result of the analysis, i.e. that the metal hydride is competitive when the hydrogen to be separated is present in relatively small amount in the initial gas mixture. The pre-design considered the entire hydrogen absorption process to be static in the $LaNi_{4.8}Mn_{0.3}Fe_{0.1}$ tank and two fundamental aspects of the solid-state purification/storage technology were neglected: reaction kinetics and thermal management.
The equilibrium of the reaction belongs to the domain of thermodynamics of the metal-hydride transformation and is effectively represented by the PCT curves (figure 8), in which the concentration is the amount of hydrogen in the metal alloy. The rate at which a reaction takes place instead belongs to the domain of chemical kinetics and describes the temporal behavior of the phenomena of absorption and desorption characteristic of the material.
Thermal management refers to the interaction between metal hydrides and tanks from a thermal point of view, as temperature variations occur during the charge and discharge phase due to reactions between metal, metal hydride and hydrogen, and which influence the flow rate of hydrogen in or out.

6.1 Methodology

To take all these aspects into account, it is possible to build a mathematical model made up of several physical relationships which represents, with some assumptions or simplifying hypotheses, the behavior of a real phenomenon, or at least it is as faithful as possible. The model explained below, developed at FBK in the Dymola simulation environment, is based on a cylindrical geometry inside which there are heat exchange tubes that allow the passage of water and the volume of metal alloy. Figure 40 shows how the cylindrical tank is approximated by multiple cylindrical tanks, and how each of these cylindrical tanks is discretized in the radial and longitudinal directions. Figure 41 shows the graphical representation of the model where the volume inside which the gaseous mixture is adsorbed is a component called "volume", and the tube filled with water is indicated with "pipe", connected to the exchange fluid ports. The model is based on an adiabatic assumption that the volumes do not exchange heat with each other underestimating the capacity to absorb hydrogen of the metal hydride. The metal of the heat transfer tube indicated with "SS_Case" is thermal inertia for the system and is modeled like a thermal conductive resistance with a constant heat transfer coefficient.

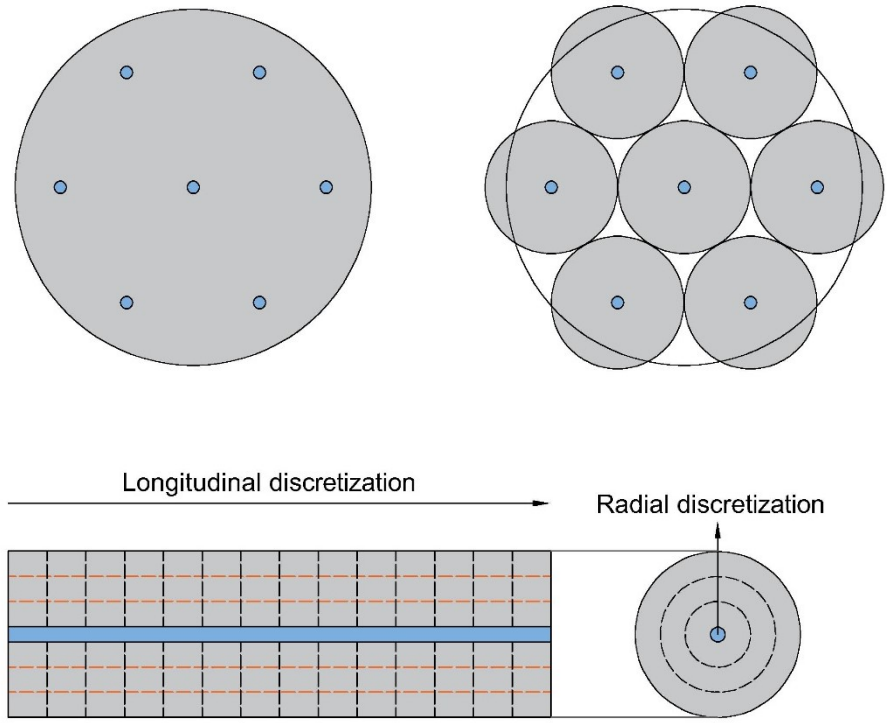

Figure 40: Cylinder tank approximated by multiple cylindrical tanks. Pseudo 2D discretization of each cylindrical tank.

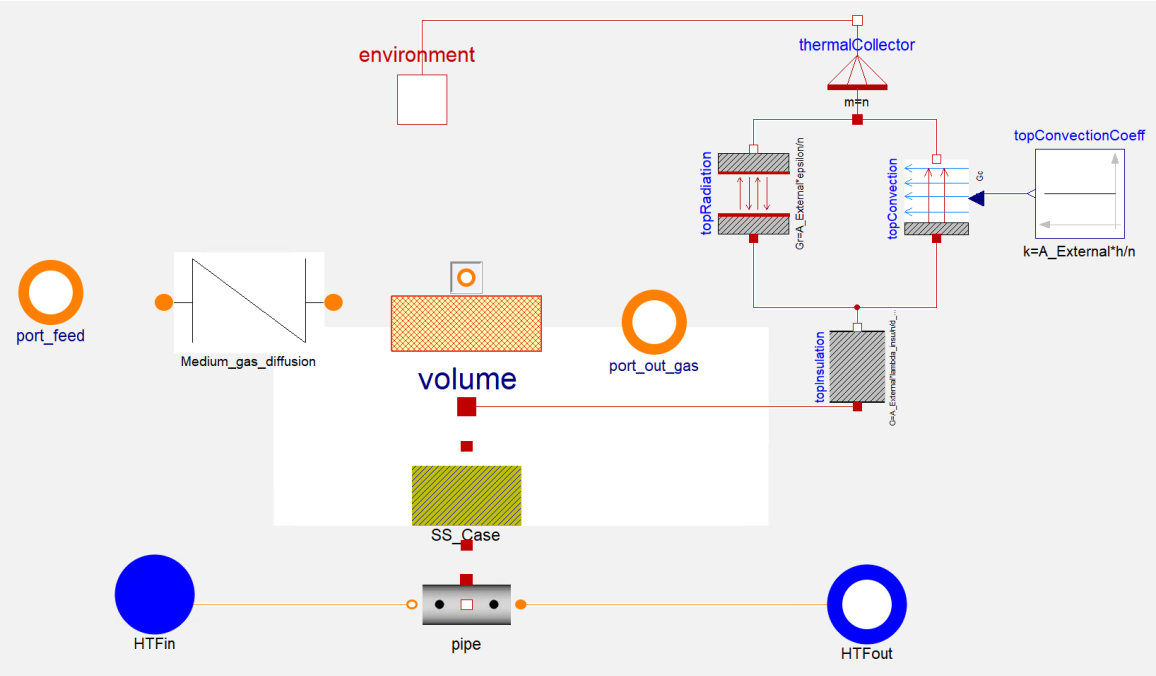

Figure 41: Graphic display of the model with components from Dymola software.

The gas-tight container in which the metal hydride is placed must insulate from the external environment and is shaped by a lumped thermal element to transport heat without storing it. The heat dispersion according to the thermal radiation, heat convection and conduction mechanisms is modeled with lumped thermal components. The diffusion of gases inside the tank is modeled using a gas pressure loss model defined by a friction model ("Medium_gas_diffusion" in figure 41).
Within the "volume" component there are energy and mass balances, and the equations to express the temporal evolution of the process since all equations are time dependent. The absorption rate in the charge phase [kg/s] and the desorption rate in the discharge phase [kg/s] are expressed by the following equations:

$$r_{ABS} = k_{ABS} \cdot (Cap_0 - Cap) \cdot DF_{ABS}$$

Eq. 45

$$r_{DES} = k_{DES} \cdot Cap \cdot DF_{DES}$$

Eq. 46

where $k_{ABS,DES}$ are the kinetic constants [1/s], Cap_0 the maximum amount of hydrogen stored in the metal hydride [kg], Cap the actual amount of hydrogen stored [kg], and $DF_{ABS,DES}$ the driving force. Expressing in kg the amount of metal hydride $mass_{MH}$, the maximum reversible capacity Cap_{rev}, and the number of heat exchange tubes n_{pipes}, the maximum amount of hydrogen stored is expressed as:

$$Cap_0 = mass_{MH} \cdot Cap_{rev} \cdot n_{pipes}$$

Eq. 47

The expression can be used in calculating the amount of hydrogen actual stored using the percentage of hydrogen stored at the beginning:

$$Cap = Cap_0 \cdot Cap_{start}$$

Eq. 48

The driving force is the comparison between the partial pressure of hydrogen p_{H_2} and the equilibrium pressure of the system, in the absorption phase $p_{eq_{ABS}}$ and desorption $p_{eq_{DES}}$:

$$DF_{ABS} = \frac{p_{H_2} - p_{eq_{ABS}}}{p_{eq_{ABS}}}$$

Eq. 49

$$DF_{DES} = \frac{p_{eq_{DES}} - p_{H_2}}{p_{eq_{DES}}}$$

Eq. 50

In particular, above $p_{eq_{ABS}}$, the metallic material and gaseous hydrogen tend to form the hydride phase, on the contrary, when the pressure is lower than the equilibrium one, the hydride tends to return to metallic phase releasing hydrogen. The PCT curves for the absorption and desorption phases have been provided as input to the algorithm for $LaNi_{4.8}Mn_{0.3}Fe_{0.1}$ from the work of Dunikov [109] and are represented in figure 42 for five different temperature values. The other parameters of the metal hydride are shown in table 30.

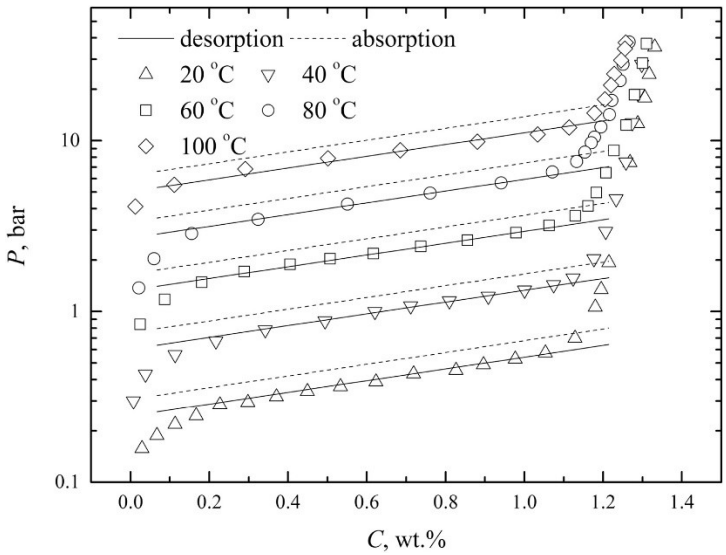

Figure 42: PCT-isotherms for $LaNi_{4.8}Mn_{0.3}Fe_{0.1}$.

Table 30: Principal properties of $LaNi_{4.8}Mn_{0.3}Fe_{0.1}$.

	Unit	$LaNi_{4.8}Mn_{0.3}Fe_{0.1}$	$LaNi_5$	Ref
Desorption enthalpy	kJ/mol_{H2}	34		[98]
Desorption entropy	J/mol_{H2}	108		
Max adsorption capacity	wt%	1.35		
Hysteresis $\ln(p_{abs}/p_{des})$		0.13		
Density	kg/m^3		8400	[99]
Adsorption capacity	mmol/g		7	[100]
Specific heat	J/kgK		419	[110]
Thermal conductivity	W/mK		1.087	
Kinetic absorption constant	Hz	0.01		
Kinetic desorption constant	Hz	0.01		

The cycle simulation parameters are shown in table 31 and the parameters relating to the metal hydride tank in table 32.

Table 31- Main characteristics of adsorption cycle for the MH bed.

	Unit	Value
Adsorption time	s	300
Cycle time	s	2000
Feed composition	kg/kg	H_2 0.0065 CH_4 0.9935
Feed pressure	bar	70
Feed temperature	°C	20
Off gas pressure	bar	68.5
Product pressure	bar	1

Table 32- Principal characteristics of the MH bed.

Parameter	Unit	Value
General		
Longitudinal discretization tank		20
Radial discretization tank		6
Ambient temperature	°C	25
Water		
Heat transfer coefficient single phase	$W/(m^2K)$	100
Mass flow rate fixed	kg/s	1.5
Inlet temperature	°C	8
Outlet temperature	°C	20
Metal wall		
Thickness	m	0.001
Mass	kg	20
Specific heat capacity	J/(kgK)	502
Density	kg/m^3	7500
Thermal conductivity	W/(mK)	50
Geometry		
Number of pipes		30
Length of tank	m	0.3
Radius of pipe	m	0.00955
Free volume in the tank	m^3	0.000001
Insulation		
External area of insulation	m^2	2
Thickness of insulation	m	0.06
Thermal conductivity of the liquid phase	W/(mK)	0.32
Emission value body		0.04
Heat transfer coefficient	$W/(m^2K)$	50

6.2 Model validation

An important step that must be done after the proposal of a mathematical model is the study of its validity. Comparison of numerical data with robust experimental results is a reliable method for validation. In this case a reliable way to validate the numerical data with real experiments is the comparison of the hydrogenation/absorption kinetics during the charging phase. One method for characterizing the absorption properties of materials is the volumetric method in which a sample under study is placed in a chamber in which the pressure variation of the control volume is controlled, which will decrease during the absorption phase. These conditions are reproduced in the simulation software. Usually, in the experimental procedure, the temporal evolution of the pressure of the control volume is measured to determine the evolution of the metal-hydrogen atomic ratio for different values of temperature and pressure. In the literature there are no data on the kinetic process for the $LaNi_{4.8}Mn_{0.3}Fe_{0.1}$ alloy, therefore, it was decided to validate the model with the more common $LaNi_5$ alloy, which has a maximum gravimetric capacity of 1.5 %wt. Moreover, for $LaNi_5$, at room temperature (20-25°C) the absorption plateau pressure is very close to ambient pressure. The results calculated by the model show good agreement with the experimental data of Jemni et al. [111]. However, the difference is present and attributable to the fact that the two are different materials with slightly different capacities. The amount of hydrogen compared to the amount of metal by weight is plotted in figure 43 for the temperature of 20 and 40°C at a pressure of 5 and 10 bar. The model is placed between the two trends examined, and, although it does not intend to faithfully reproduce the physical reality, it approximates the kinetics at 40°C particularly well. Considering the metal alloy$LaNi_{4.8}Mn_{0.3}Fe_{0.1}$ separately, the model underestimates the absorption capacity of the alloy as the curves plateau below the maximum capacity value (1.35 %wt).

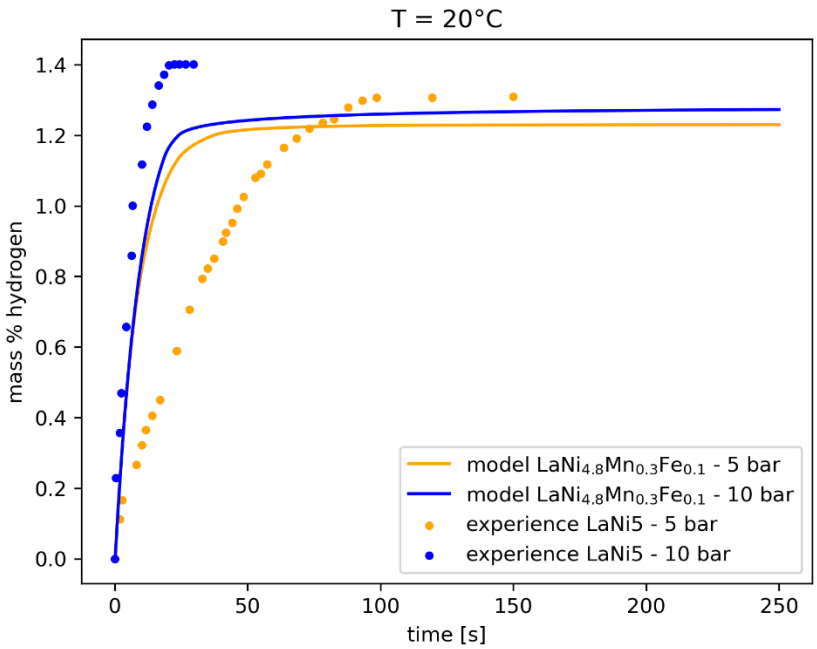

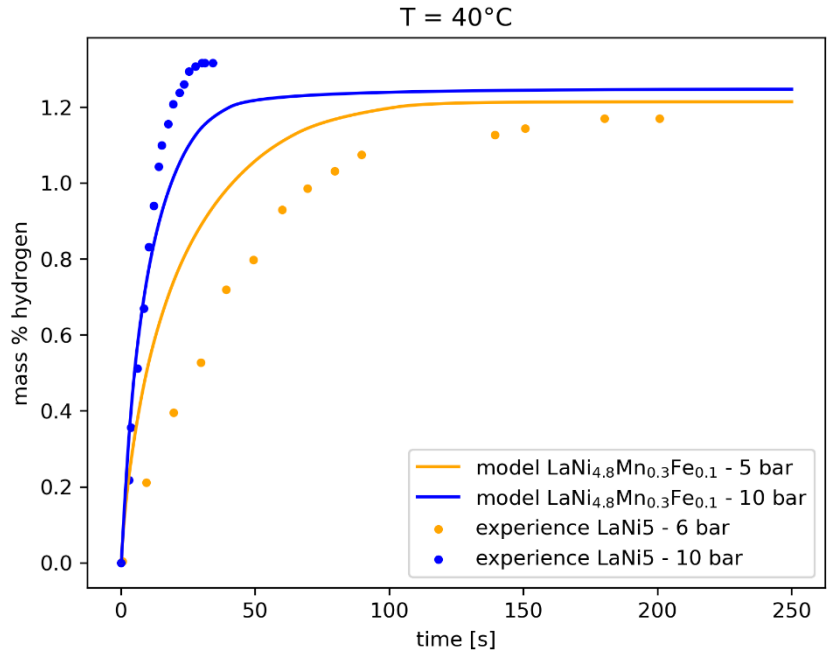

Figure 43: model validation. Mass% hydrogen absorbed under different condition for the absorption case.

6.3 Simulation

The model is applied to simulate a purification cycle according to the steps set out in Chapter 2 and reported below:

1) Absorption step: the mixture is introduced into the metal hydride tank through the feed port where the hydrogen begins to be absorbed following the hydrogenation reaction with heat release. The methane passes through the tank as gas inert, not reacting with the metal alloy, leaving the volume at the outlet port at the same inlet pressure unless pressure drops.

2) Depressurization: the absorption phase ends when the hydrogen is no longer absorbed due to bed saturation and begins to flow out as offgas without being trapped. The feed mixture is interrupted and a communication is opened with another tank that is in a temporally displaced phase. This means that the second tank begins to pressurize and prepare for complete pressurization and the start of a new cycle.

3) Desorption: hydrogen is still present inside the tank and must be discharged. The desorption is driven by the reduction of the system pressure, from the outlet port pure hydrogen can be removed as a product of the cycle.

4) Once the complete or partial regeneration of the bed has been reached, the pressure inside the tank increases to reach the starting conditions, ready to carry out step 1. No purge phase is considered.

Figure 44 shows the opening time sequence of the valves starting from the first instant of the feed phase, where 0 represents the complete closure of the valve and 1 represents the complete opening.

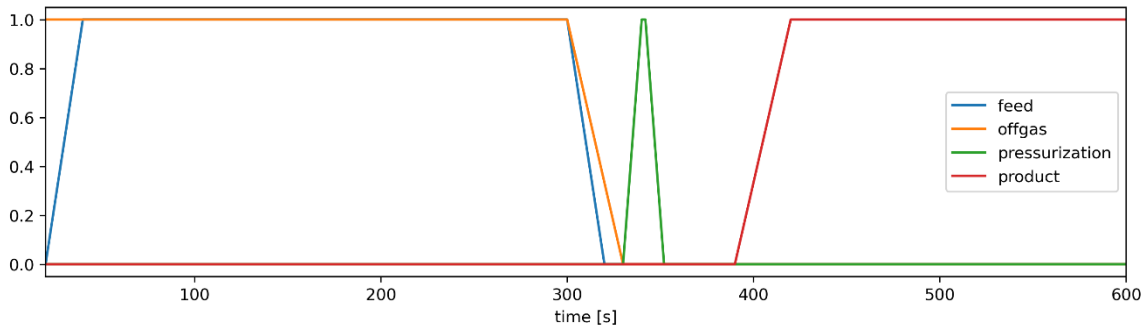

Figure 44: valve opening time sequence up to the desorption phase.

6.4 Results

The first result to evaluate is the hydrogen recovery by simulating an entire purification cycle with the process parameters used in the pre-design. Figure 45 shows that the instantaneous recovery remains above the assumed 80% mean value for almost the entire absorption cycle. The reduction in hydrogen recovery means an increase in the amount of hydrogen gas leaving the tank with the offgas.

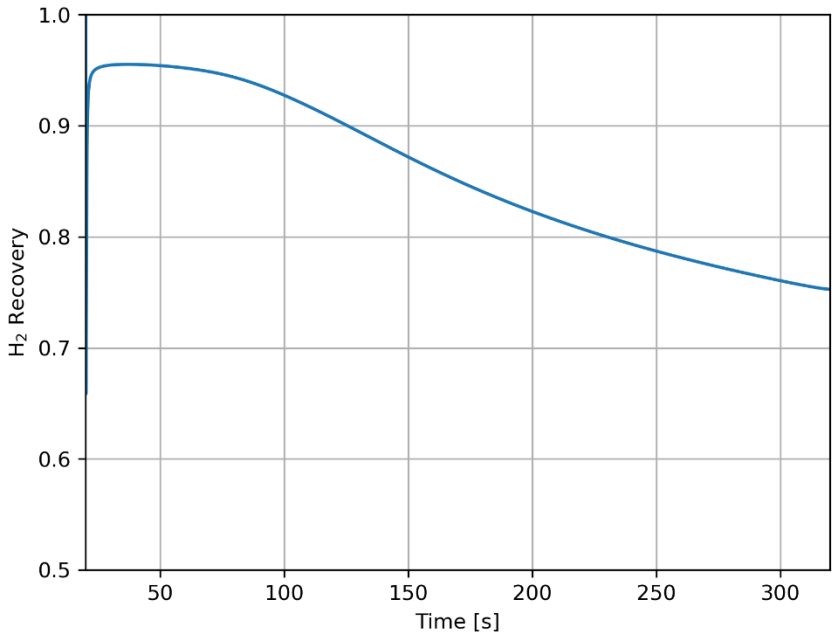

Figure 45: hydrogen recovery in the charge phase.

The other important KPI for the purification process is the purity of the hydrogen as it leaves the tank in the product stream. This is calculated in the post-process analysis and the system allows to reach a purity of 99.97% in line with the PEMFC requirements.

In chapter 5 the amount of hydrogen stored after the absorption phase is 128 g. But instead, as shown in figure 46, the capacity, i.e. the quantity of hydrogen in grams stored in the tank is lower and equal to 100 g. This is probably related to the already mentioned feature of the model to underestimate the capacity of the metal hydride. The same figure shows another important result, after about 30 minutes it is not possible to completely regenerate (empty) the bed, and some residual hydrogen remains. This may be due to the equilibrium pressure reached in the desorption phase.
The tank is not completely filled, at the end of the absorption phase the state of charge does not exceed 35%.
The absorption behavior is not the same inside the tank; the characteristics is evident in the plot of figure 47. Here, the three different discretization picked along the longitudinal direction are reported, the first the tenth and the twentieth volumes represent the initial, the middle and final volume reached by the flowing gas. It can be seen that the amount of stored hydrogen is greater in the first part of the tank reducing towards the outlet port due to the lowering of the partial pressure of hydrogen (figure 48), which regulates the driving force. It is this difference that affects recovery because when the last volume starts to fill up, hydrogen starts to come out of the tank. For the three longitudinal volumes drawn in the figure, the radial volume closest to the pipe is considered (also indicated with [1]), and therefore subjected to the best conditions of heat exchange with water.

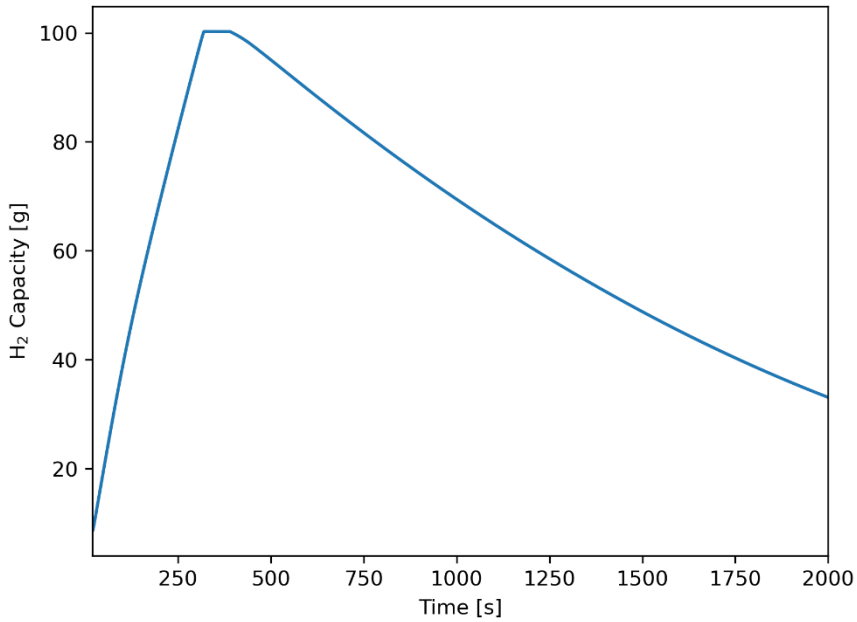

Figure 46: storage capacity in the metal hydride until the desorption step is complete.

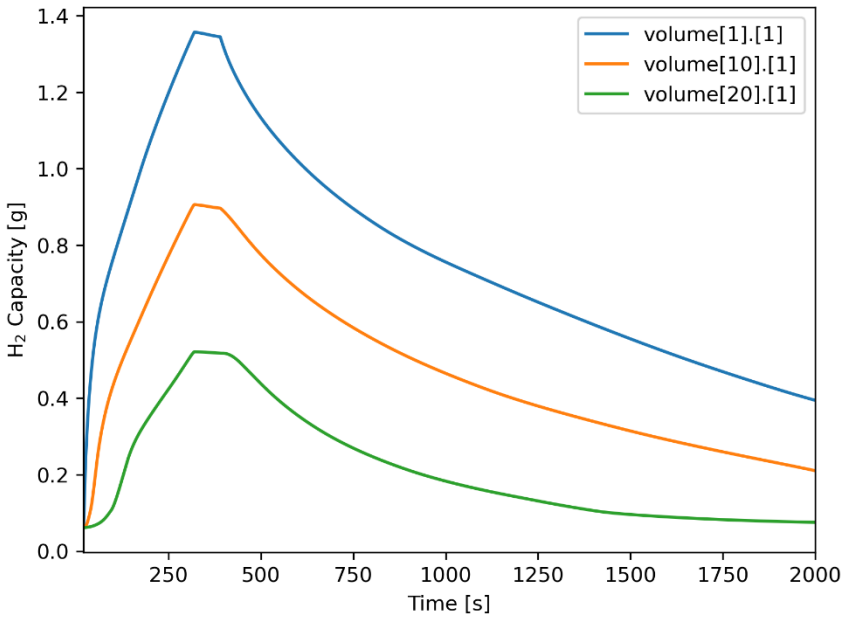

Figure 47: different absorption and desorption capacity of a longitudinal discretized volumes.

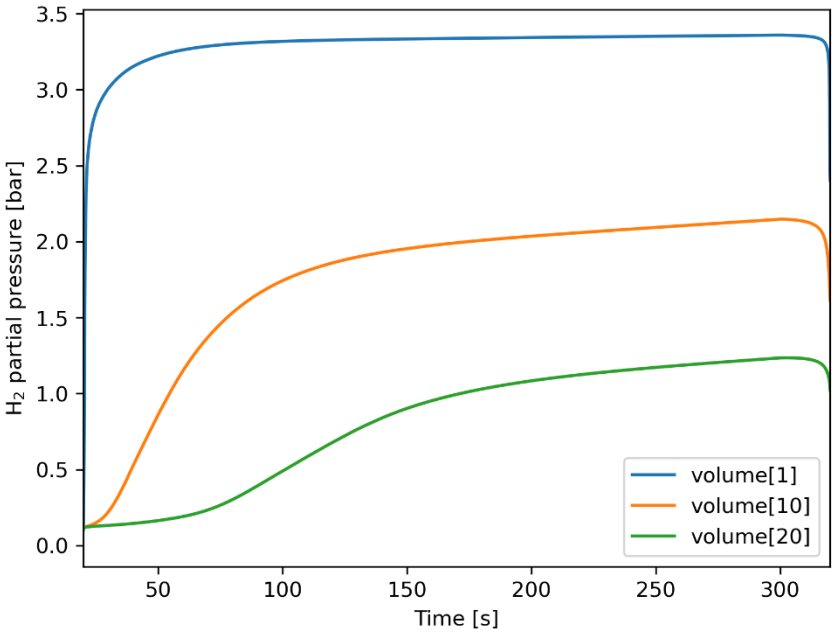

Figure 48: hydrogen partial pressure for the charge phase for 3 different longitudinally discretized volumes.

Indicative of absorption is the temperature of the metal hydride. Figure 49 shows the temperature inside the metal hydride for several longitudinally discrete volumes; the initial volumes have a greater value than the volumes placed near the outgas port. If the same longitudinal volume is considered, the temperature is not the same in the radial discretizations, as shown in figure 50.

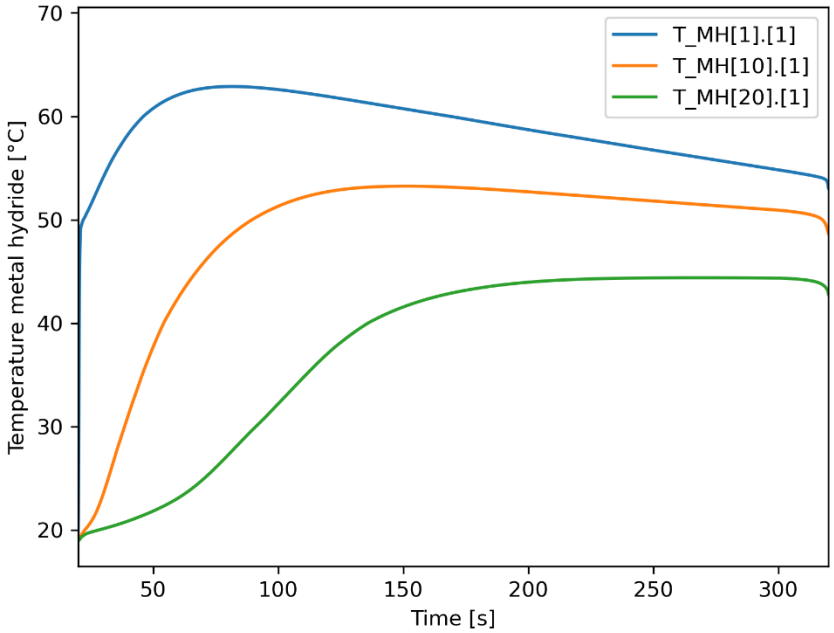

Figure 49: metal hydride temperature in different longitudinal volumes.

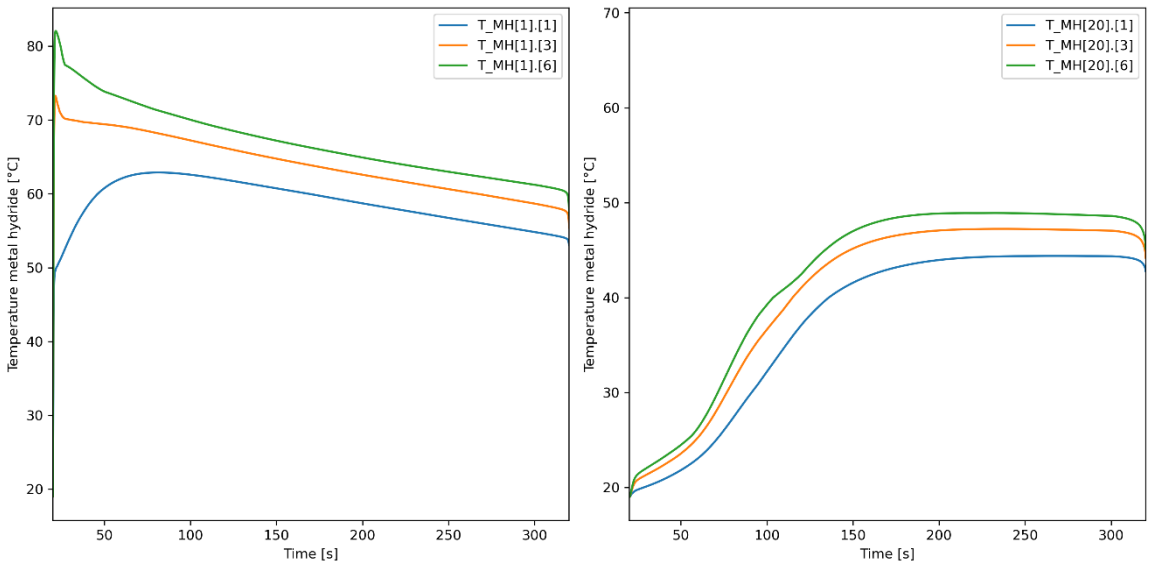

Figure 50: Variation of metal hydride temperature in different radial volumes, for the longitudinal volume placed near the feed gas port (left), and the one placed near the outgas port (right).

The purification cycle includes the first absorption phase, in which the hydrogen is trapped inside the tank, and the methane escapes as offgas. When the feed valve closes, the tank is connected to another tank to pressurize it to about 34 bar. Once the pressurization phase is completed, the hydrogen is released as a product at 1 bar. The pressure trend inside the tank is shown in figure 51.

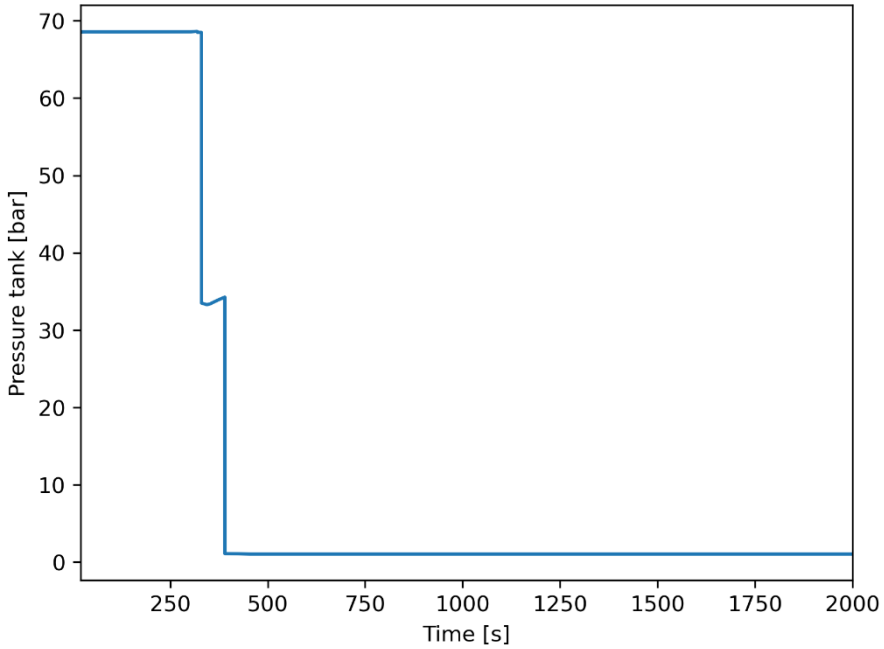

Figure 51: pressure trend inside the tank.

The same volumetric flow rate used in the deblending case is now expressed as mass flow rate in the gas flow rate (figure 52) from the feed port and the outgas port. The difference is the hydrogen stored inside the metal hydride tank.

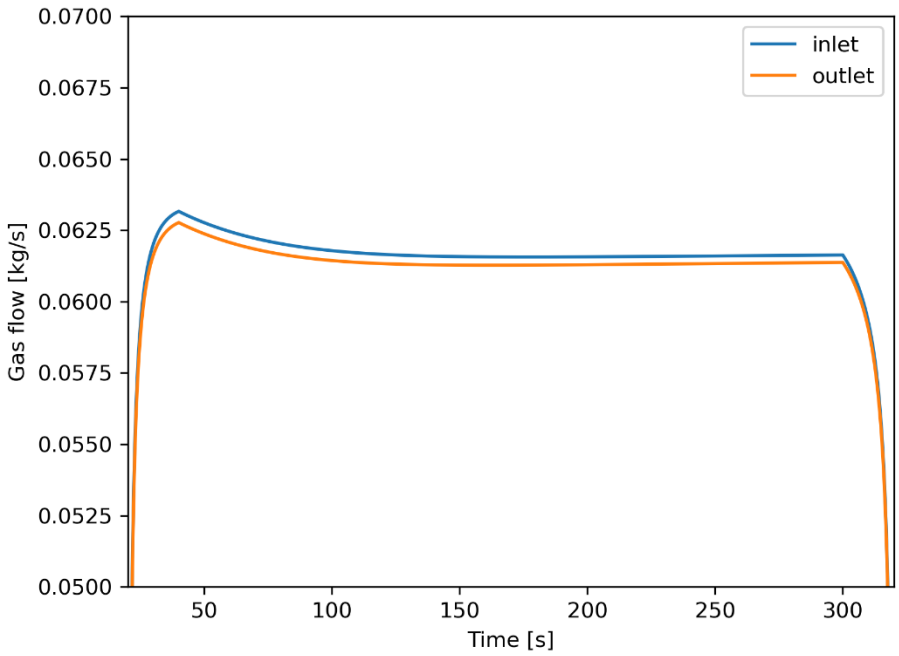

Figure 52: gas flow rate at the ports.

Conclusion

In this thesis, a TEA is conducted to determine which purification technology to adopt in the need to purify a gaseous mixture containing hydrogen in a certain amount, mixed with other components, and to achieve the purity required by PEMFCs. Mainstream technologies for purification are chosen, such as PSA, metal and carbon-based membranes, and metal hydrides. Excluded from the analysis were cryogenic distillation systems, which have high capital and operating costs incompatible with the chosen study cases, but also due to their difficulty in liquefying all impurities present in the gas phase, making hydrogen unsuitable for the fuel cell. All technologies are studied separately without hybrid configurations.

The PSA system is design by assessing the amount of fixed-bed adsorbent material to be installed inside the metal tank, which is proportional to the amount of impurities present in the mixture with hydrogen. A minimum of four adsorber vessels are required to have a continuous process that releases a stream of purified hydrogen product at feed pressure.

The purification unit using membrane technology is design by assessing the membrane area required to achieve a fixed hydrogen recovery value. At least three membrane stages are always required to achieve the required purity, whereby carbon membranes are effective to perform bulk separation, and subsequently palladium-based metallic membranes due to a high selectivity are able to obtain extremely pure hydrogen, with values above 99.999%.

The metal hydride is design similarly to the PSA technology by combining 4 beds in parallel, so that the batch process is, at the boundaries of the control volume, a continuous process producing a flow of purified hydrogen. The amount of hydrogen to be stored within the tank and which is released during desorption phase as a purified product affects the amount of metal alloy to be installed in the tank.

The analysis is based on two case studies representing some of the scenarios in which hydrogen may be used in the coming years. Case study 1 proposes the deblending and purification of hydrogen injected into the natural gas grid, for 5% and 30% H_2 by volume. Case study 2 proposes the purification of a hydrogen stream produced by gasification of biomass, and compared to the previous case study, identifies the purification of a stream with a high hydrogen content. Each case study involved the definition of different boundary conditions, but which remain the same when comparing the different technologies.

In the scenario of deblending from the natural gas grid with 5% hydrogen, the analysis shows that metal hydride is a winning technology with a specific separation cost in the range of 1.1-1.7 €/kg_{H2}, for an extraction or recovery rate of 43 kg/day. This is due to the inherent ability of metal hydrides to absorb small quantities of hydrogen in the feed, reducing investment (small containers) and operational (reduced compression

and electrical costs) costs. The specific cost of separation using PSA or membranes is about 6-7 times higher which makes hydrogen recovery potentially uneconomical. From the energy point of view, the metal hydride system, which uses a doped $LaNi_5$ alloy, has a specific separation cost of about 6 kWh/kg_{H2}, at least 6 times lower than the energy costs of PSA and membranes.

As the percentage of hydrogen within the natural gas increases up to the 30%, reaching an extraction scale of about 260 kg/day, metal hydride remains the one with the lowest specific separation cost (range 0.8-1.2 €/kgH2). In general, if an increase in the amount of hydrogen causes an increase in investment and operating costs, there is a reduction in the final separation cost for the higher amount of purified hydrogen product. In conclusion, costs are very sensitive to hydrogen content in feed gas as less hydrogen can be recovered for practically the same volume of gas processed, and metal hydride presents itself as an interesting solution at an experimental stage of blending hydrogen into the natural gas grid for reduced % H_2 values. The cost of hydrogen extraction from a natural gas pipeline is largely due to high OPEX costs, consisting of the fixed and variable costs for the utilities.

In case study 2, which involves the purification of hydrogen mixed with carbon dioxide, PSA is the leading technology for this type of application. In fact, for a purification capacity of about 600 kg/day, the specific separation cost for PSA is around 0.5 €/kg_{H2}.

The design provided orders of magnitude to complete the economic analysis but deliberately neglected important features of the purification processes. The relevant metal hydride result prompted the 5% H_2 deblending process to be studied in more detail by developing a dynamic model using the commercial software Dymola, proposing a kinetic absorption model and considering thermal management. The cylindrical geometry model with heat exchange tubes is validated with literature data and demonstrates the goodness of the design and the feasibility of adopting a metal hydride tank system to purify the hydrogen, achieving the goal of 99.97% purity and approaching 80% hydrogen recovery. The selectivity of metal hydrides to bind to a pressurized hydrogen stream can be used to separate a hydrogen that will be of high purity from the feed gas.

It is the chosen case studies and their boundary conditions that heavily influence the cost-effectiveness of each purification technology analyzed. The advantage of the metal hydride purification is absorption of the minor fraction from the feed, thus it is preferable for dilute mixtures, and the highest selectivity of metal hydride beds makes practical applications possible.
It is noted that these are costs for hydrogen purification which would contribute to the total hydrogen supply costs. The H_2 purification technology is not only a fundamental step but also an essential prerequisite for the widespread adoption of hydrogen.

References

[1] M. R. and P. R. Hannah Ritchie, "CO_2 and Greenhouse Gas Emissions," *Published online at OurWorldInData.org*, 2020. https://ourworldindata.org/co2-and-greenhouse-gas-emissions (accessed May 14, 2023).

[2] S. S. Penner, "Steps toward the hydrogen economy," *Energy*, vol. 31, no. 1, pp. 33–43, Jan. 2006, doi: 10.1016/j.energy.2004.04.060.

[3] Lawrence W Jones, "Toward a liquid hydrogen fuel economy," *University of Michigan Enviromental Action for Survival Teach In.*, 1970.

[4] IEA, "World Energy Outlook 2016," Paris, 2016. Accessed: May 14, 2023. [Online]. Available: https://www.iea.org/reports/world-energy-outlook-2016

[5] IEA, "Global Hydrogen Review," Paris, 2022.

[6] D. Tarvydas, "The role of hydrogen in decarbonisation energy scenarios – Views on 2030 and 2050," 2022. Accessed: May 14, 2023. [Online]. Available: https://data.europa.eu/doi/10.2760/899528

[7] IEA, "Renewable Electricity," Paris, 2022. Accessed: May 06, 2023. [Online]. Available: https://www.iea.org/reports/renewable-electricity

[8] K. Mazloomi and C. Gomes, "Hydrogen as an energy carrier: Prospects and challenges," *Renewable and Sustainable Energy Reviews*, vol. 16, no. 5, pp. 3024–3033, Jun. 2012, doi: 10.1016/j.rser.2012.02.028.

[9] S. K. Dwivedi and M. Vishwakarma, "Hydrogen embrittlement in different materials: A review," *Int J Hydrogen Energy*, vol. 43, no. 46, pp. 21603–21616, Nov. 2018, doi: 10.1016/j.ijhydene.2018.09.201.

[10] Irvin Glassman, Richard A. Yetter, and Nick G. Glumac, *Combustion*, 5th ed. 2014.

[11] Ian Tiseo, "Annual global emissions of carbon dioxide 1940-2022," 2023. https://www.statista.com/statistics/276629/global-co2-emissions/ (accessed May 14, 2023).

[12] L. Kaiwen, Y. Bin, and Z. Tao, "Economic analysis of hydrogen production from steam reforming process: A literature review," *Energy Sources, Part B: Economics, Planning, and Policy*, vol. 13, no. 2, pp. 109–115, Feb. 2018, doi: 10.1080/15567249.2017.1387619.

[13] T. research consultancy for energy technologies Thunder Said Energy, "Costs of hydrogen from coal gasification?" https://thundersaidenergy.com/downloads/costs-of-hydrogen-from-coal-gasification/ (accessed May 14, 2023).

[14] A. Molino, S. Chianese, and D. Musmarra, "Biomass gasification technology: The state of the art overview," *Journal of Energy Chemistry*, vol. 25, no. 1, pp. 10–25, Jan. 2016, doi: 10.1016/j.jechem.2015.11.005.

[15] A. Mohammadi and M. Mehrpooya, “A comprehensive review on coupling different types of electrolyzer to renewable energy sources,” *Energy*, vol. 158, pp. 632–655, Sep. 2018, doi: 10.1016/j.energy.2018.06.073.

[16] IEA, “Global average levelised cost of hydrogen production by energy source and technology, 2019 and 2050.” https://www.iea.org/data-and-statistics/charts/global-average-levelised-cost-of-hydrogen-production-by-energy-source-and-technology-2019-and-2050 (accessed May 14, 2023).

[17] ENTSO-E, “Electricity in Europe,” 2017.

[18] IPCC, “AR5 Climate Change 2014: Mitigation of Climate Change,” 2014.

[19] C. Tarhan and M. A. Çil, “A study on hydrogen, the clean energy of the future: Hydrogen storage methods,” *J Energy Storage*, vol. 40, p. 102676, Aug. 2021, doi: 10.1016/j.est.2021.102676.

[20] J. O. Abe, A. P. I. Popoola, E. Ajenifuja, and O. M. Popoola, “Hydrogen energy, economy and storage: Review and recommendation,” *Int J Hydrogen Energy*, vol. 44, no. 29, pp. 15072–15086, Jun. 2019, doi: 10.1016/j.ijhydene.2019.04.068.

[21] R. Kurz *et al.*, “Transport and storage,” in *Machinery and Energy Systems for the Hydrogen Economy*, Elsevier, 2022, pp. 215–249. doi: 10.1016/B978-0-323-90394-3.00003-5.

[22] K Shashikala, “Hydrogen storage materials,” *Functional Materials* , 2012.

[23] “Hydrogen Insights, A perspective on hydrogen investment, market development and cost competitiveness,” 2021.

[24] N. Sazali, W. N. Wan Salleh, A. S. Jamaludin, and M. N. Mhd Razali, “New Perspectives on Fuel Cell Technology: A Brief Review,” *Membranes (Basel)*, vol. 10, no. 5, p. 99, May 2020, doi: 10.3390/membranes10050099.

[25] Daniele Reschiotto, “Effects of anode fuel recirculation on SOFCs fuelled with biogas,” Politecnico di Torino, 2018.

[26] “2022 Hydrogen Supply Capacity and Demand, Chapter 2,” 2022.

[27] J. L. Aprea, “‘Quality specification and safety in hydrogen production, commercialization and utilization,’” *Int J Hydrogen Energy*, vol. 39, no. 16, pp. 8604–8608, May 2014, doi: 10.1016/j.ijhydene.2014.01.005.

[28] A. Murugan and A. S. Brown, “Review of purity analysis methods for performing quality assurance of fuel cell hydrogen,” *Int J Hydrogen Energy*, vol. 40, no. 11, pp. 4219–4233, Mar. 2015, doi: 10.1016/j.ijhydene.2015.01.041.

[29] Y. Ligen, H. Vrubel, and H. Girault, “Energy efficient hydrogen drying and purification for fuel cell vehicles,” *Int J Hydrogen Energy*, vol. 45, no. 18, pp. 10639–10647, Apr. 2020, doi: 10.1016/j.ijhydene.2020.02.035.

[30] C.-C. Cormos, “Hydrogen production from fossil fuels with carbon capture and storage based on chemical looping systems,” *Int J Hydrogen Energy*, vol. 36, no. 10, pp. 5960–5971, May 2011, doi: 10.1016/j.ijhydene.2011.01.170.

[31] F. Dawood, M. Anda, and G. M. Shafiullah, “Hydrogen production for energy: An overview,” *Int J Hydrogen Energy*, vol. 45, no. 7, pp. 3847–3869, Feb. 2020, doi: 10.1016/j.ijhydene.2019.12.059.

[32] Z. Luo, Y. Hu, H. Xu, D. Gao, and W. Li, “Cost-Economic Analysis of Hydrogen for China’s Fuel Cell Transportation Field,” *Energies (Basel)*, vol. 13, no. 24, p. 6522, Dec. 2020, doi: 10.3390/en13246522.

[33] D. Wickham, A. Hawkes, and F. Jalil-Vega, “Hydrogen supply chain optimisation for the transport sector – Focus on hydrogen purity and purification requirements,” *Appl Energy*, vol. 305, p. 117740, Jan. 2022, doi: 10.1016/j.apenergy.2021.117740.

[34] IEA, “Hydrogen Supply,” 2022. https://www.iea.org/reports/hydrogen-supply

[35] “Global Oil and Gas Pipelines Market Outlook, 2021-2025 – Capacity and Capital Expenditure Outlook with Details of All Operating and Planned Pipelines,” *GlobalData*. https://www.globaldata.com/store/report/oil-and-gas-pipelines-market-analysis/ (accessed May 20, 2023).

[36] Frontier Economics, “GAS FRAMEWORK CHANGES TO ENABLE HYDROGEN DEBLENDING,” 2022.

[37] MW Melaina, O Antonia, and M Penev, “Blending hydrogen into natural gas pipeline networks: a review of key issues,” 2013.

[38] “Hydrogen Deblending in the GB Gas Network,” 2021.

[39] “Flexible Hybrid separation system for H2 recovery from NG Grids.” https://cordis.europa.eu/project/id/700355 (accessed May 20, 2023).

[40] W. Liemberger, M. Groß, M. Miltner, and M. Harasek, “Experimental analysis of membrane and pressure swing adsorption (PSA) for the hydrogen separation from natural gas,” *J Clean Prod*, vol. 167, pp. 896–907, Nov. 2017, doi: 10.1016/j.jclepro.2017.08.012.

[41] “Preparing for the hydrogen economy by using the existing natural gas system as a catalyst (NATURALHY).” https://cordis.europa.eu/project/id/502661 (accessed May 20, 2023).

[42] H. Balat and E. Kırtay, “Hydrogen from biomass – Present scenario and future prospects,” *Int J Hydrogen Energy*, vol. 35, no. 14, pp. 7416–7426, Jul. 2010, doi: 10.1016/j.ijhydene.2010.04.137.

[43] Donatella Barisano, “Green hydrogen through biomass gasification,” *ENEA magazine*, 2021.

[44] A. Albuloushi, “Optimization of a Water Gas Shift Reaction,” *Undergraduate Journal of Mathematical Modeling: One + Two*, vol. 8, no. 2, Jan. 2018, doi: 10.5038/2326-3652.8.2.4892.

[45] Matthias Binder, Michael Kraussler, Matthias Kuba, and Markus Luisser, “Hydrogen from biomass gasification,” 2018.

[46] S. Fail *et al.*, "Wood Gas Processing To Generate Pure Hydrogen Suitable for PEM Fuel Cells," *ACS Sustain Chem Eng*, vol. 2, no. 12, pp. 2690–2698, Dec. 2014, doi: 10.1021/sc500436m.

[47] L. Schorer, S. Schmitz, and A. Weber, "Membrane based purification of hydrogen system (MEMPHYS)," *Int J Hydrogen Energy*, vol. 44, no. 25, pp. 12708–12714, May 2019, doi: 10.1016/j.ijhydene.2019.01.108.

[48] "UNIQUE gasifier for hydrogen Production." Accessed: May 20, 2023. [Online]. Available: https://cordis.europa.eu/project/id/299732

[49] M. Luberti and H. Ahn, "Review of Polybed pressure swing adsorption for hydrogen purification," *Int J Hydrogen Energy*, vol. 47, no. 20, pp. 10911–10933, Mar. 2022, doi: 10.1016/j.ijhydene.2022.01.147.

[50] Ruthven, Farooq, and Knaebel, *Pressure swing adsorption*. John Wiley & Sons, 1996.

[51] A. PE. Gabelman, "Adsorption Basics: Part 1," *Chem Eng Prog*, 2017.

[52] Michael C. Georgiadis, Julio R. Banga, and Efstratios N. Pistikopoulos, "Modeling of Pressure Swing Adsorption Processes," in *Process Systems Engineering*, 2011.

[53] P. N. Sharratt, "Chemicals manufacture by batch processes," in *Handbook of Batch Process Design*, Dordrecht: Springer Netherlands, 1997, pp. 1–23. doi: 10.1007/978-94-009-1455-1_1.

[54] C. A. Grande, "Advances in Pressure Swing Adsorption for Gas Separation," *ISRN Chemical Engineering*, vol. 2012, pp. 1–13, Dec. 2012, doi: 10.5402/2012/982934.

[55] H. T. Lu, W. Li, E. S. Miandoab, S. Kanehashi, and G. Hu, "The opportunity of membrane technology for hydrogen purification in the power to hydrogen (P2H) roadmap: a review," *Front Chem Sci Eng*, vol. 15, no. 3, pp. 464–482, Jun. 2021, doi: 10.1007/s11705-020-1983-0.

[56] R. W. Baker, *Membrane Technology and Applications*. Wiley, 2012. doi: 10.1002/9781118359686.

[57] M. R. Rahimpour, F. Samimi, A. Babapoor, T. Tohidian, and S. Mohebi, "Palladium membranes applications in reaction systems for hydrogen separation and purification: A review," *Chemical Engineering and Processing: Process Intensification*, vol. 121, pp. 24–49, Nov. 2017, doi: 10.1016/j.cep.2017.07.021.

[58] A. ISMAIL and L. DAVID, "A review on the latest development of carbon membranes for gas separation," *J Memb Sci*, vol. 193, no. 1, pp. 1–18, Oct. 2001, doi: 10.1016/S0376-7388(01)00510-5.

[59] M. Martin, C. Gommel, C. Borkhart, and E. Fromm, "Absorption and desorption kinetics of hydrogen storage alloys," *J Alloys Compd*, vol. 238, no. 1–2, pp. 193–201, May 1996, doi: 10.1016/0925-8388(96)02217-7.

[60] Jin Zhong Zhang, Jinghong Li, Yat Li, and Yiping Zhao, "Chemical Storage Based on Metal Hydrides and Hydrocarbons," in *Hydrogen Generation, Storage and Utilization*, 2014.

[61] M. Dornheim, "Thermodynamics of Metal Hydrides: Tailoring Reaction Enthalpies of Hydrogen Storage Materials," in *Thermodynamics - Interaction Studies - Solids, Liquids and Gases*, InTech, 2011. doi: 10.5772/21662.

[62] Batta L.B., "Selective adsorption process," 3564816, 1971

[63] Warren D. Seider, Daniel R. Lewin, J. D. Seader, Soemantri Widagdo, Rafiqul Gani, and Ka Ming Ng, *Product and Process Design Principles: Synthesis, Analysis and Evaluation*, 4th ed. Wiley, 2016.

[64] *Chemical Engineering Design*. Elsevier, 2022. doi: 10.1016/C2019-0-02025-0.

[65] D. S. N. F. Pg Hj Mohd Yussof, M. H. A. H. Ibrahim, M. Z. Ramli, M. I. F. H. Sahari, R. R. Karri, and M. H. Azri, "Design of pressure swing adsorber and absorption column for production of hydrogen by steam methane reforming using biogas," 2023, p. 060001. doi: 10.1063/5.0110290.

[66] M. Mulder, *Basic Principles of Membrane Technology*. Dordrecht: Springer Netherlands, 1996. doi: 10.1007/978-94-009-1766-8.

[67] Christie John Geankoplis, Daniel H. Lepek, and Allen Hersel, *Transport Processes and Separation Process Principles*, 5th ed. Pearson, 2021.

[68] M. Thundyil, "Mathematical modeling of gas separation permeators — for radial crossflow, countercurrent, and cocurrent hollow fiber membrane modules," *J Memb Sci*, vol. 125, no. 2, pp. 275–291, Mar. 1997, doi: 10.1016/S0376-7388(96)00218-9.

[69] D. GRAINGER and M. HAGG, "The recovery by carbon molecular sieve membranes of hydrogen transmitted in natural gas networks," *Int J Hydrogen Energy*, vol. 33, no. 9, pp. 2379–2388, May 2008, doi: 10.1016/j.ijhydene.2008.03.001.

[70] J. J. Sheridan, F. G. Eisenberg, E. J. Greskovich, G. D. Sandrock, and E. L. Huston, "Hydrogen separation from mixed gas streams using reversible metal hydrides," *Journal of the Less Common Metals*, vol. 89, no. 2, pp. 447–455, Feb. 1983, doi: 10.1016/0022-5088(83)90355-7.

[71] S. Miura, A. Fujisawa, and M. Ishida, "A hydrogen purification and storage system using metal hydride," *Int J Hydrogen Energy*, vol. 37, no. 3, pp. 2794–2799, Feb. 2012, doi: 10.1016/j.ijhydene.2011.03.150.

[72] Y. Taniguchi and M. Ishida, "Passive load following method for PEFC system with reformer and its efficiency improvement evaluated by using the concept of exergy," *Electrical Engineering in Japan*, vol. 152, no. 4, pp. 17–26, Sep. 2005, doi: 10.1002/eej.20148.

[73] P. Hao, S. Li, S. Li, Y. Shi, and N. Cai, “Hydrogen Direct Adsorptive Separation: Development Status and Trends,” *Energy & Fuels*, vol. 34, no. 12, pp. 15126–15140, Dec. 2020, doi: 10.1021/acs.energyfuels.0c02317.

[74] B. SAKINTUNA, F. LAMARIDARKRIM, and M. HIRSCHER, “Metal hydride materials for solid hydrogen storage: A review☆,” *Int J Hydrogen Energy*, vol. 32, no. 9, pp. 1121–1140, Jun. 2007, doi: 10.1016/j.ijhydene.2006.11.022.

[75] D. Chandra, J. J. Reilly, and R. Chellappa, “Metal hydrides for vehicular applications: The state of the art,” *JOM*, vol. 58, no. 2, pp. 26–32, Feb. 2006, doi: 10.1007/s11837-006-0005-0.

[76] K. D. Modibane, M. Williams, M. Lototskyy, M. W. Davids, Ye. Klochko, and B. G. Pollet, “Poisoning-tolerant metal hydride materials and their application for hydrogen separation from CO2/CO containing gas mixtures,” *Int J Hydrogen Energy*, vol. 38, no. 23, pp. 9800–9810, Aug. 2013, doi: 10.1016/j.ijhydene.2013.05.102.

[77] N. Hanada *et al.*, “Dependence of constituent elements of AB5 type metal hydrides on hydrogenation degradation by CO2 poisoning,” *J Alloys Compd*, vol. 647, pp. 198–203, Oct. 2015, doi: 10.1016/j.jallcom.2015.05.253.

[78] G. Sdanghi, G. Maranzana, A. Celzard, and V. Fierro, “Review of the current technologies and performances of hydrogen compression for stationary and automotive applications,” *Renewable and Sustainable Energy Reviews*, vol. 102, pp. 150–170, Mar. 2019, doi: 10.1016/j.rser.2018.11.028.

[79] J. André, S. Auray, D. De Wolf, M.-M. Memmah, and A. Simonnet, “Time development of new hydrogen transmission pipeline networks for France,” *Int J Hydrogen Energy*, vol. 39, no. 20, pp. 10323–10337, Jul. 2014, doi: 10.1016/j.ijhydene.2014.04.190.

[80] Inc. Nexant, “H2A Hydrogen Delivery Infrastructure Analysis Models and Conventional Pathway Options Analysis Results,” 2008.

[81] *Natural Gas Engineering Handbook*. Elsevier, 2005. doi: 10.1016/C2013-0-15534-1.

[82] “Euro foreign exchange reference rates.” https://www.ecb.europa.eu/stats/policy_and_exchange_rates/euro_reference_exchange_rates/html/eurofxref-graph-usd.en.html (accessed Mar. 30, 2023).

[83] “Cost Indices.” https://toweringskills.com/financial-analysis/cost-indices/ (accessed Mar. 30, 2023).

[84] E. Popovski, T. Fleiter, H. Santos, V. Leal, and E. O. Fernandes, “Technical and economic feasibility of sustainable heating and cooling supply options in southern European municipalities-A case study for Matosinhos, Portugal,” *Energy*, vol. 153, pp. 311–323, Jun. 2018, doi: 10.1016/j.energy.2018.04.036.

[85] I. Burgers, “Novel Technology for Hydrogen Separation from Natural Gas using Pressure Swing Adsorption.”

[86] M. Penev, G. Saur, C. Hunter, and J. Zuboy, “H2A Hydrogen Production Model: Version 3.2018 User Guide (DRAFT).”

[87] D. Chen, F. Yang, D. S. Karousos, L. Lei, E. P. Favvas, and X. He, “Process parametric testing and simulation of carbon membranes for H2 recovery from natural gas pipeline networks,” *Sep Purif Technol*, vol. 307, p. 122842, Feb. 2023, doi: 10.1016/j.seppur.2022.122842.

[88] M. Nordio, S. A. Wassie, M. Van Sint Annaland, D. A. Pacheco Tanaka, J. L. Viviente Sole, and F. Gallucci, “Techno-economic evaluation on a hybrid technology for low hydrogen concentration separation and purification from natural gas grid,” *Int J Hydrogen Energy*, vol. 46, no. 45, pp. 23417–23435, Jul. 2021, doi: 10.1016/j.ijhydene.2020.05.009.

[89] A. N. L. Nuclear Science Engineering Division, “Economic Data and Modeling Support for the Two Regional Case Studies,” 2018.

[90] Wade A. Amos, “Costs of Storing and Transporting Hydrogen.”

[91] G. Parks, R. Boyd, J. Cornish, and R. Remick, “Hydrogen Station Compression, Storage, and Dispensing Technical Status and Costs,” 2014.

[92] N. Kohlheb, M. Wluka, A. Bezama, D. Thrän, A. Aurich, and R. A. Müller, “Environmental-Economic Assessment of the Pressure Swing Adsorption Biogas Upgrading Technology,” *Bioenergy Res*, vol. 14, no. 3, pp. 901–909, Sep. 2021, doi: 10.1007/s12155-020-10205-9.

[93] J. B. Cristello, J. M. Yang, R. Hugo, Y. Lee, and S. S. Park, “Feasibility analysis of blending hydrogen into natural gas networks,” *Int J Hydrogen Energy*, Feb. 2023, doi: 10.1016/j.ijhydene.2023.01.156.

[94] L. Roses, G. Manzolini, S. Campanari, E. De Wit, and M. Walter, “Techno-economic Assessment of Membrane Reactor Technologies for Pure Hydrogen Production for Fuel Cell Vehicle Fleets,” *Energy & Fuels*, vol. 27, no. 8, pp. 4423–4431, Aug. 2013, doi: 10.1021/ef301960e.

[95] “Misura qualità - Snam.” https://misura.snam.it/portmis/coortecDocumentoController.do?menuSelected=4300 (accessed Apr. 05, 2023).

[96] F. Dreisbach, R. Staudt, and J. U. Keller, “High Pressure Adsorption Data of Methane, Nitrogen, Carbon Dioxide and their Binary and Ternary Mixtures on Activated Carbon,” *Adsorption*, vol. 5, no. 3, pp. 215–227, 1999, doi: 10.1023/A:1008914703884.

[97] “SAFETY DATA SHEET.” https://www.cabotcorp.jp/-/media/files/msds/nac/eghs/en/r1e-eghs-en.pdf?la=en&rev=221f3184a112499ca28fce5afabfc3f6&hash=7F3AC50CFFFCA661142B4AA966A5F8FB (accessed Apr. 08, 2023).

[98] D. Dunikov and D. Blinov, “Extraction of hydrogen from a lean mixture with methane by metal hydride,” *Int J Hydrogen Energy*, vol. 45, no. 16, pp. 9914–9926, Mar. 2020, doi: 10.1016/j.ijhydene.2020.01.201.

[99] F. Yang, X. Cao, Z. Zhang, Z. Bao, Z. Wu, and N. N. Serge, "Assessment on the Long Term Performance of a LaNi5 based Hydrogen Storage System," *Energy Procedia*, vol. 29, pp. 720–730, 2012, doi: 10.1016/j.egypro.2012.09.084.

[100] H. Wang, Y. Liu, and J. Zhang, "Hydrogen purification by Mg alloy hydrogen adsorbent," *Adsorption*, vol. 28, no. 1–2, pp. 85–95, Feb. 2022, doi: 10.1007/s10450-021-00348-2.

[101] L. Cao *et al.*, "Biorenewable hydrogen production through biomass gasification: A review and future prospects," *Environ Res*, vol. 186, p. 109547, Jul. 2020, doi: 10.1016/j.envres.2020.109547.

[102] D. S. Newsome, "The Water-Gas Shift Reaction," *Catalysis Reviews*, vol. 21, no. 2, pp. 275–318, Jan. 1980, doi: 10.1080/03602458008067535.

[103] B. Ohs, M. Falkenberg, and M. Wessling, "Optimizing hybrid membrane-pressure swing adsorption processes for biogenic hydrogen recovery," *Chemical Engineering Journal*, vol. 364, pp. 452–461, May 2019, doi: 10.1016/j.cej.2019.01.136.

[104] B. Axelberg, "Application of a Water-Gas shift reaction to the WoodRoll process," KTH, Stockholm, 2017.

[105] Y. Park, D.-K. Moon, Y.-H. Kim, H. Ahn, and C.-H. Lee, "Adsorption isotherms of CO2, CO, N2, CH4, Ar and H2 on activated carbon and zeolite LiX up to 1.0 MPa," *Adsorption*, vol. 20, no. 4, pp. 631–647, May 2014, doi: 10.1007/s10450-014-9608-x.

[106] H.-S. Lee, S. Y. Lee, K. Yoo, H. W. Kim, E. Lee, and N. G. Im, "Biohydrogen production and purification: Focusing on bioelectrochemical systems," *Bioresour Technol*, vol. 363, p. 127956, Nov. 2022, doi: 10.1016/j.biortech.2022.127956.

[107] M. Pan, H. Omar, and S. Rohani, "Application of Nanosize Zeolite Molecular Sieves for Medical Oxygen Concentration," *Nanomaterials*, vol. 7, no. 8, p. 195, Jul. 2017, doi: 10.3390/nano7080195.

[108] L. Lei, A. Lindbråthen, M. Hillestad, and X. He, "Carbon molecular sieve membranes for hydrogen purification from a steam methane reforming process," *J Memb Sci*, vol. 627, p. 119241, Jun. 2021, doi: 10.1016/j.memsci.2021.119241.

[109] D. Dunikov *et al.*, "Biohydrogen purification using metal hydride technologies," *Int J Hydrogen Energy*, vol. 41, no. 46, pp. 21787–21794, Dec. 2016, doi: 10.1016/j.ijhydene.2016.08.190.

[110] A. A. Rabienataj Darzi, H. Hassanzadeh Afrouzi, E. Alizadeh, V. Shokri, and M. Farhadi, "Numerical Simulation of Heat and Mass Transfer during Absorption of Hydrogen in Metal Hydride Tank," *Heat Transfer-Asian Research*, vol. 46, no. 1, pp. 75–90, Jan. 2017, doi: 10.1002/htj.21199.

[111] A. Jemni, “Experimental and theoretical study of ametal–hydrogen reactor,” *Int J Hydrogen Energy*, vol. 24, no. 7, pp. 631–644, Jul. 1999, doi: 10.1016/S0360-3199(98)00117-7.

[112] B. Fumey, T. Buetler, and U. F. Vogt, “Ultra-low NOx emissions from catalytic hydrogen combustion,” *Appl Energy*, vol. 213, pp. 334–342, Mar. 2018, doi: 10.1016/j.apenergy.2018.01.042.